Electronic Supplementary Material (ESI) for ChemComm.

Accessing Three Oxidation States of Cobalt in M_6L_3 Nanoprisms with Cobalt-Porphyrin Walls

P. Thomas Blackburn, Iram F. Mansoor, Kaitlyn G. Dutton, Alexei M. Tyryshkin, and Mark C. Lipke*

Department of Chemistry and Chemical Biology, Rutgers The State University of New Jersey
123 Bevier Road, Piscataway NJ 08854

Email: ml1353@chem.rutgers.edu

Supporting Information

Table of Contents:

1. General Considerations

Sources: Unless otherwise specified, commercially available chemicals and solvents were used as received from (1) Fisher: acetonitrile, diethyl ether, dichloromethane, sulfuric acid, pyridine, toluene; (2) Acros Organics: tetrabutylammonium hexafluorophosphate, cobalt acetate tetrahydrate, silver(I) hexafluorophosphate, zinc acetate dihydrate; (3) Alfa-Aesar: ferrocene (Fc); (4) Cambridge Isotopes: acetonitrile-d_3 (CD_3CN, D-99.8%) and benzene-d_6 (C_6D_6, D-99.5%); (5) Sigma Aldrich: ferrous sulfate, cobaltocene (Cp_2Co), potassium bromide; (6) TCI Chemicals: thianthrene; (7) Oakwood Chemical: trimethyloxonium tetrafluoroborate ($[Me_3O]BF_4$), sodium nitrite; (8) Matrix Scientific: potassium hexafluorophosphate. The nanocages **1a**•12PF$_6$ and **1b**•12PF$_6$ were prepared as we have previously described.[1] [tetrakis(N-methyl-3-pyridinium)porphyrin]•4PF$_6$ was prepared following a reported procedure.[2] Thianthrenium hexafluorophosphate[3] and nitric oxide[4] were generated using adapted literature procedures, and specific details are described in Sections 2 and 3.

Purification: NMR solvents for oxygen or moisture sensitive procedures were dried over a suitable drying agent (CaH_2 for CD_3CN; NaK alloy for C_6D_6), subjected to three freeze-pump-thaw cycles, distilled by vacuum transfer, and then stored in an N_2 atmosphere glovebox prior to use. Dry, air-free solvents for electrochemistry and EPR spectroscopy were obtained by sparging HPLC grade solvents with argon for 1 h before passage through solvent drying columns supplied by Pure Process Technologies. Ferrocene was sublimated under static vacuum prior to use. Cobaltocene (Cp_2Co) was sublimated under dynamic vacuum and stored at −25 °C in an N_2 atmosphere glovebox prior to use. Tetrabutylammonium hexafluorophosphate ($TBAPF_6$) was recrystallized three times from absolute ethanol, dried at 125 °C under dynamic vacuum for ≥ 12 hours, and stored in an N_2 atmosphere glovebox prior to use.

Air-Sensitive Procedures: All air sensitive experiments were carried out under an inert atmosphere (N_2), either in an MBraun Unilab glovebox or using standard Schlenk techniques. Solids were weighed inside the glovebox using a Sartorius Secura 225D-1S semimicro analytical balance accompanied by an electronic ionizer to eliminate static. Liquids were measured and transferred using Hamilton microliter syringes. Spectra were acquired on samples that were sealed under N_2 in PTFE-valved (J-Young type) NMR tubes.

Physical Measurements: NMR spectra were recorded on samples in CD_3CN at 298 K using a Bruker AVANCE Neo 500 MHz spectrometer or a Varian VNMRS 500 MHz spectrometer. ^1H NMR spectra were referenced using the residual proteo signal of CD_2HCN, and $^{13}C\{^1H\}$ spectra were referenced to the nitrile $^{13}C\{^1H\}$ signal of CD_3CN. High resolution mass spectra were obtained via direct infusion of acetonitrile solutions of the analyte into a Waters Xevo G2-XS QTOF mass spectrometer. EPR spectra were recorded on samples frozen in 50:50 MeCN/toluene at 77 K using a Bruker Elexsys580e EPR spectrometer operating at X-band microwave frequency. UV-vis-NIR spectra were recorded at 298 K on samples in MeCN in 1.0 mm quartz cuvettes using a Shimadzu UV-2600i spectrophotometer. Cyclic voltammetry (CV) measurements were performed using a CH Instruments 600E potentiostat. For CV experiments, a 3 mm glassy carbon working electrode was employed, along with a Pt wire counter electrode and Ag wire pseudo-reference electrode. FTIR spectra were recorded on samples in pressed KBr pellets using a Thermo Scientific Smart OMNI-Transmission FTIR spectrometer. Additional details of physical measurements are provided below in their respective sections.

2. Synthetic Procedures for Isolated Compounds (**2, 5, 7, Co$_3$-1a**,**b**, and **Zn$_3$-1a**,**b**).

2.a. Synthesis of **2**•4PF$_6$

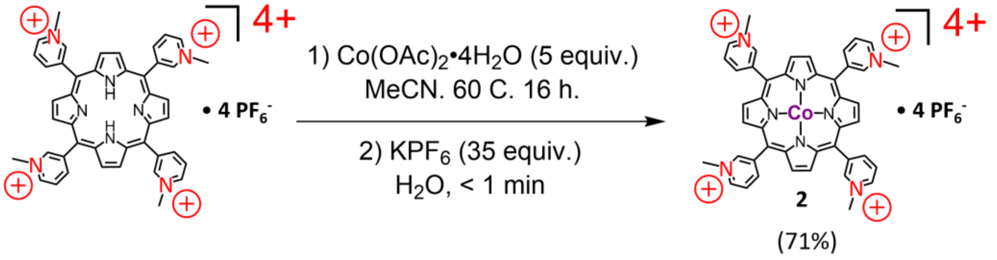

Scheme S1. Synthesis of complex **2**•4PF$_6$.

[tetrakis(*N*-methyl-3-pyridinium)porphyrin]•4PF$_6$ (48.3 mg, 38.4 µmol) was dissolved in 50 mL of MeCN in a 100 mL round bottom flask to give a dark purple solution. Co(OAc)$_2$•4H$_2$O (47.8 mg, 192 µmol) was added as a solid, a reflux condenser was attached to the flask, and the reaction heated to 60 °C for 16 h, resulting in a dark orange-purple solution. The reaction mixture was concentrated to 20 mL under reduced pressure, followed by the addition of solid KPF$_6$ (254 mg, 1.38 mmol) and then 200 mL of water, resulting in a fine orange precipitate. The supernatant was removed by vacuum filtration on a fine mesh frit, and the solids were washed with water (50 mL) and then Et$_2$O (50 mL). The product was washed through the frit with 10 mL of MeCN and the resulting solution was dried by rotary evaporation, providing 35.8 mg of **2**•4PF$_6$ as a dark orange-purple solid (71 % yield). ^{1}H NMR (500 MHz, CD$_3$CN): δ 12.58 (br, 8 H, β CH), 10.40 (br, 4 H), 10.13 (br, 4 H), 9.46 (s, 4 H), 9.19 (s, 4 H), 4.99 (s, 12 H, *N*CH$_3$). ESI(+)-MS: [**2** – PF$_6$]$^{1+}$ Calculated: 1170.1320 m/z, Found: 1170.1433 m/z; [[**2**]$_2$ – 3PF$_6$]$^{3+}$ Calculated: 731.7666 m/z, Found: 731.7778 m/z; [**2** – 2PF$_6$]$^{2+}$ Calculated: 512.5839 m/z, Found: 512.5924 m/z; [**2** – 4PF$_6$]$^{4+}$ Calculated: 183.8099 m/z, Found: 183.8052 m/z. UV-vis (MeCN): λ_{max} = 417 (ε = 119,620 M^{-1} cm^{-1}), 534 nm (ε = 12,770 M^{-1} cm^{-1}).

2.b. Synthesis of **5**•5PF$_6$

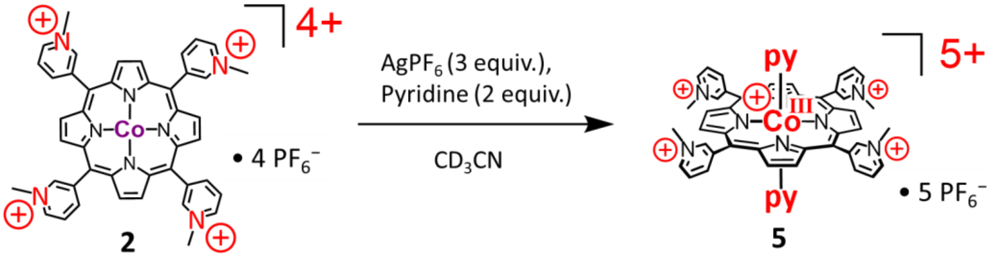

Scheme S2. Synthesis of **5**•5PF$_6$**.**

2•4PF$_6$ (11.6 mg, 8.8 µmol) was dissolved in 0.60 mL of CD$_3$CN and the resulting solution was transferred to an NMR tube. AgPF$_6$ (6.7 mg, 27 µmol) was added as a solid along with pyridine (1.4 µL, 18 µmol). The NMR sample was sealed with a PTFE stopper and the tube was turned over repeatedly to mix the solutions, resulting in the formation of a fine precipitate of Ag^0 without any other visually apparent changes. Ag^0 particles were removed using a 0.2 µm PTFE syringe filter and solvent was removed by rotary evaporation. The resulting solid was washed with dichloromethane (3 x 5 mL) and dried under vacuum to provide 10.9 mg of **5**•5PF$_6$ as a dark purple/orange solid (76% yield). ^{1}H NMR (500 MHz, CD$_3$CN): δ 9.33 (s, 4 H), 9.26 (s, 8 H, β CH), 9.09 (dt, *J* = 6.2, 1.31 Hz, 4 H), 8.92 (d, 8.18 Hz, 4 H), 8.39 (dd, *J* = 7.89, 6.31 Hz, 4 H), 6.25 (tt, *J* = 7.56, 1.41 Hz, 2 H, py), 5.14 (t, *J* = 7.07 Hz, 4 H, py), 4.59 (s, 12 H, *N*CH$_3$), 0.79 (dd, *J* = 6.74, 1.42 Hz, 4 H, py). ^{13}C{^{1}H} NMR (125 MHz, CD$_3$CN): δ 149.19, 147.92, 147.59, 146.42, 143.47, 139.99, 138.78, 137.49, 127.95, 123.57, 112.80, 49.54. UV-vis (MeCN): λ_{max} = 434 (ε = 205,180 M^{-1} cm^{-1}), 548 nm (ε = 12,780 M^{-1} cm^{-1}).

2.c. Synthesis of **7**•4PF$_6$

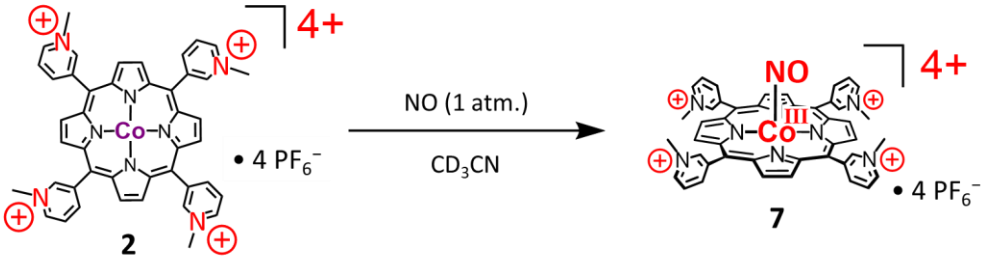

Scheme S3. Synthesis of **7**•4PF$_6$**.**

Generation of Nitric Oxide. Adapting a reported procedure,[4] iron(II) sulfate (8.06 g, 29.0 mmol) and sulfuric acid (2.33 mL, 43.5 mmol) were added to 50 mL of water in a filter flask. The flask was sealed with a rubber septum and Tygon tubing was attached to the sidearm of the flask, leading to a drying tube packed with 3 Å molecular sieves followed by a needle as an outlet. The solution was sparged with N$_2$ for 30 min, allowing the N$_2$ to flush the entire system of air. Meanwhile, sodium sulfite (2.00 g, 29.0 mmol) was dissolved in 10 mL of water and sparged with N$_2$ gas for 30 min. The sodium sulfite solution was then added slowly to the filter flask via syringe, causing the resulting mixture to turn from a light green color to a dark black color with visible gas evolution. The system was allowed to fill with nitric oxide for 2 min before using the output to add NO to solutions of **7**•4PF$_6$ as described below.

7•4PF$_6$. **2**•4PF$_6$ (8.3 mg, 6.3 µmol) was dissolved in 0.60 mL of CD$_3$CN and the resulting solution was transferred to a J-Young style air-free NMR tube. The NMR sample was sealed with a PTFE stopper, the solution was degassed via three freeze-pump-thaw cycles, and the tube was then filled with N$_2$. The PTFE stopper was replaced with a rubber septum and nitric oxide was passed through the tube for 5 min using needles for the inlet and outlet. The NMR tube was resealed with the PTFE stopper and turned over repeatedly to saturate the solution with NO, resulting in an immediate color change from dark orange to dark red. The ^{1}H NMR spectrum of the sample was acquired to confirm the complete disappearance of the signals of **2** and the clean formation of a diamagnetic porphyrin complex. The sample was degassed via three freeze-pump-thaw cycles to remove excess nitric oxide before being cycled into a N$_2$ atmosphere glove box, where the solvent was removed under vacuum to afford 8.2 mg of **7**•4PF$_6$ as a dark red-purple solid (98 % yield). ^{1}H NMR (500 MHz, CD$_3$CN): δ 9.46 (s, 4H), 9.20 (m, 4H), 9.14 (d, *J* = 6.29 Hz, 4H), 9.09 (s, 8 H, β CH), 8.48 (dd, *J* = 8.04, 6.31 Hz, 4 H), 4.63 (s, 12 H, *N*CH$_3$). ^{13}C{^{1}H} NMR (125 MHz, CD$_3$CN): δ 149.05, 147.87, 146.25, 145.55, 144.62, 141.73, 135.74, 135.17, 127.96, 114.55, 49.70. UV-vis (MeCN): λ_{max} = 435 (ε = 238,930 M^{-1} cm^{-1}), 546 nm (ε = 17,060 M^{-1} cm^{-1}). FTIR (KBr): 1738.5 cm^{-1} (NO stretch).

2.d. Synthesis of **Co_3-1a**•12PF_6 and **Co_3-1b**•12PF_6

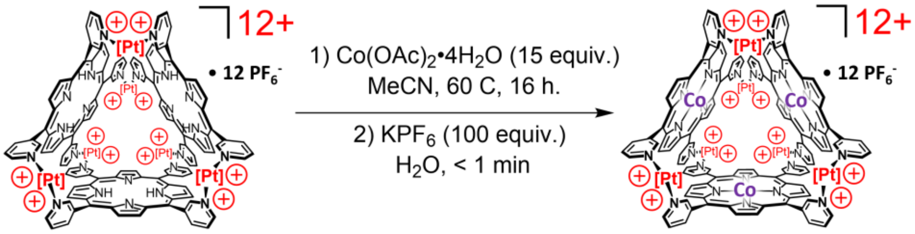

1a,b

$[Pt]^{2+}$ = (tmeda)Pt^{2+} (**1a**)
(bipy)Pt^{2+} (**1b**)

Co_3-1a,b

1a (86%)
1b (79%)

Scheme S4. Synthesis of **Co_3-1a**•12PF_6 and **Co_3-1b**•12PF_6.

Co_3-1a•12PF_6. **1a**•12PF_6 (27.2 mg, 4.98 µmol) was dissolved in 50 mL of MeCN in a 100 mL round bottom flask to give a dark purple solution. $Co(OAc)_2$•$4H_2O$ (18.6 mg, 74.7 µmol) was added as a solid, a reflux condenser was attached to the flask, and the mixture was heated to 60 °C for 16 h, resulting in a dark orange-purple solution. This solution was concentrated to 20 mL under reduced pressure, followed by the addition of solid KPF_6 (91.6 mg, 498 µmol) and then 200 mL of water, resulting in a fine orange precipitate. The supernatant was removed by vacuum filtration on a fine mesh frit, and the solids were washed with water (3 x 50 mL) and then Et_2O (50 mL). The product was washed through the frit with 10 mL of MeCN and the resulting solution was dried by rotary evaporation, providing 23.4 mg of **Co_3-1a**•12PF_6 as a dark orange-purple solid (86 % yield). ^{1}H NMR (500 MHz, CD_3CN): δ 12.37 (s, br, 12 H, β CH), 11.74 (s, br, 12 H, β CH), 10.54-9.48 (br, m, 36 H), 9.07 (s, 12 H), 4.25-3.38 (m, 96 H). ESI(+)-MS: [**Co_3-1a** – 3PF_6]$^{3+}$ Calculated: 1732.8873 m/z, Found: 1732.8146 m/s; [**Co_3-1a** – 4PF_6]$^{4+}$ Calculated: 1263.4244 m/z, Found: 1263.3702 m/z; [**Co_3-1a** – 5PF_6]$^{5+}$ Calculated: 981.7467 m/z, Found 981.7063 m/z; [**Co_3-1a** – 6PF_6]$^{6+}$ Calculated: 793.9616 m/z, Found: 793.9294 m/z; [**Co_3-1a** – 7PF_6]$^{7+}$ Calculated: 659.8293 m/z, Found: 659.8066 m/z; [**Co_3-1a** – 8PF_6]$^{8+}$ Calculated: 559.2301 m/z, Found: 559.2089 m/z; [**Co_3-1a** – 9PF_6]$^{9+}$ Calculated: 480.9863 m/z, Found: 480.9668 m/z. UV-vis (MeCN): λ_{max} = 412 (ε = 416,909 M^{-1} cm^{-1}), 533 nm (ε = 32,575 M^{-1} cm^{-1}).

Co_3-1b•12PF_6. **1b**•12PF_6 (31.0 mg, 5.44 µmol) was dissolved in 50 mL of MeCN in a 100 mL round bottom flask to give a dark purple solution. $Co(OAc)_2$•$4H_2O$ (20.3 mg, 81.5 µmol) was added as a solid, a reflux condenser was attached to the flask, and the mixture was heated to 60 °C for 16 h, resulting in a dark orange-purple solution. The reaction mixture was concentrated to 20 mL under reduced pressure, followed by the addition of solid KPF_6 (100 mg, 544 µmol) and 200 mL of water, resulting in a fine orange precipitate. The supernatant was removed by vacuum filtration on a fine mesh frit, and the solids were washed with water (3 x 50 mL) and then Et_2O (50 mL). The product was washed through the frit with 10 mL of MeCN and the resulting solution was dried by rotary evaporation, providing 25.1 mg of **Co_3-1b**•12PF_6 as a dark orange-purple solid (79 % yield). ^{1}H NMR (500 MHz, CD_3CN): δ 12.62 (br, 12 H, β CH), 11.74 (br, 12 H, β CH), 10.97-9.51 (m, 36 H), 9.16 (s, 12 H), 9.10-8.90 (m, 36 H), 8.47 (12 H). ESI(+)-MS: [**Co_3-1b** – 3PF_6]$^{3+}$ Calculated: 1812.7621 m/z, Found: 1812.7026 m/z; [**Co_3-1b** – 4PF_6]$^{4+}$ Calculated: 1323.3305 m/z, Found: 1323.2996 m/z; [**Co_3-1b** – 5PF_6]$^{5+}$ Calculated: 1029.6716 m/z, Found: 1029.6469 m/z; [**Co_3-1b** – 6PF_6]$^{6+}$ Calculated: 833.8990 m/z, Found: 833.8822 m/z; [**Co_3-1b** – 7PF_6]$^{7+}$ Calculated: 694.0614 m/z, Found: 694.0493 m/z. UV-vis (MeCN): λ_{max} = 413 (ε = 412,969 M^{-1} cm^{-1}), 534 nm (ε = 33,090 M^{-1} cm^{-1}).

2.e. Synthesis of **Zn_3-1a•**$12PF_6$ and **Zn_3-1b•**$12PF_6$

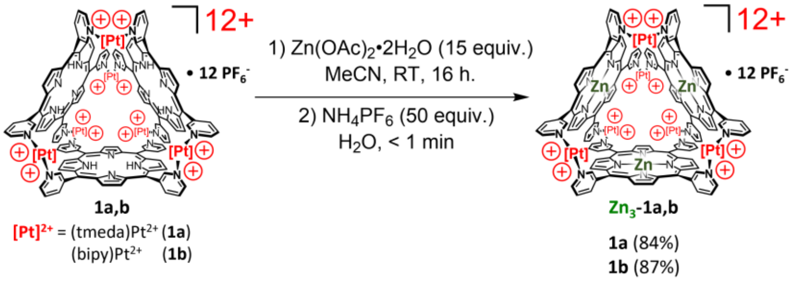

Scheme S5: Synthesis of **Zn_3-1a•**$12PF_6$ and **Zn_3-1b•**$12PF_6$.

Zn_3-1a•$12PF_6$. **1a•**$12PF_6$ (50.0 mg, 9.15 µmol) was dissolved in 50 mL of MeCN in a 100 mL round bottom flask to give a dark purple solution. $Zn(OAc)_2$•$2H_2O$ (30.1 mg, 137 µmol) was added as a solid and the mixture was left to stir at room temperature for 16 h, resulting in a dark green-purple solution. This solution was concentrated to 20 mL under reduced pressure, followed by the addition of solid NH_4PF_6 (74.6 mg, 458 µmol) and then 200 mL of water, resulting in a fine green precipitate. The supernatant was removed by vacuum filtration on a fine mesh frit, and the solids were washed with water (3 x 50 mL) and then Et_2O (50 mL). The product was washed through the frit with 10 mL of MeCN and the resulting solution was dried by rotary evaporation, providing 43.5 mg of **Zn_3-1a•**$12PF_6$ as a dark green-purple solid (84 % yield). ^1H NMR (500 MHz, CD_3CN): δ 9.54 (d, *J* = 5.3 Hz, 12 H), 9.23 (s, 12 H), 8.60 (s, 12 H), 8.58 (d, *J* = 8.3 Hz, 12 H), 8.34 (s, 12 H), 8.18 (dd, *J* = 7.7, 5.9 Hz, 12 H), 3.37 (m, 24 H), 3.21 (s, 36 H, *N*CH_3), 3.20 (s, 36 H, *N*CH_3). $^{13}C\{^1H\}$ NMR (125 MHz, CD_3CN): δ 155.38, 152.19, 150.48, 150.31, 147.01, 143.08, 133.07, 132.44, 138.08, 115.04, 65.55, 53.10, 52.81. ESI(+)-MS: [**Zn_3-1a** – $3PF_6]^{3+}$ Calculated: 1739.2166 m/z, Found: 1739.1913 m/z; [**Zn_3-1a** – $4PF_6]^{4+}$ Calculated: 1268.1714 m/z, Found: 1268.1602; [**Zn_3-1a** – $5PF_6]^{5+}$ Calculated: 985.5443 m/z, Found: 985.5308 m/z; [**Zn_3-1a** – $6PF_6]^{6+}$ Calculated: 797.1208 m/z, Found: 797.1262 m/z; [**Zn_3-1a** – $7PF_6]^{7+}$ Calculated: 662.5419 m/z, Found: 662.5370 m/z [**Zn_3-1a** – $8PF_6]^{8+}$ Calculated 561.6036 m/z, Found: 561.6016 m/z. UV-vis (MeCN): λ_{max} = 424 (ε = 598,212 M^{-1} cm^{-1}), 562 (ε = 32,000 M^{-1} cm^{-1}), 603 nm (ε = 8,121 M^{-1} cm^{-1}).

Zn_3-1b•$12PF_6$. **1b•**$12PF_6$ (26.7 mg, 4.68 µmol) was dissolved in 50 mL of MeCN in a 100 mL round bottom flask to give a dark purple solution. $Zn(OAc)_2$•$2H_2O$ (14.3 mg, 70.2 µmol) was added as a solid, and the mixture was allowed to stir at room temperature for 16 h, resulting in a dark green-purple solution. The reaction mixture was concentrated to 20 mL under reduced pressure, followed by the addition of solid NH_4PF_6 (38.2 mg, 234 µmol) and then 200 mL of water, resulting in a fine green precipitate. The supernatant was removed by vacuum filtration on a fine mesh frit, and the solids were washed with water (3 x 50 mL) and Et_2O (50mL). The product was dissolved through the frit with 10 mL of MeCN and dried by rotary evaporation, providing 24.1 mg of **Zn_3-1b•**$12PF_6$ as a dark green-purple solid (87 % yield). ^1H NMR (500 MHz, CD_3CN): δ 9.66 (d, *J* = 5.4 Hz, 12 H), 9.39 (s, 12 H), 8.66 (t, *J* = 7.6 Hz, 12 H), 8.63-8.57 (m, 36 H), 8.53 (s, 12 H), 8.26 (dd, *J* = 8.0, 5.4 Hz, 12 H), 8.14 (d, *J* = 5.7 Hz, 12 H), 7.96 (t, *J* = 6.5 Hz, 12 H). $^{13}C\{^1H\}$ NMR (125 MHz, CD_3CN): δ 175.73, 154.32, 152.77, 150.61, 150.39, 150.12, 148.09, 144.04, 143.55, 133.12, 129.73, 128.40, 126.54, 114.93. ESI(+)-MS: [**Zn_3-1b** – $5PF_6]^{5+}$ Calculated: 1033.6692 m/z, Found: 1033.6824 m/z; [**Zn_3-1b** – $6PF_6]^{6+}$ Calculated: 837.2303 m/z, Found: 837.2374 m/z; [**Zn_3-1b** – $7PF_6]^{7+}$ Calculated: 696.9168 m/z, Found: 696.9240 m/z; [**Zn_3-1b** – $8PF_6]^{8+}$ Calculated: 591.6817 m/z, Found: 591.6849 m/z; [**Zn_3-1b** – $9PF_6]^{9+}$ Calculated: 509.8321 m/z, Found: 509.8367 m/z; [**Zn_3-1b** – $10PF_6]^{10+}$ Calculated: 444.3525 m/z, Found: 444.2571 m/z UV-vis (MeCN): λ_{max} = 424 (ε = 537,939 M^{-1} cm^{-1}), 561 (35,000 M^{-1} cm^{-1}), 602 nm (ε = 8,818 M^{-1} cm^{-1}).

3. Procedures for In Situ Preparation of 3, 4, 6, Co$^{I}_{3}$-1a,b, and [Co^{III}NO]$_3$-1a,b

3.a. In situ formation of 3

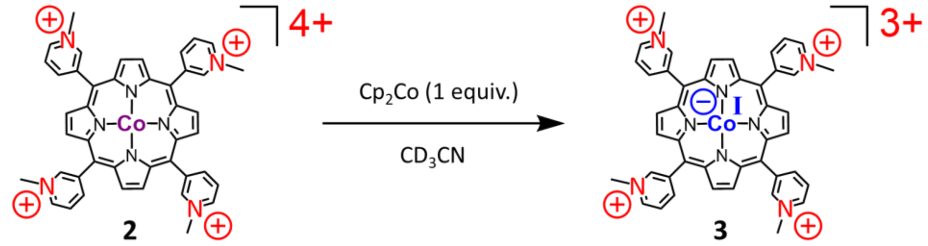

Scheme S6. Formation of **3** from **2.**

In an N_2 atmosphere glovebox, 6.2 mg of **2**•PF_6 (4.7 μmol) was dissolved in 0.55 mL of CD_3CN and the resulting solution was transferred to an air-free NMR tube. Then 50 μL of a 0.094 M solution of Cp_2Co (4.7 μmol) in C_6D_6 was added. The NMR tube was sealed with a PTFE stopper and then turned over repeatedly to mix the solutions. No significant color change was observed. The ^{1}H NMR spectrum was acquired, showing the disappearance of all resonances downfield of 10 ppm and the appearance of well-defined signals indicative of the clean formation of a diamagnetic Co^{I} porphyrin complex. ^{1}H NMR (500 MHz, CD_3CN): δ 9.24 (s, 4 H), 9.08 (d, *J* = 7.87 Hz, 4 H), 8.88 (d, *J* = 6.14 Hz, 4 H), 8.35 (s, 8 H, β CH), 8.26 (dd, *J* = 8.01, 6.17 Hz, 4 H), 4.48 (s, 12 H, *N*CH_3). ^{13}C{^{1}H} NMR (125 MHz, CD_3CN): δ 157.65, 147.35, 145.78, 145.41, 144.50, 135.22, 119.37, 49.42. UV-vis (MeCN): λ_{max} = 434 (62,190 M^{-1} cm^{-1}), 554 (14,550 M^{-1} cm^{-1}) nm.

3.b. In situ formation of 4

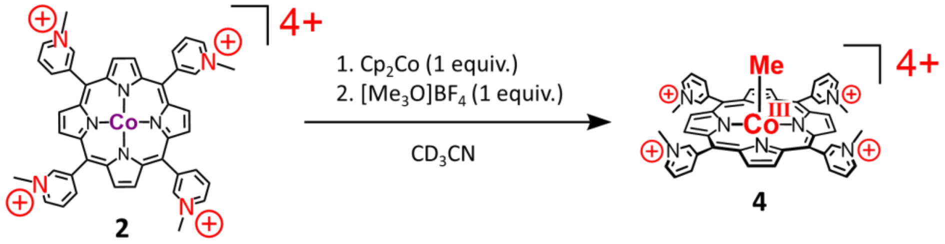

Scheme S7. Formation of **4** from **2.**

A solution of **3** (0.60 mL, 7.9 mM, 4.7 μmol) was prepared in CD_3CN in a J-Young style NMR tube as described above. After confirming the clean formation of **3** by ^{1}H NMR spectroscopy, the NMR tube was wrapped with foil, returned to an N_2 atmosphere glovebox, and 50 μL of a 0.094 M stock solution of $[Me_3O]BF_4$ (4.7 μmol) in CD_3CN was added. The NMR tube was sealed with a PTFE stopper and then turned over repeatedly to mix the solutions. No significant color change was observed. The ^{1}H NMR spectrum was acquired, showing clean formation of a new diamagnetic complex exhibiting an upfield ^{1}H NMR signal consistent with a porphyrin-supported Co^{III}-CH_3 group.^{1}H NMR (500 MHz, CD_3CN): δ 9.36 (s, 4 H), 9.12 (br, 4 H), 9.09 (d, J = 5.9 Hz, 4 H), 8.91 (s, 8 H, β CH), 8.42 (t, *J* = 7.06 Hz, 4 H), 4.60 (s, 12 H, *N*CH_3), −4.66 (s, 3 H, CoCH_3). ^{13}C{^{1}H} NMR (125 MHz, CD_3CN): δ 148.69, 147.64, 145.88, 145.38, 142.30, 134.88, 127.65, 113.36, 60.45, 49.5. UV-vis (MeCN): λ_{max} = 426 (131,891 M^{-1} cm^{-1}), 549 (14,990 M^{-1} cm^{-1}) nm.

3.c. In Situ Formation of **6**

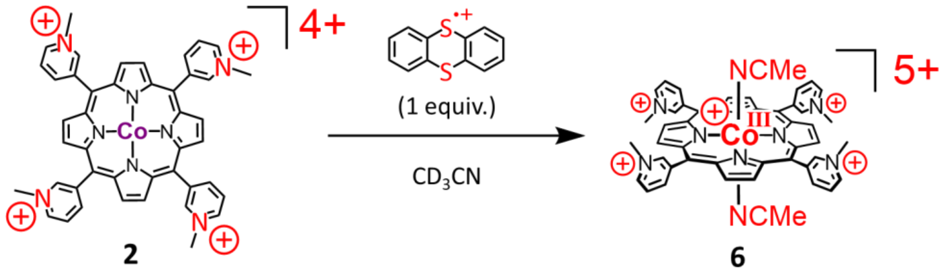

Scheme S8. Formation of **6** from **2.**

Preparation of thianthrenium stock solution. A reported procedure was adapted.[3] In an N_2 atmosphere glovebox, thianthrene (102 mg, 0.470 mmol) was added to 3.00 mL of CD_3CN in a scintillation vial and a magnetic stir bar was used to vigorously stir this suspension. Then 1.00 mL of a 0.456 M solution of $[NO]PF_6$ (0.456 mmol) in CD_3CN was added to the vial, resulting in an immediate change in appearance from a white suspension to a deep-blue homogeneous solution. To remove nitric oxide, the solution of was degassed by cycling five times between active vacuum (10 s each cycle) and N_2 (15 s each cycle). Some solvent loss occurred during this procedure, so the remaining solution was diluted with additional CD_3CN to provide a total volume of 3.00 mL. The concentration of this stock solution was determined to be 0.14 M based on the amount required to fully oxidize a solution of **2**•$4PF_6$ of a known concentration.

6. In an N_2 atmosphere glovebox, **2**•$4PF_6$ (7.0 mg, 5.3 μmol) was dissolved in 0.60 mL of CD_3CN and the resulting solution was transferred to an NMR tube. Then 35.5 μL of a 0.14 M solution of thianthrenium hexafluorophosphate (5.3 μmol) in CD_3CN was added. The tube was sealed with a polypropylene cap and then turned over repeatedly to mix the solutions, resulting in an immediate change of appearance from a dark orange color to a dark red color. The cap was secured with PTFE tape, and the ^{1}H NMR spectrum of the sample was acquired, showing the disappearance of all resonances downfield of 10 ppm and the appearance of well-defined signals indicative of the clean formation of a diamagnetic Co^{III} porphyrin complex. ^{1}H NMR (500 MHz, CD_3CN): δ 9.44 (s, 4 H), 9.36 (s, 8 H, β CH), 9.29 (m, 4 H), 9.18 (d, *J* = 6.35 Hz, 4 H), 8.53 (t, *J* = 7.04 Hz, 4 H), 4.65 (s, 12 H, *N*CH_3). $^{13}C\{^1H\}$ NMR (125 MHz, CD_3CN): δ 149.25, 148.08, 146.50, 144.35, 141.04, 137.42, 136.05, 128.17, 112.71, 49.77. UV-vis (MeCN): λ_{max} = 434 (254,310 M^{-1} cm^{-1}), 545 (15,820 M^{-1} cm^{-1}) nm.

3.d. In situ formation of **Co$^{I}_{3}$-1a** and **Co$^{I}_{3}$-1b**

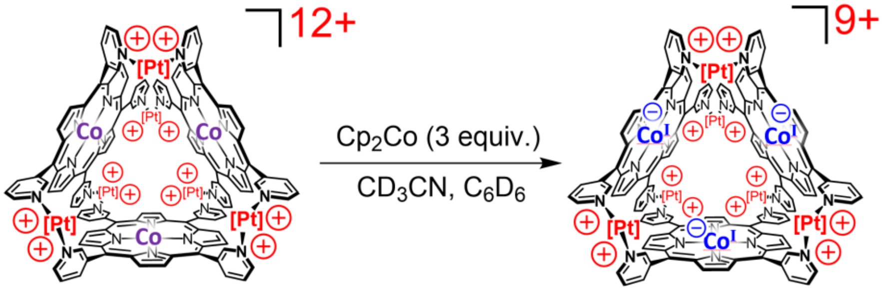

Co$_3$-1a,b **Co$^{I}_{3}$-1a,b**

Scheme S9. In situ reduction of **Co$_3$-1a**,**b** to form **Co$^{I}_{3}$-1a**,**b**.

Co$^{I}_{3}$-1a. In an N_2 atmosphere glovebox, **Co$_3$-1a**•12PF$_6$ (12.0 mg, 2.1 μmol) was dissolved in 0.60 mL of CD_3CN and the resulting solution was transferred to an air-free NMR tube. 50 μL of a 0.128 M solution of Cp_2Co (6.4 μmol, 3 equiv.) in C_6D_6 was added. The NMR tube was sealed with a PTFE stopper and then turned over repeatedly to mix the solutions. No significant color change was observed. The ^{1}H NMR spectrum was acquired, showing the disappearance of all resonances downfield of 10 ppm and the appearance of well-defined signals indicative of the clean formation of a diamagnetic tris-[Co^{I}-porphyrin] nanoprism. ^{1}H NMR (500 MHz, CD_3CN): δ 9.29 (d, *J* = 5.76 Hz, 12 H), 9.05 (s, 12 H), 8.38 (dt, *J* = 7.29, 1.61 Hz, 12 H), 8.04 (s, 12 H, β CH), 7.95 (dd, *J* = 7.80, 5.62 Hz, 12 H), 7.70 (s, 12 H, β CH), 3.40-3.32 (m, 12 H), 3.32-3.23 (m, 12H), 3.02 (s, 36 H, *N*CH$_3$), 2.99 (s, 36 H, *N*CH$_3$). $^{13}C\{^{1}H\}$ NMR (125 MHz, CD_3CN): δ 156.75, 152.66, 151.42, 144.87, 144.37, 140.52, 134.31, 133.38, 65.60, 50.88, 52.48. UV-vis (MeCN): λ_{max} = 425 (208,757 M^{-1} cm^{-1}), 552 nm (31,393 M^{-1} cm^{-1}).

Co$^{I}_{3}$-1b. In an N_2 atmosphere glovebox, **Co$_3$-1b**•12PF$_6$ (9.37 mg, 1.66 μmol) was dissolved in 0.60 mL of CD_3CN and the resulting solution was transferred to an air-free NMR tube. 50 μL of a 0.099 M solution of Cp_2Co (5.0 μmol, 3 equiv.) in C_6D_6 was added. The NMR sample was sealed with a PTFE stopper and the tube was turned over repeatedly to mix the solutions. No significant color change was observed. The ^{1}H NMR spectrum was acquired, showing the disappearance of all resonances downfield of 10 ppm and the appearance of well-defined signals indicative of the clean formation of a diamagnetic tris-[Co^{I}-porphyrin] nanoprism. ^{1}H NMR (500 MHz, CD_3CN): δ 9.19 (d, *J* = 5.37 Hz, 12 H), 9.09 (s, 12 H), 8.60-8.43 (m, broad, 24H), 8.40 (d, *J* = 7.85 Hz, 12 H), 7.96-7.89 (m, 36 H), 7.78 (s, 12 H), 7.73 (s, br, 12 H). ^{13}C NMR (125 MHz, CD_3CN): δ 156.88, 152.15, 151.40, 145.14, 134.67, 133.67. UV-vis (MeCN): λ_{max} = 427 (208,030 M^{-1} cm^{-1}), 548 nm (39,636 M^{-1} cm^{-1}).

3.f. In situ formation of **[Co^{III}NO]$_3$-1a** and **[Co^{III}NO]$_3$-1b**

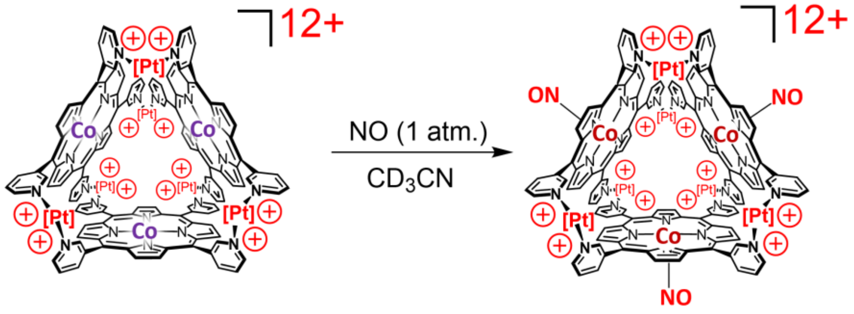

Co$_3$-1a,b **[Co^{III}NO]$_3$-1a,b**

Scheme S10. Reaction of **Co$_3$-1a**,**b** with nitric oxide to form **[Co^{III}NO]$_3$-1a**,**b**.

[Co^{III}NO]$_3$-1a. A sample of **Co$_3$-1a**•12PF$_6$ (9.33 mg, 1.66 µmol) was dissolved in 0.60 mL of CD_3CN and the resulting solution was transferred to an air-free NMR tube. The NMR tube was sealed with a PTFE stopper, the solution was degassed via three freeze-pump-thaw cycles, and the tube was then filled with N_2. The PTFE stopper was replaced with a rubber septum and nitric oxide, generated as described in Section 2.c., was passed through the tube for 5 min using needles for the inlet and outlet. The NMR tube was resealed with the PTFE stopper and turned over repeatedly to saturate the solution with NO, resulting in an immediate color change from dark orange to dark red. The ^{1}H NMR spectrum of the sample was acquired to confirm the complete disappearance of the signals of **Co$_3$-1a** and the formation of a diamagnetic nanoprism. The sample was degassed via three freeze-pump-thaw cycles to remove excess nitric oxide before evaporating under vacuum in an N_2 atmosphere glovebox to provide a solid sample for FTIR analysis. ^{1}H NMR (500 MHz, CD_3CN): δ 9.57 (d, *J* = 8.52 Hz, 12 H), 9.18 (s, 12 H), 8.61 (s, 12 H), 8.55 (d, *J* = 8.34 Hz, 12 H), 8.47 (s, 12 H), 8.20 (dd, *J* = 8.03, 5.74 Hz), 3.39-3.26 (m, 24 H), 3.16 (s, 36 H, *N*CH_3), 3.10 (s, 36 H, *N*CH_3). ^{13}C{^{1}H} NMR (125 MHz, CD_3CN): δ 154.81, 153.07, 146.67, 145.97, 141.83, 134.27, 133.75, 128.44, 116.00, 65.54, 53.09, 52.55. UV-vis (MeCN): λ_{max} = 427 (539,666 M^{-1} cm^{-1}), 548 nm (40,424 M^{-1} cm^{-1}). FTIR (KBr): 1732.6 cm^{-1} (NO stretch).

[Co^{III}NO]$_3$-1b. A sample of **Co$_3$-1b**•12PF$_6$ (9.41 mg, 1.60 µmol) was dissolved in 0.60 mL of CD_3CN and the resulting solution was transferred to a J-Young style air-free NMR tube. The NMR tube was sealed with a PTFE stopper, the solution was degassed via three freeze-pump-thaw cycles, and the tube was then filled with N_2. The PTFE stopper was replaced with a rubber septum and nitric oxide, generated as described in Section 2.c., was passed through the tube for 5 min using needles for the inlet and outlet. The NMR tube was resealed with the PTFE stopper and turned over repeatedly to saturate the solution with NO, resulting in an immediate color change from dark orange to dark red. The ^{1}H NMR spectrum of the sample was acquired to confirm the complete disappearance of the signals of **Co$_3$-1b** and the formation of a diamagnetic nanoprism. The sample was degassed via three freeze-pump-thaw cycles to remove excess nitric oxide before evaporating under vacuum in an N_2 atmosphere glovebox to provide a solid sample for FTIR analysis. ^{1}H NMR (500 MHz, CD_3CN): δ 9.70 (d, *J* = 5.76 Hz, 12 H), 9.34 (s, 12 H), 9.78-9.56 (m, 60 H), 8.30 (t, *J* = 8.67 Hz, 12 H), 8.09 (d, *J* = 5.60 Hz, 12 H), 7.96 (dd, *J* = 7.60, 5.17 Hz, 12 H). ^{13}C{^{1}H} NMR (125 MHz, CD_3CN): δ 157.27, 153.80, 153.07, 150.05, 147.23, 145.39, 145.14, 143.60, 141.88, 133.82, 133.68, 129.27, 128.39, 125.82, 115.50. UV-vis (MeCN): λ_{max} = 427 (292,212 M^{-1} cm^{-1}), 548 nm (22,666 M^{-1} cm^{-1}). FTIR (KBr): 1713.4 cm^{-1} (NO stretch).

4. Unsuccessful Attempts to Generate tris-Co^{III} states of Co$_3$-1a,b

4.a. Attempted generation of **[Co^{III}Me]$_3$-1a**,**b**.

Representative Procedure. A solution of **Co$^{I}_3$-1a** (0.60 mL, 2.8 mM, 1.68 μmol) was prepared in CD_3CN in a J-Young style air-free NMR tube as described above in Section 3.d. After confirming the clean formation of **Co$^{I}_3$-1a** by ^{1}H NMR spectroscopy, the sample was returned to an N_2 atmosphere glovebox and 50 μL of a 1.00 M solution of $[Me_3O]BF_4$ (5.00 μmol) in CD_3CN was added, using foil to shield the sample from light. The NMR tube was sealed with a PTFE stopper and turned over repeatedly to mix the solutions. No significant color change was observed. The ^{1}H NMR spectrum (Figure S30) was acquired, showing broad, poorly defined resonances in the aromatic, aliphatic, and Co^{III}-CH_3 regions of the spectrum. A small, broad signal downfield of 11 ppm suggested the formation of some Co^{II} species.

Similar results were obtained when attempting to prepare **[Co^{III}Me]$_3$-1b** except that the aromatic and Co^{III}-CH_3 regions of the resulting ^{1}H NMR spectrum (Figure S31) were somewhat better defined.

4.b. Attempted Oxidations of **Co$_3$-1a**,**b** with $AgPF_6$ in the presence of pyridine.

Representative Procedure. A sample of **Co$_3$-1a**•12PF_6 (2.87 mg, 0.51 μmol) was dissolved in 0.60 mL of CD_3CN and the resulting solution was transferred to an NMR tube. 1.2 mg of $AgPF_6$ (4.6 μmol) was added as a solid along with 0.25 μL of pyridine (3.1 μmol). The NMR tube was sealed with a PTFE stopper and turned over repeatedly to mix the solutions, resulting in the formation of a fine precipitate of Ag^0. No significant color change was observed. The ^{1}H NMR spectrum (Figure S32) was acquired after 30 min, showing broad, poorly defined signals in the aromatic region and downfield of 11 ppm, suggesting the cobalt centers remained primarily in the Co^{II} oxidation state. After 45 min, the sample was diluted to 0.033 mM and the UV-vis spectrum was acquired (Figure S77), showing a Soret band at λ_{max} = 412 nm with a shoulder at 433 nm, consistent with only partial oxidation of the Co^{II} centers to Co^{III}.

Similar results were obtained upon treating **Co$_3$-1b** with $AgPF_6$ and pyridine, except that the resulting ^{1}H NMR spectrum (Figure S33) did not clearly display signals downfield of 11 ppm. The UV-vis spectrum (Figure S78) did, however, confirm that the cobalt centers remained primarily in the Co^{II} oxidation state.

4.c. Oxidation of **Co$_3$-1a**,**b** with thianthrenium hexafluorophosphate**.**

Representative Procedure. In an N_2 atmosphere glovebox, 6.2 mg of **Co$_3$-1a**•12PF_6 (1.1 μmol) was dissolved in 0.45 mL of CD_3CN and then sealed in an NMR tube with a polyethylene cap that was secured with PTFE tape. After acquiring the ^{1}H NMR spectrum, the sample was returned to the glovebox and 24 μL of a 0.14 M solution of thianthrenium hexafluorophosphate (3.3 μmol) in CD_3CN was added (thianthrenium was prepared as described in Section 3.c.). The tube was sealed and turned over repeatedly to mix the solutions, resulting in an immediate color change from dark orange to dark red-orange. The ^{1}H NMR spectrum (Figure S34) of the sample was acquired, showing disappearance of all resonances downfield of 11 ppm, indicating complete oxidation of Co^{II} to Co^{III}, which was confirmed by UV-vis spectroscopy (Figure S79). However, the appearance of many overlapping signals in the aromatic and aliphatic regions of the ^{1}H NMR spectrum suggests the cage structure is not retained.

Similar results were obtained upon treating **Co$_3$-1b** with a solution of thianthrenium (see Figures S35, S80).

5. ^{1}H and ^{13}C{^{1}H} NMR Spectra

<u>Instrumentation:</u> Nuclear magnetic resonance (NMR) spectra were measured using a Bruker AVANCE Neo spectrometer or a Varian VNMR spectrometer, with a 500 MHz working frequency for ^{1}H nuclei and a 125 MHz working frequency for ^{13}C nuclei. All spectra were recorded at 298 K. Chemical shifts of ^{1}H NMR spectra were referenced to the residual proteo signal of the solvent (^{1}H δ 1.94 ppm for CD_2HCN in CD_3CN), and ^{13}C{^{1}H} NMR spectra were referenced to the solvent ^{13}C{^{1}H} signal (^{13}C δ 118.26 ppm for $CD_3\underline{\mathbf{C}}N$).[5]

5.a. Complex **2**

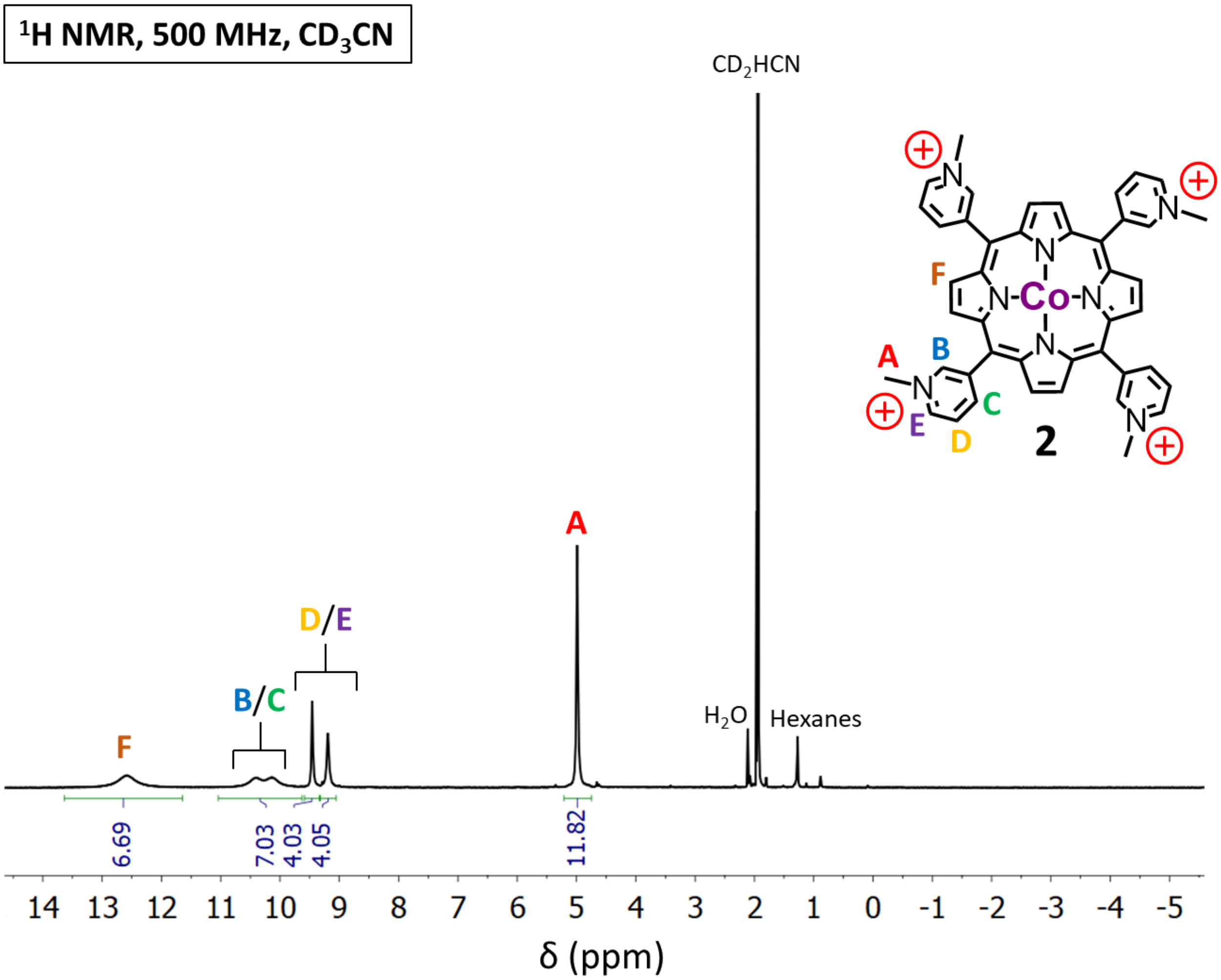

Figure S1. ^{1}H NMR spectrum of **2**•$4PF_6$ in CD_3CN.

5.b. Complex **3**

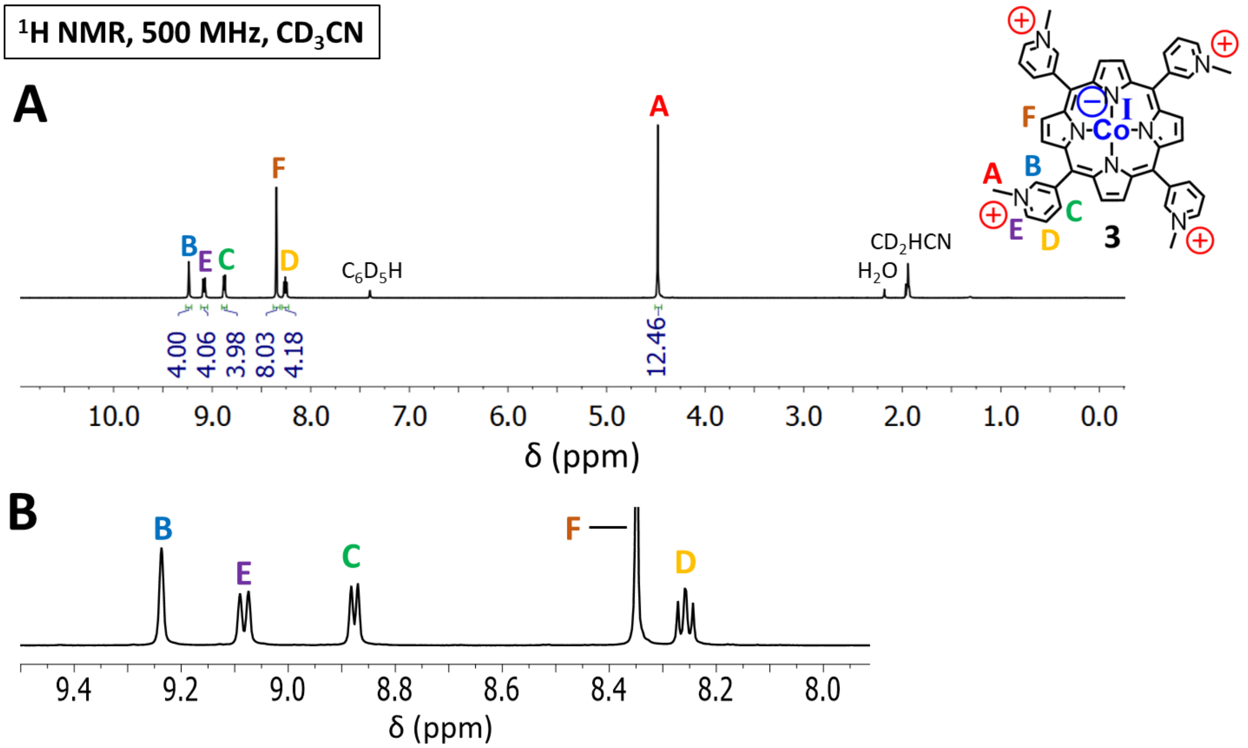

Figure S2. ^{1}H NMR spectrum of **3** prepared in situ in CD$_3$CN by reducing **2**•4PF$_6$ with a slight excess of Cp$_2$Co. (A) Full spectrum. (B) Aromatic region. Note that the top of signal "F" is cut off in this latter image.

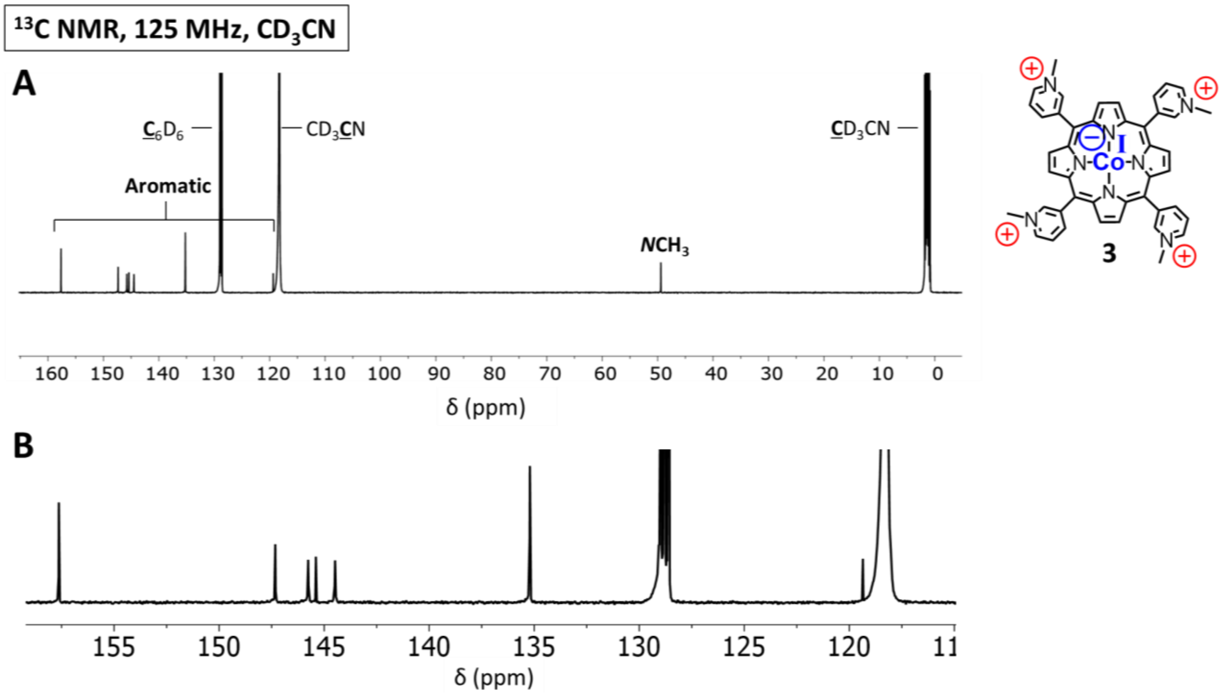

Figure S3. ^{13}C{^{1}H} NMR spectrum of **3** prepared in situ in CD$_3$CN by reducing **2**•4PF$_6$ with a slight excess of Cp$_2$Co. (A) Full spectrum. (B) Aromatic region. Seven of eight expected aromatic signals are observed.

5.c. Complex **4**

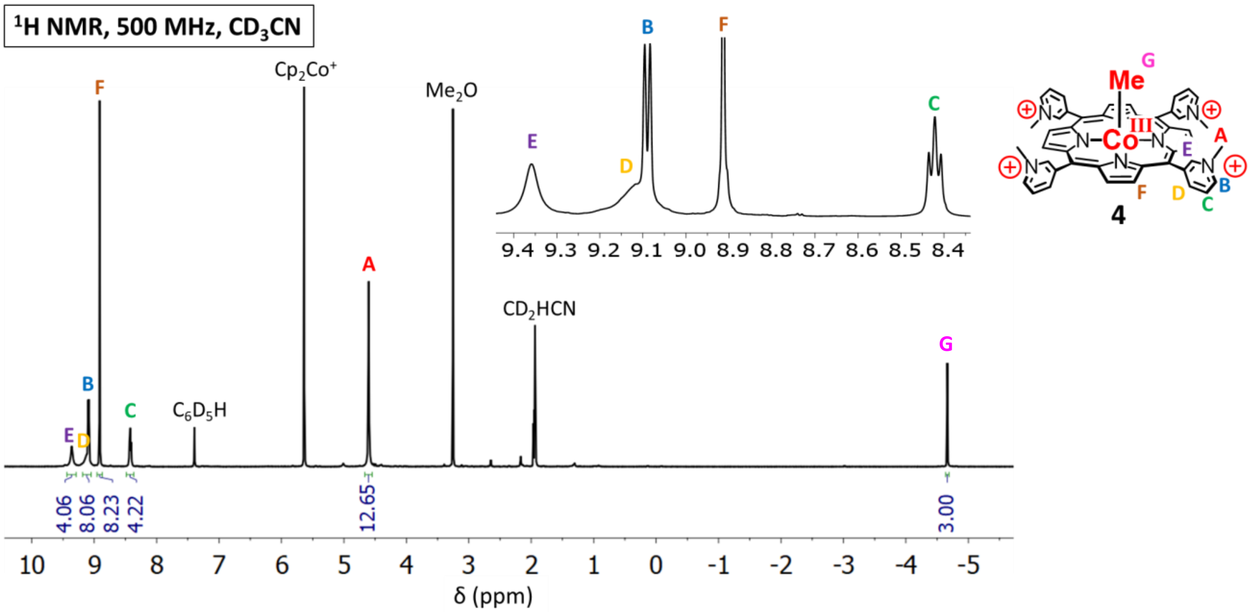

Figure S4. ^{1}H NMR spectrum of **4** prepared in situ in CD_3CN by reducing **2**•$4PF_6$ with Cp_2Co (1 equiv.) followed by the addition of $[Me_3O]BF_4$ (1 equiv.). The inset displays an expanded view of the aromatic region of the spectrum. Note that the top of signal "F" is cut off in the inset.

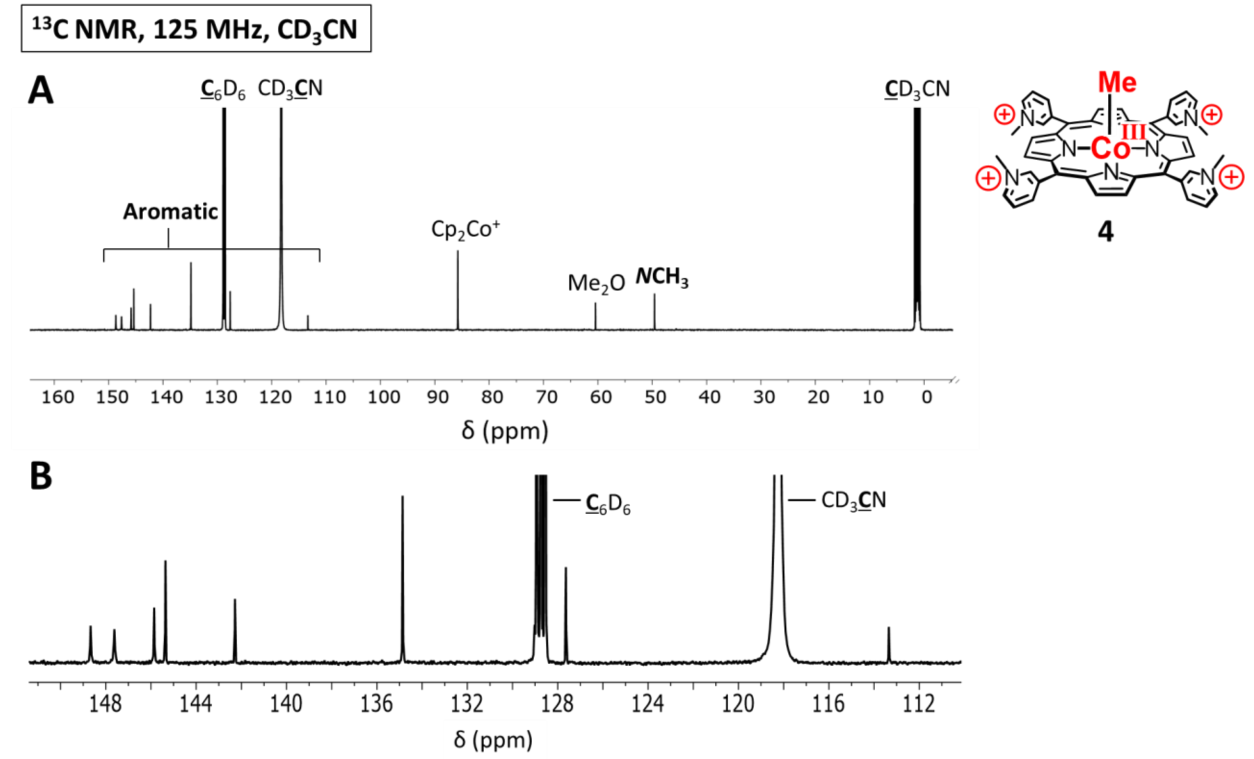

Figure S5. $^{13}C\{^1H\}$ NMR spectrum of **4** prepared in situ in CD_3CN by reducing **2**•$4PF_6$ with Cp_2Co (1 equiv.) followed by the addition of $[Me_3O]BF_4$ (1 equiv.). (A) Full spectrum. (B) Aromatic region.

5.d. Complex **5**

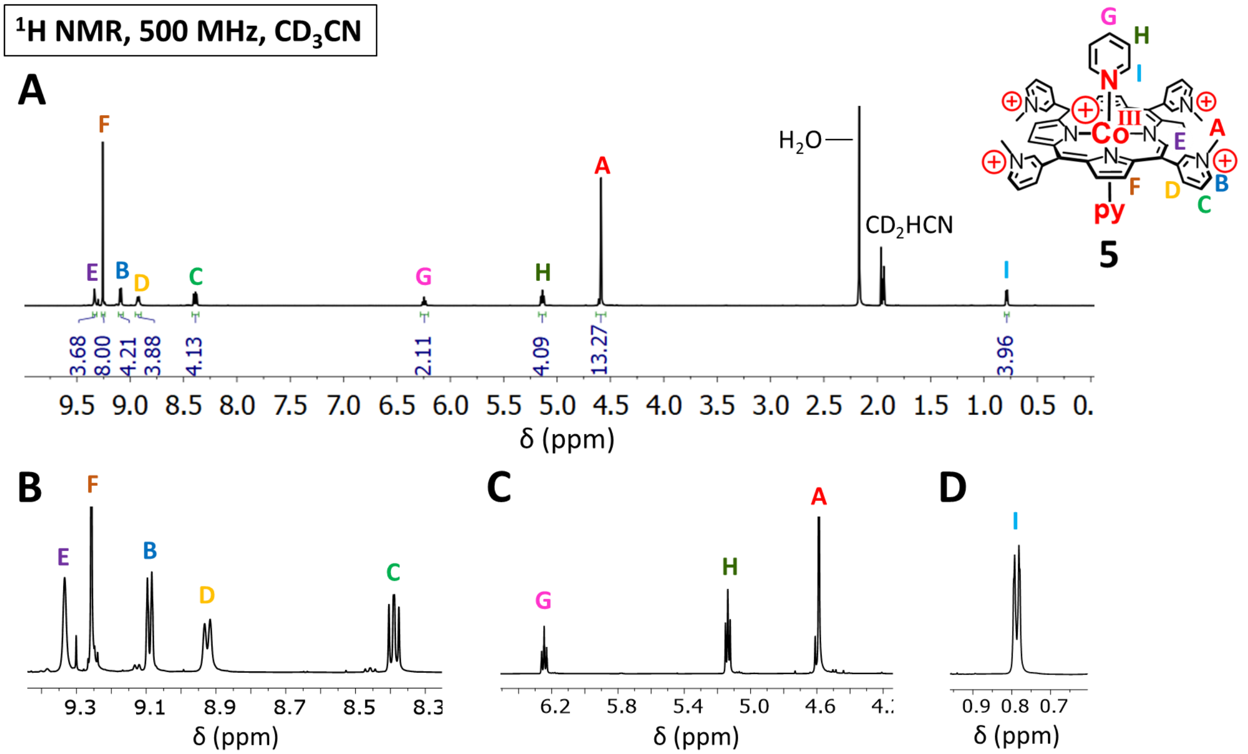

Figure S6. ^{1}H NMR spectrum of **5**•5PF$_6$ in CD$_3$CN. (A) Full Spectrum. (B-D) Expansions showing signals of the porphyrin, pyridinium groups, and pyridine ligands.

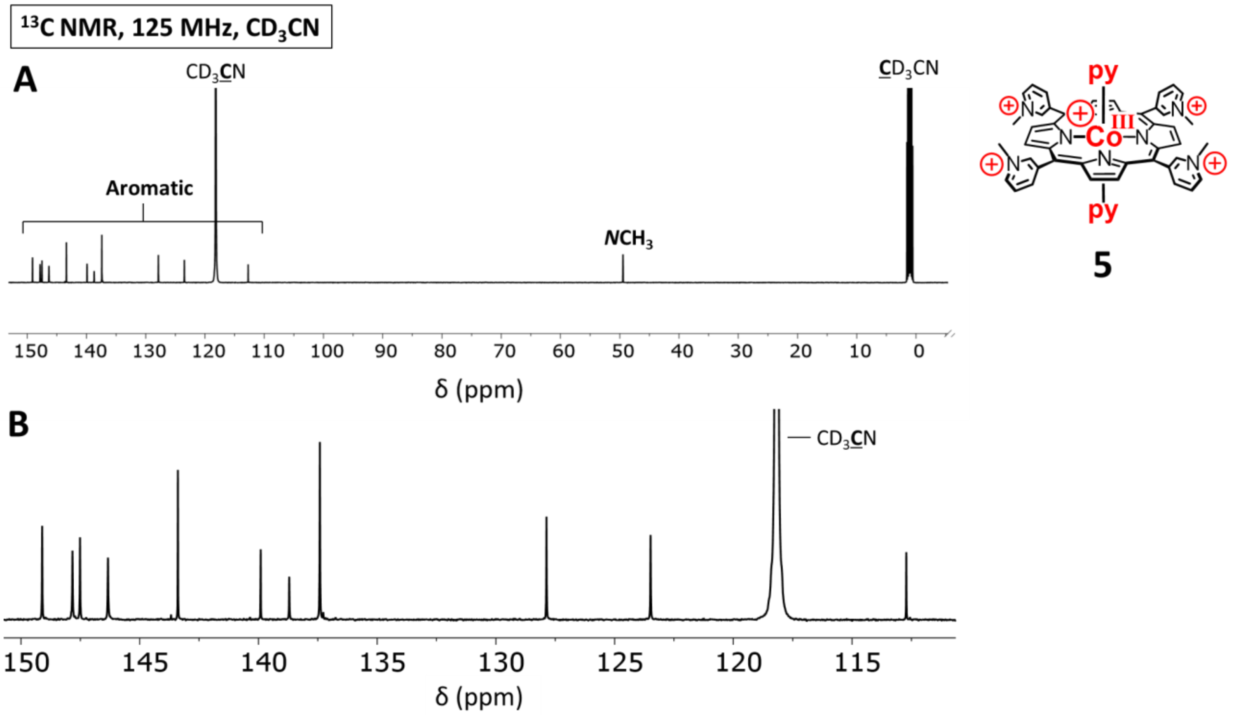

Figure S7. ^{13}C{^{1}H} NMR spectrum of **5**•5PF$_6^-$ in CD$_3$CN. (A) Full Spectrum. (B) Aromatic region.

5.e. Complex **6**

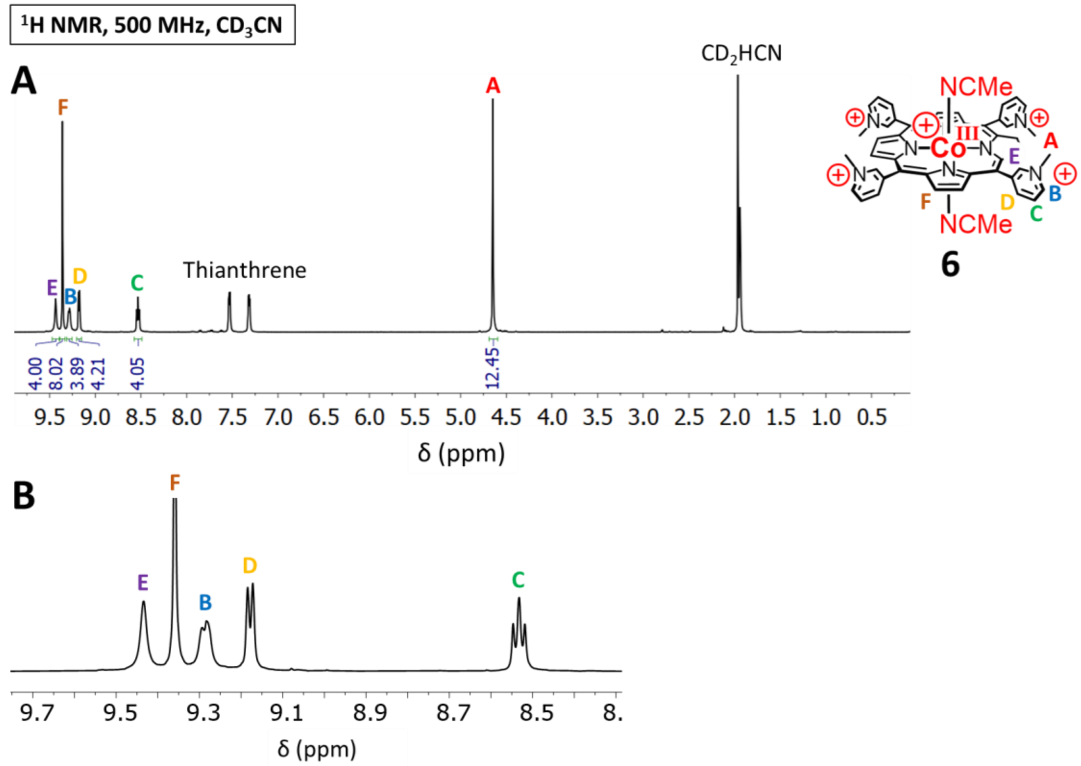

Figure S8. ^{1}H NMR spectrum of **6** prepared in situ in CD_3CN by oxidizing **2**•4PF_6 with thianthrenium hexafluorophosphate. (A) Full spectrum. (B) Aromatic region.

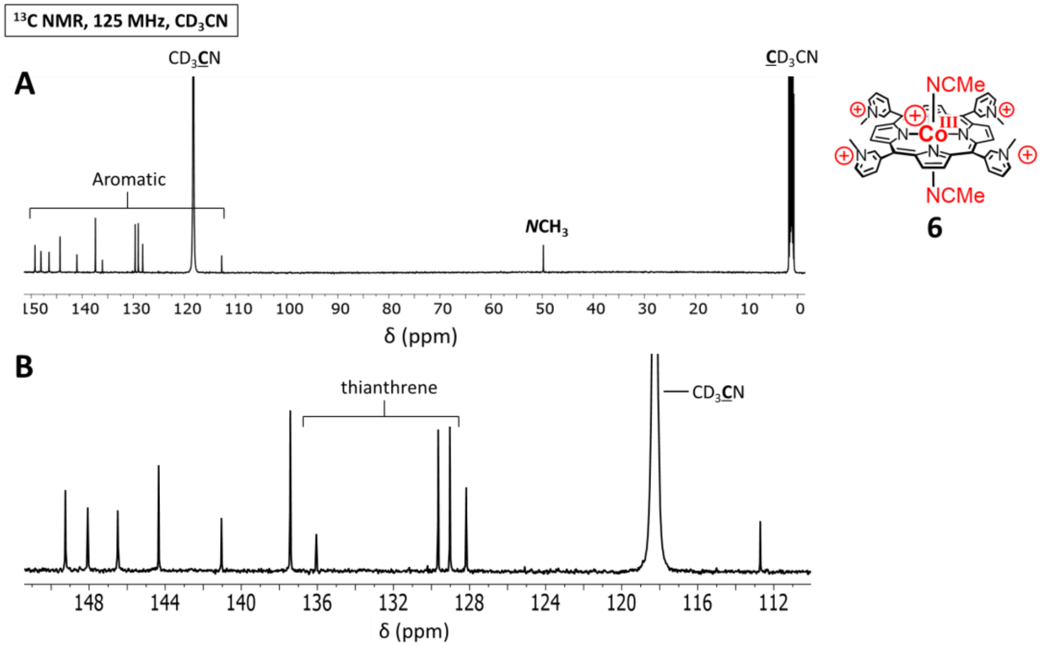

Figure S9. $^{13}C\{^{1}H\}$ NMR spectrum of **6** prepared in situ in CD_3CN by oxidizing **2**•4PF_6 with thianthrenium hexafluorophosphate. (A) Full spectrum. (B) Aromatic region, which includes three signals from the thianthrene that is produced upon reduction of thianthrenium.

5.f. Complex **7**

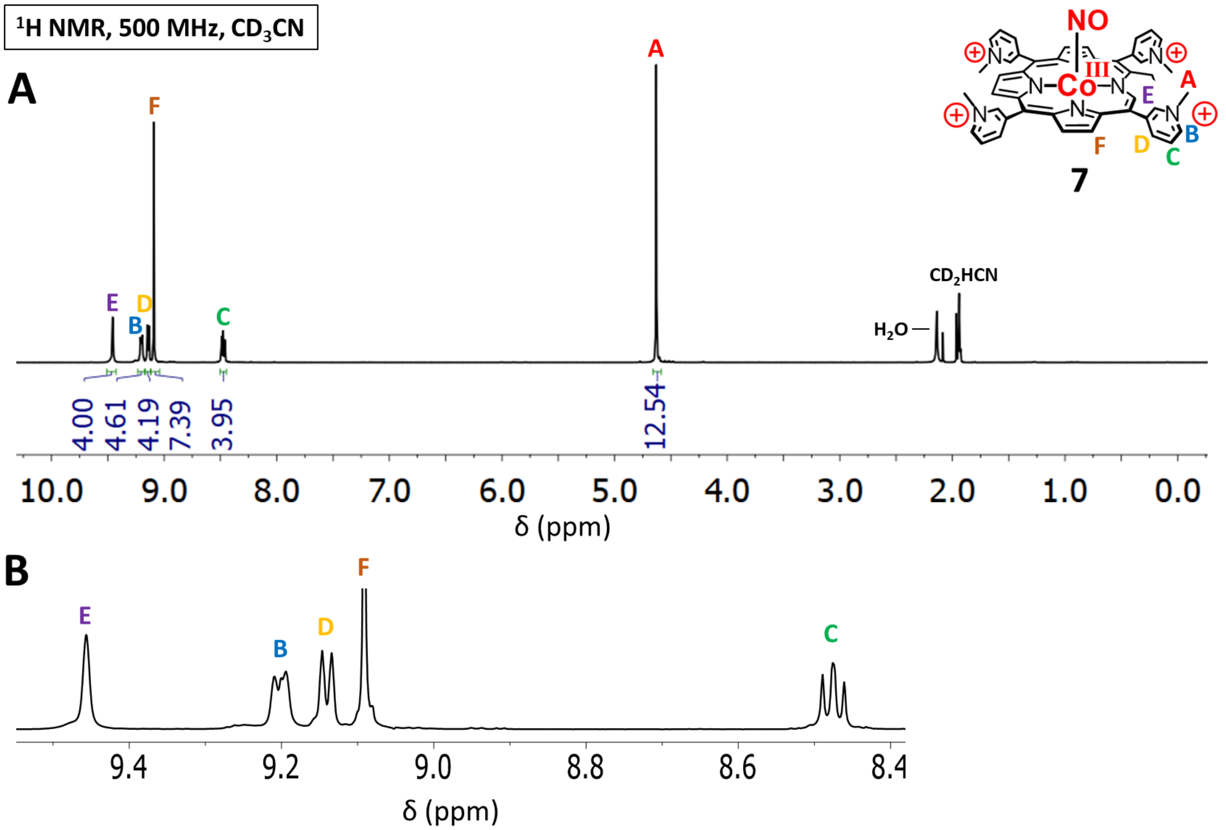

Figure S10. ^{1}H NMR spectrum of **7**•4PF$_6$ in CD$_3$CN. (A) Full spectrum. (B) Aromatic region. Note that the top of signal "F" is cut off in this latter image.

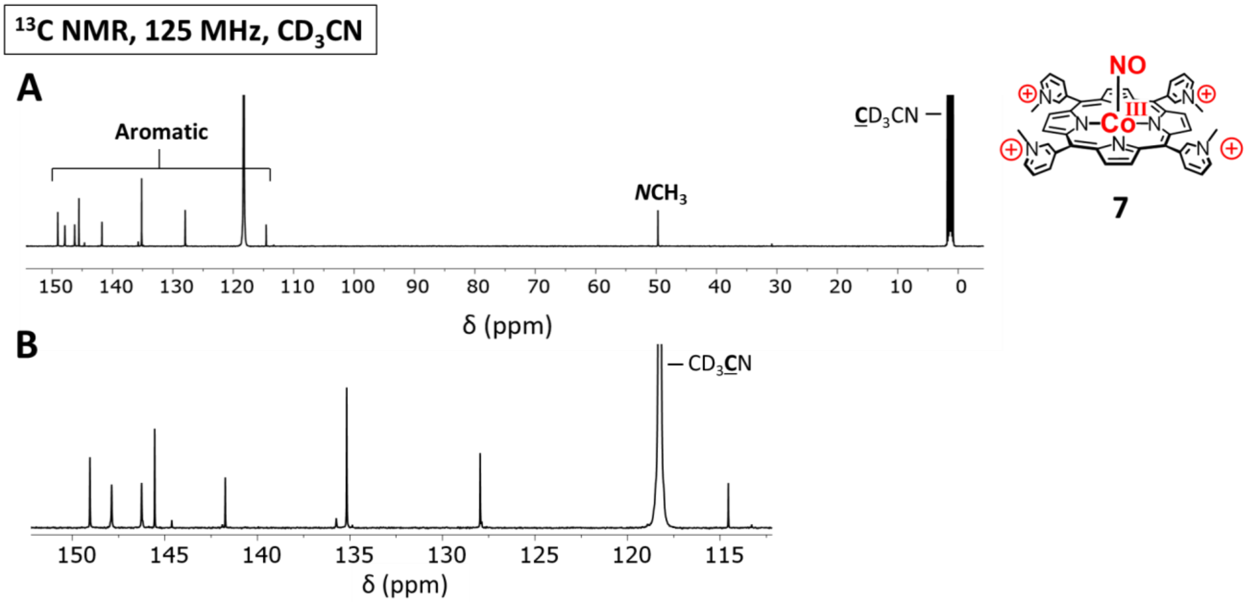

Figure S11. ^{13}C{^{1}H} NMR spectrum of **7**•4PF$_6$ in CD$_3$CN. (A) Full spectrum. (B) Aromatic region.

5.g. Cage **Co_3-1a**

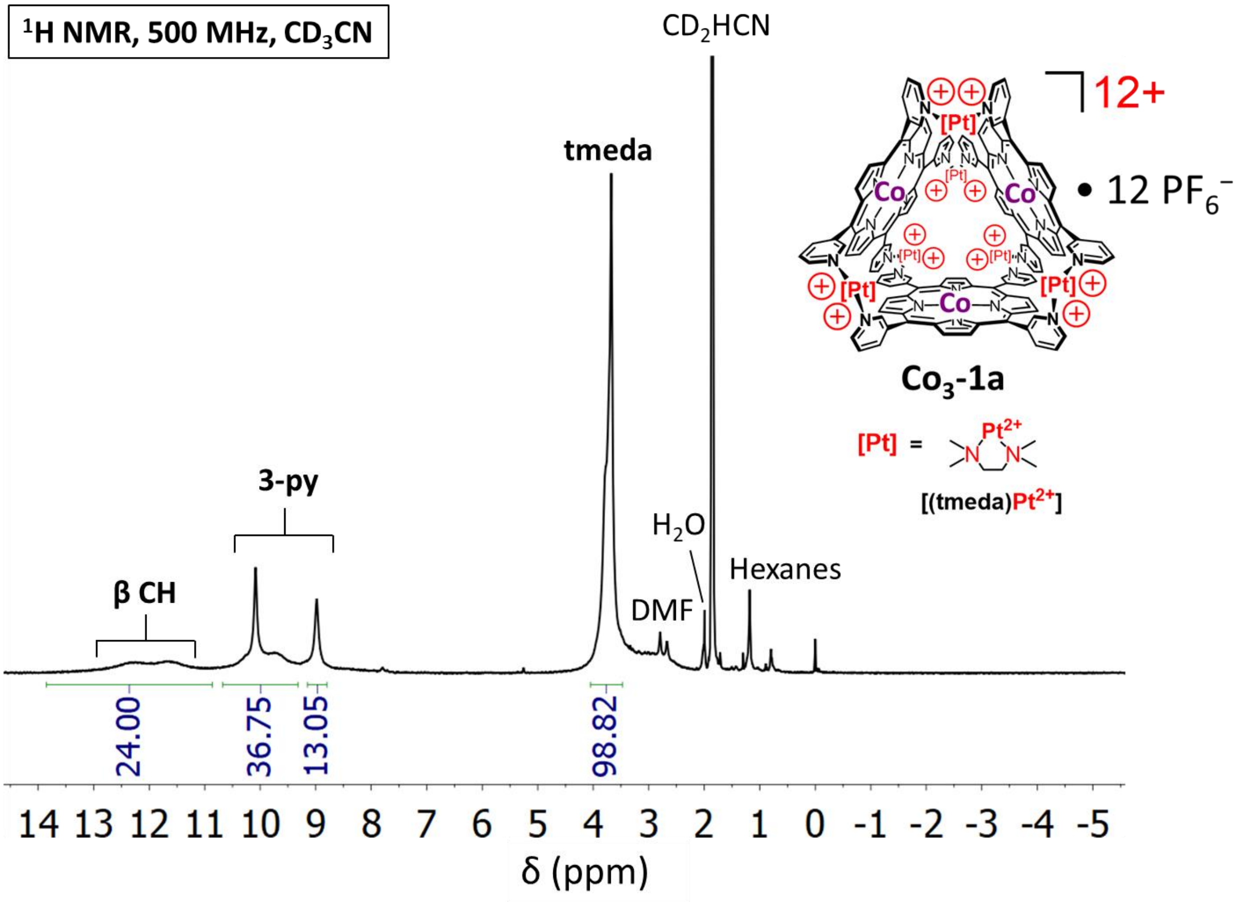

Figure S12. ^1H NMR spectrum of **Co_3-1a**•12PF_6 in CD_3CN.

5.h. Cage **Co₃-1b**

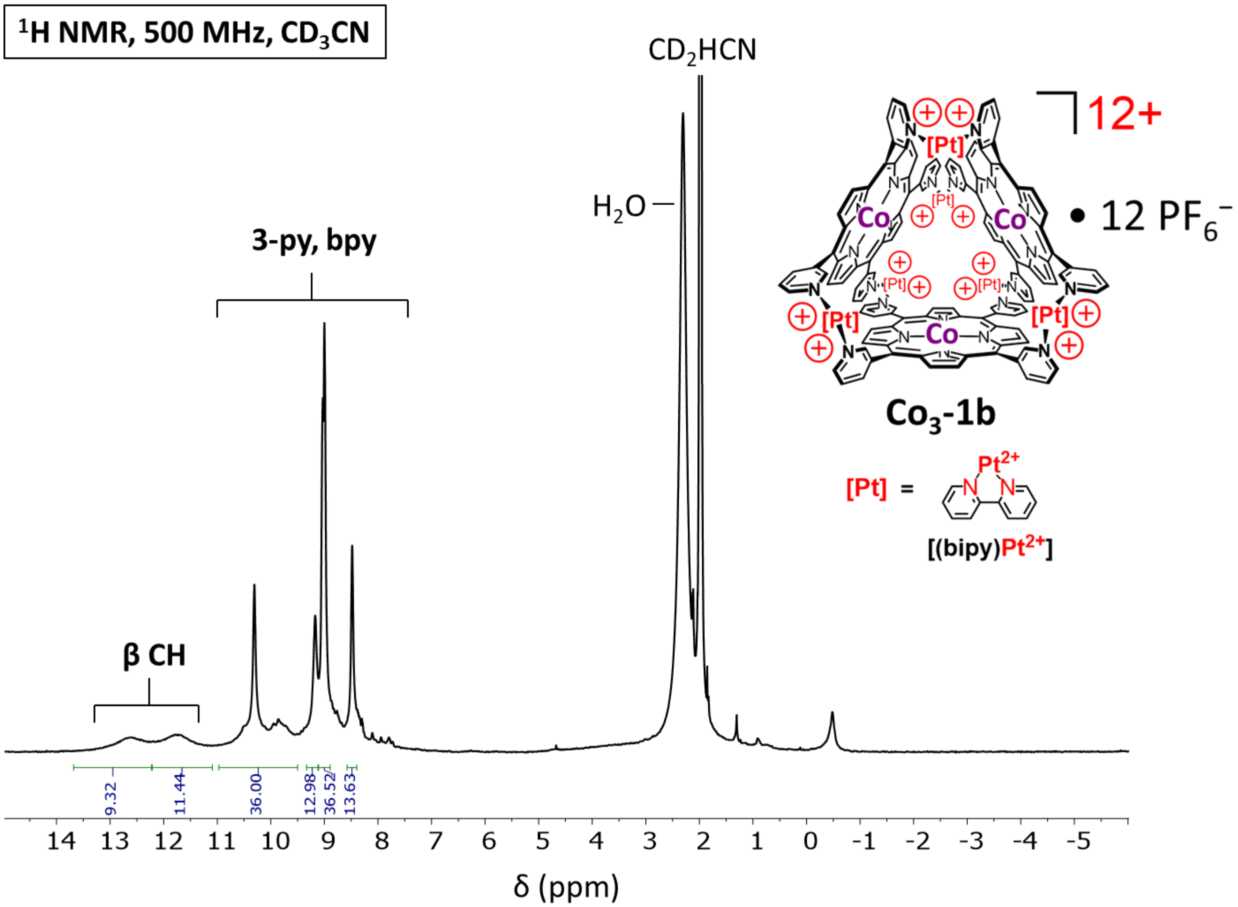

Figure S13. ^{1}H NMR spectrum of **Co$_3$-1b**•12PF$_6$ in CD$_3$CN.

5.i. Cage **Co$^{I}_{3}$-1a**

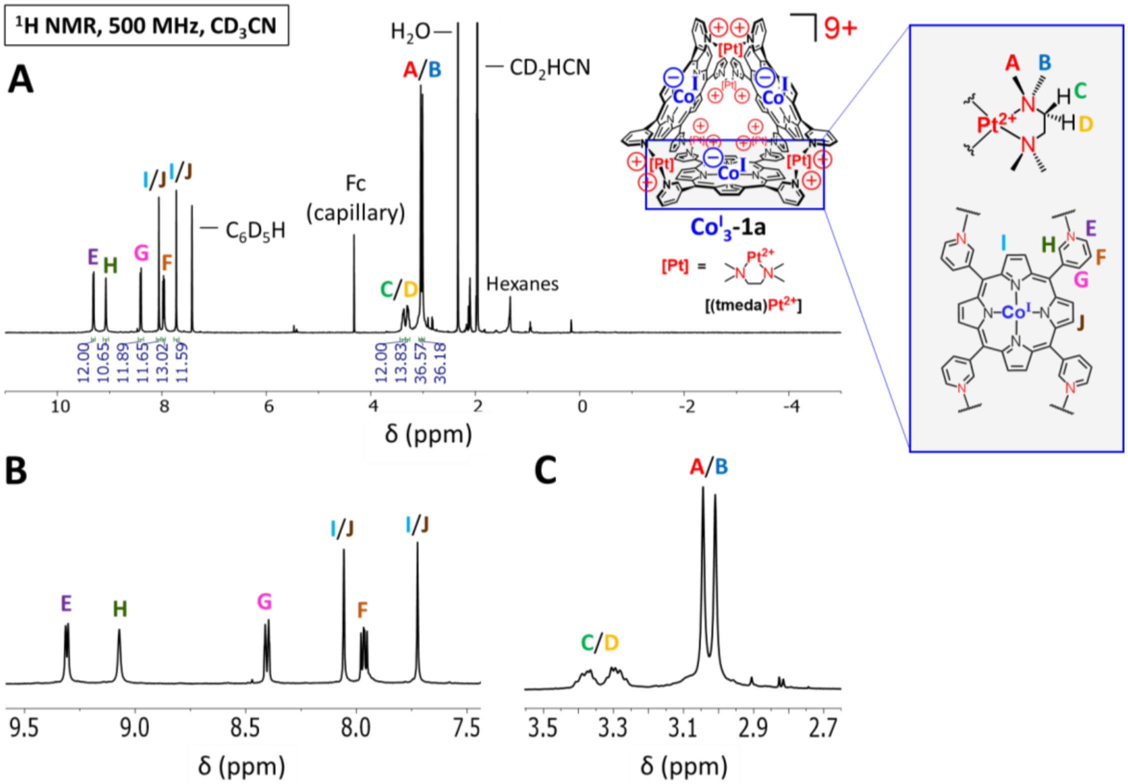

Figure S14. ^{1}H NMR spectrum of **Co$^{I}_{3}$-1a** prepared in situ by reducing **Co$_3$-1a**•12PF$_6$ with Cp$_2$Co in CD$_3$CN. (A) Full spectrum. (B) Aromatic region. (C) Aliphatic region.

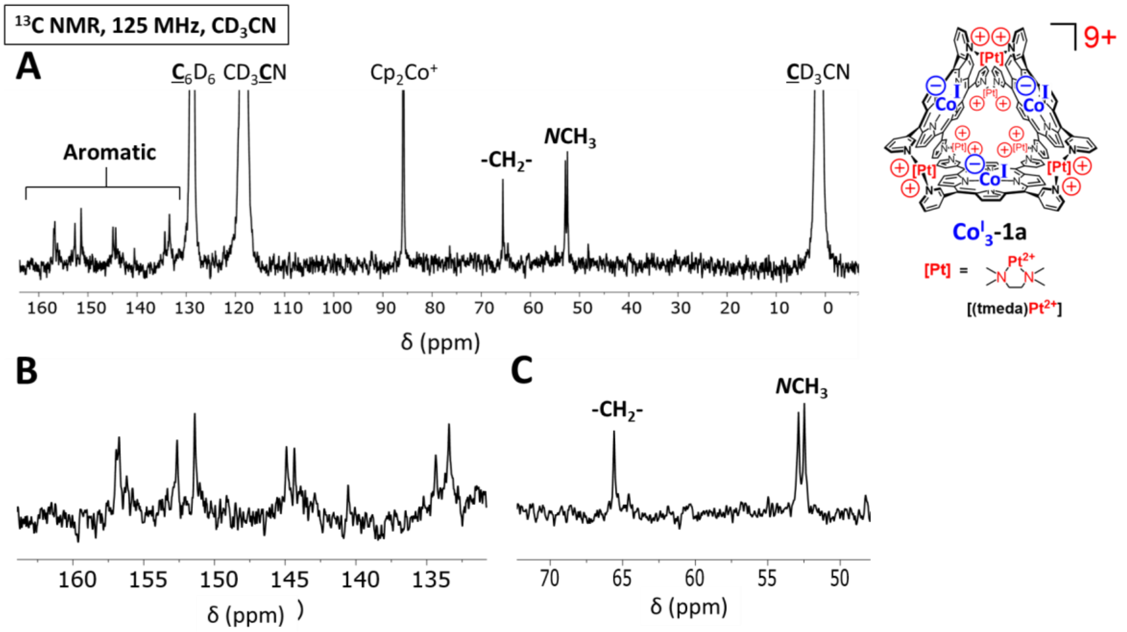

Figure S15. ^{13}C{^{1}H} NMR spectrum of **Co$^{I}_{3}$-1a** prepared in situ by reducing **Co$_3$-1a**•12PF$_6$ with Cp$_2$Co in CD$_3$CN. (A) Full spectrum. (B) Aromatic region. Aromatic signals of **Co$^{I}_{3}$-1a** were poorly defined regardless of spectral acquisition parameters and acquisition time (up to 12 h). (C) Aliphatic region.

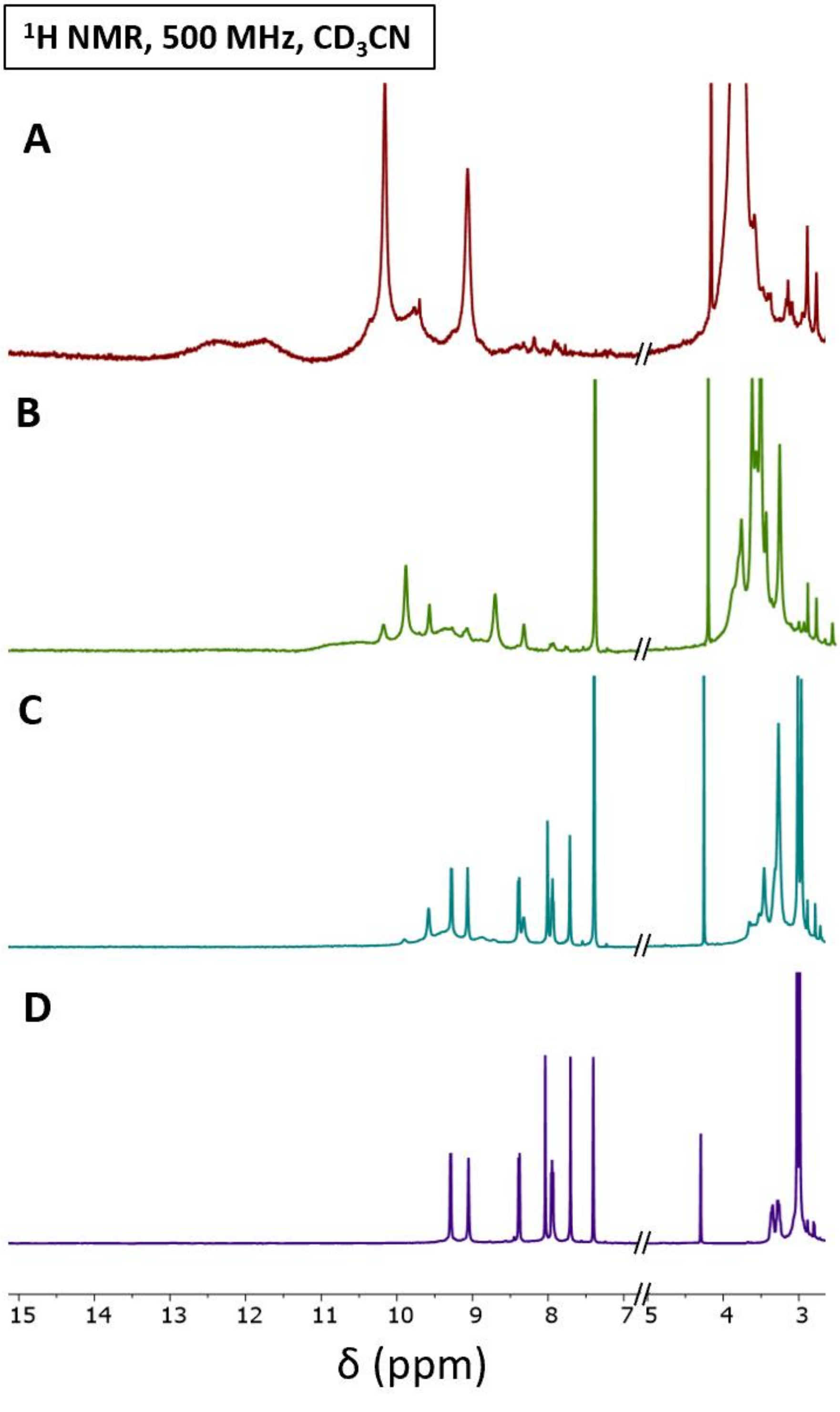

Figure S16: ^{1}H NMR spectra of the titration of a solution of **Co$_3$-1a** in CD$_3$CN with 1 – 3 equiv Cp$_2$Co. (A) Initial spectrum of **Co$_3$-1a**. (B) After adding 1 equiv Cp$_2$Co. (C) After adding 2 equiv Cp$_2$Co. (D) After adding 3 equiv Cp$_2$Co to form the fully diamagnetic state **Co$^I_3$-1a**.

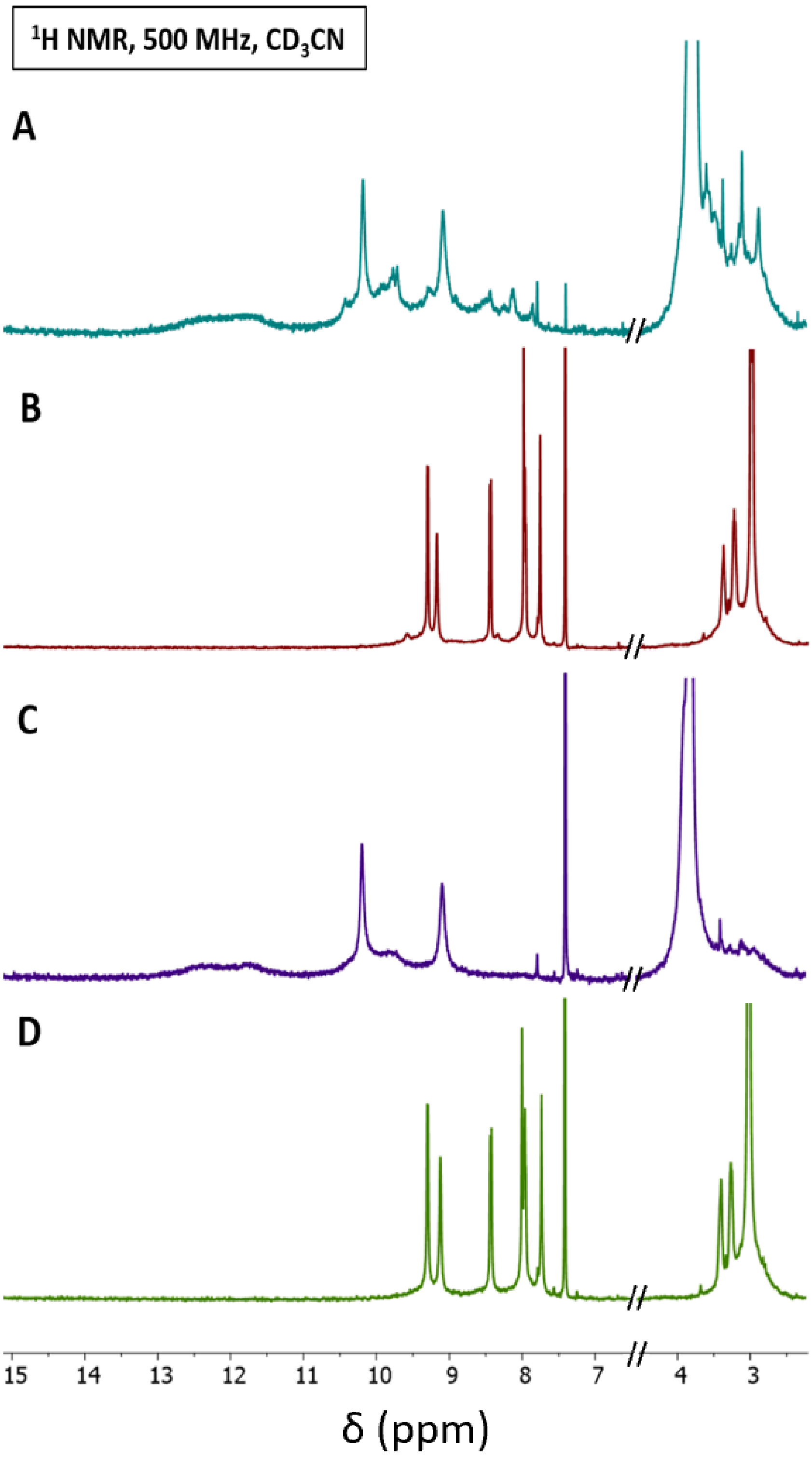

Figure S17: ^{1}H NMR spectra showing the redox cycling of **Co_3-1a** and **Co^I_3-1a** via sequential additions of Cp_2Co and $AgPF_6$. (A) Initial spectrum of **Co_3-1a**. (B) After adding 3 equiv Cp_2Co to form the fully diamagnetic state **Co^I_3-1a**. (C) After adding 3 equiv $AgPF_6$ to regenerate **Co_3-1a** (D) After adding another 3 equiv Cp_2Co to again access the **Co^I_3-1a** state.

5.j. Cage **Co$^{I}_{3}$-1b**

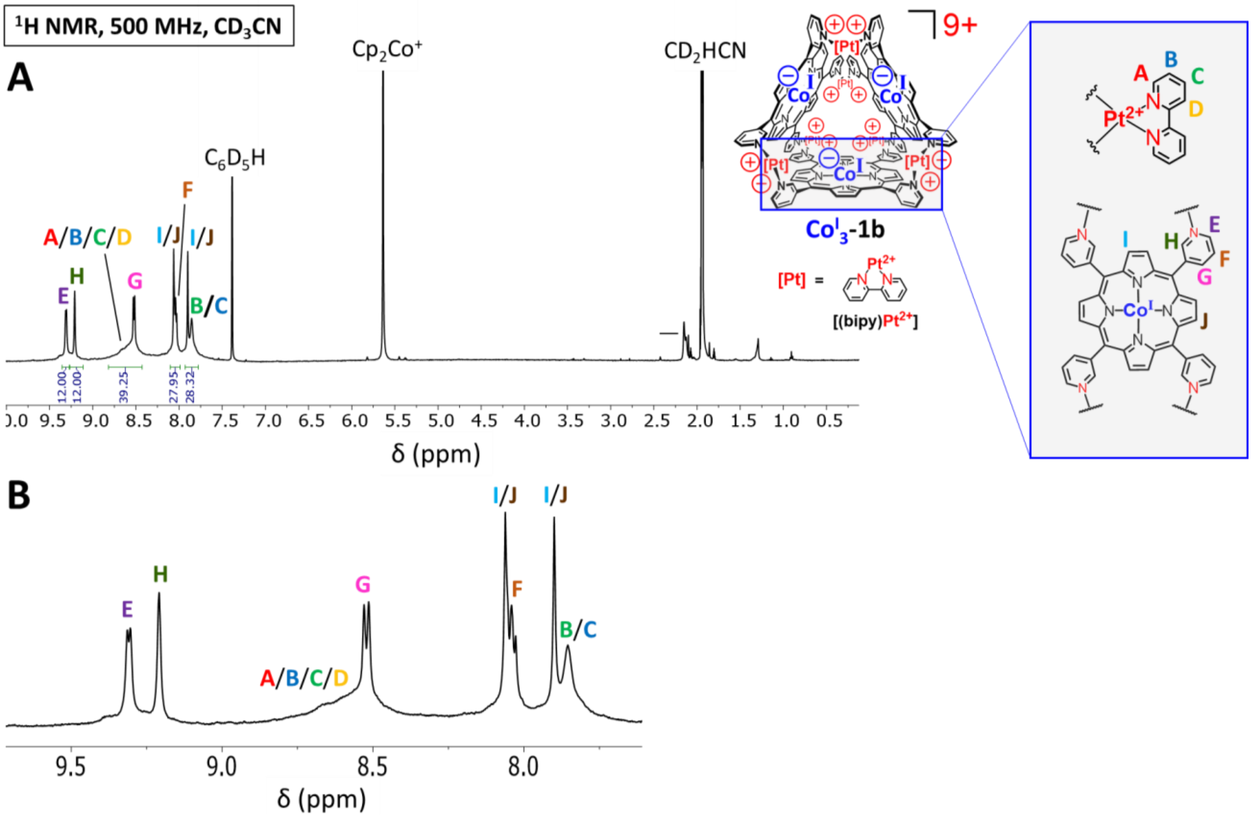

Figure S18. ^{1}H NMR spectrum of **Co$^{I}_{3}$-1b** prepared in situ by reducing **Co$_3$-1b**•12PF$_6$ with Cp$_2$Co in CD$_3$CN. (A) Full spectrum. (B) Aromatic region. Broadening of the bipy signals is attributed to slight radical character on these units from equilibration of electrons between the cobalt centers and bipy ligands.

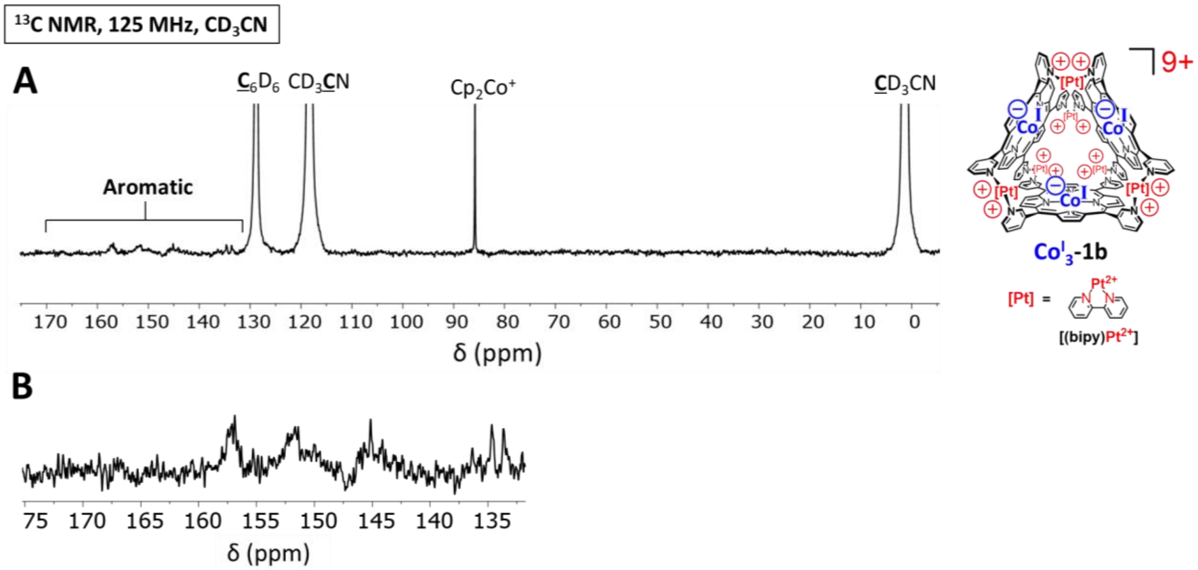

Figure S19. ^{13}C{^{1}H} NMR spectrum of **Co$^{I}_{3}$-1b** prepared in situ by reducing **Co$_3$-1b**•12PF$_6$ with Cp$_2$Co in CD$_3$CN. (A) Full spectrum. (B) Aromatic region. Aromatic signals of **Co$^{I}_{3}$-1b** were poorly defined regardless of spectral acquisition parameters and acquisition time (up to 12 h).

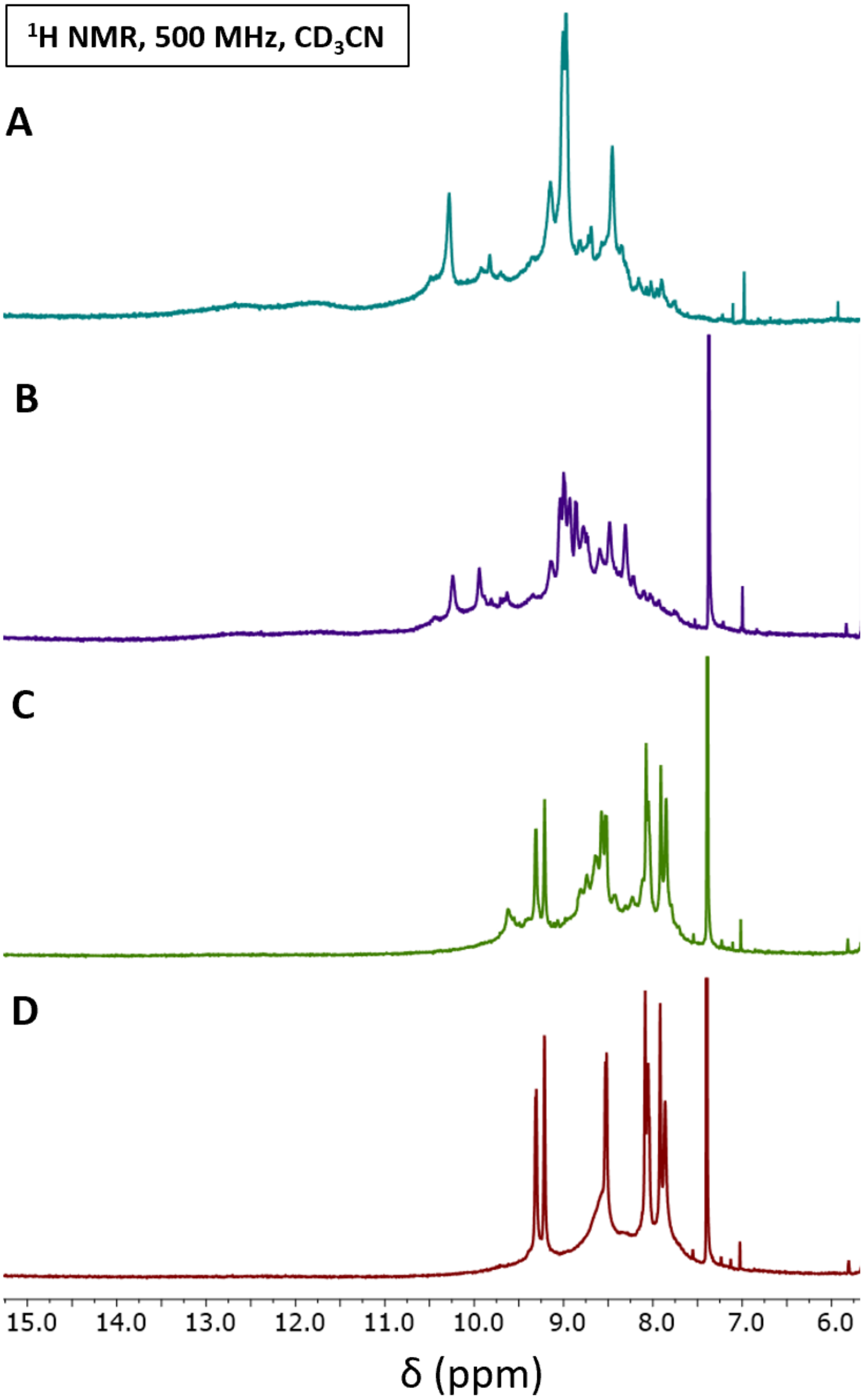

Figure S20: ^{1}H NMR spectra of the titration of a solution of **Co_3-1b** in CD_3CN with 1 – 3 equiv Cp_2Co. (A) Initial spectrum of **Co_3-1b**. (B) After adding 1 equiv Cp_2Co. (C) After adding 2 equiv Cp_2Co. (D) After adding 3 equiv Cp_2Co to form the fully diamagnetic state **Co^I_3-1b**.

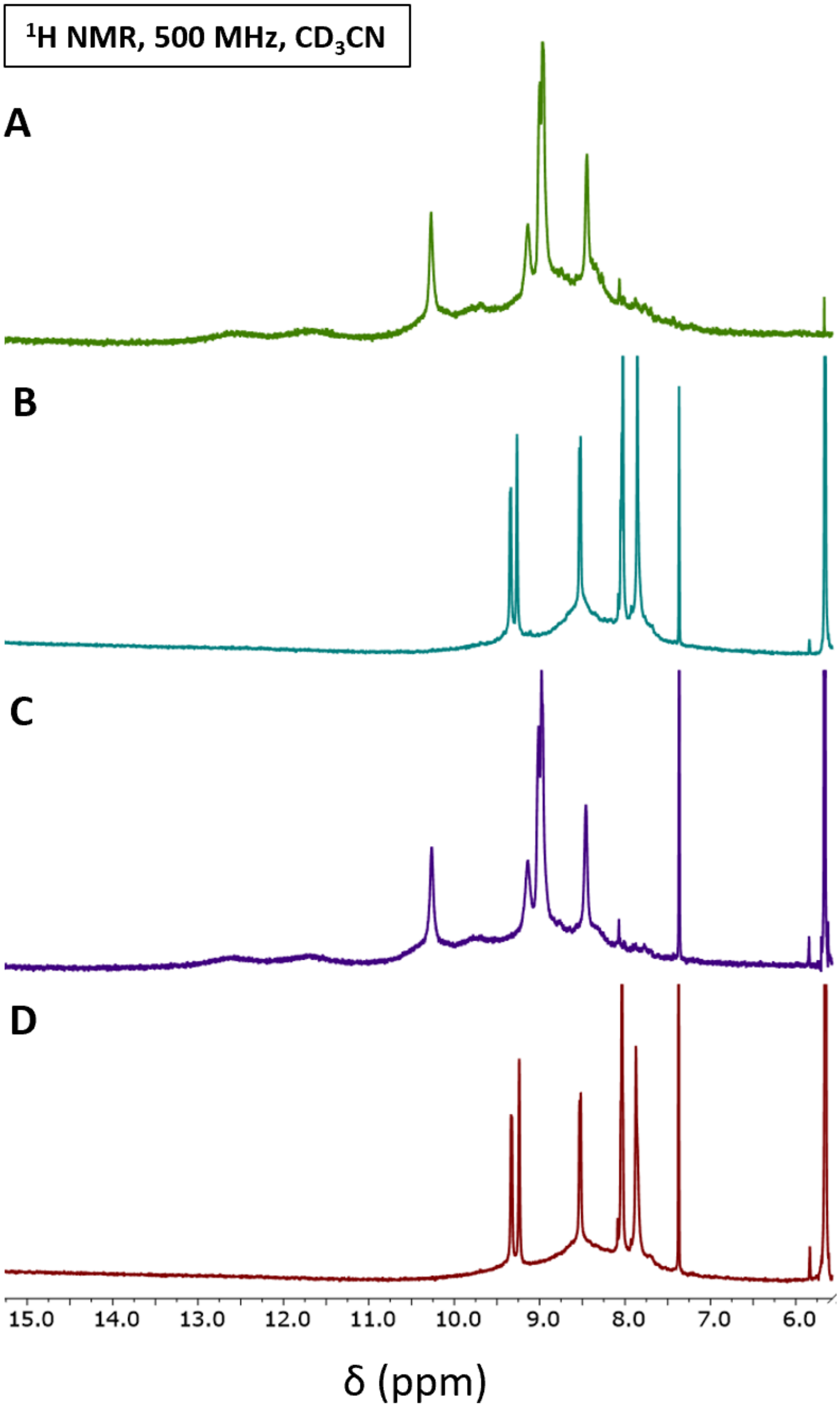

Figure S21: ^{1}H NMR spectra showing the redox cycling of **Co$_3$-1b** and **Co$^I_3$-1b** via sequential additions of Cp$_2$Co and AgPF$_6$. (A) Initial spectrum of **Co$_3$-1b**. (B) After adding 3 equiv Cp$_2$Co to form the fully diamagnetic state **Co$^I_3$-1b**. (C) After adding 3 equiv AgPF$_6$ to regenerate **Co$_3$-1b** (D) After adding another 3 equiv Cp$_2$Co to again access the **Co$^I_3$-1b** state.

5.k. Cage **[Co^{III}NO]$_3$-1a**

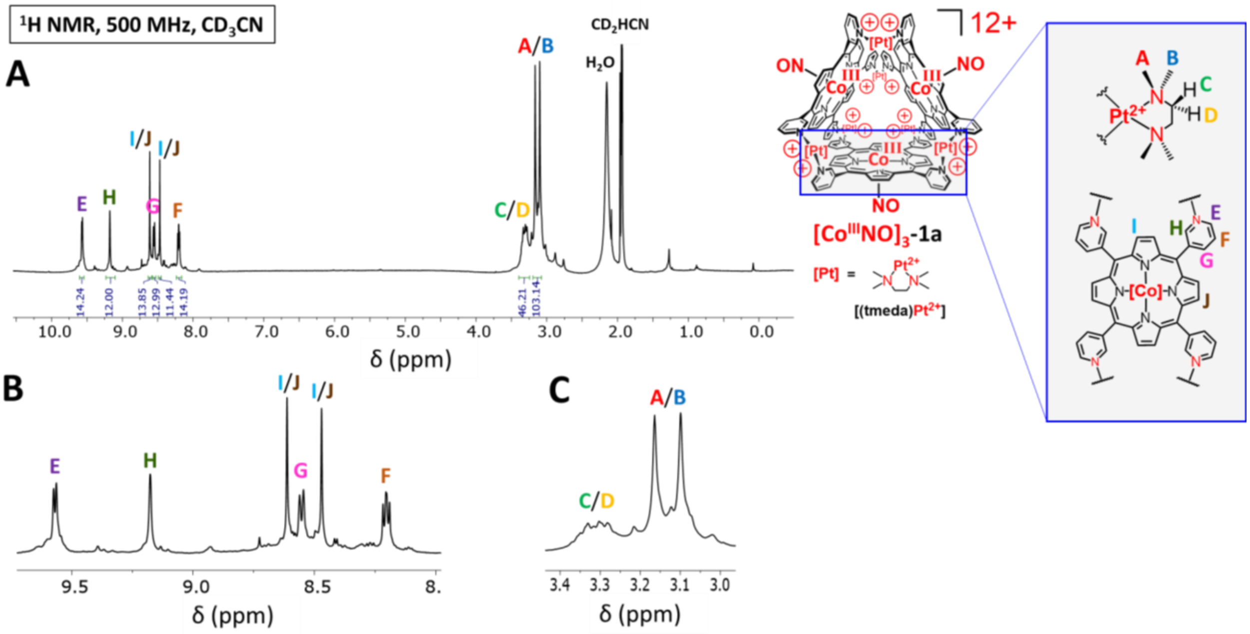

Figure S22. ^{1}H NMR spectrum of **[Co^{III}NO]$_3$-1a** prepared in situ by reaction of **Co$_3$-1a**•12PF$_6$ with NO in CD$_3$CN. (A) Full spectrum. (B) Aromatic region. (C) Aliphatic region. Major signals identified in each region confirm formation of the expected tris-Co^{III}NO derivative of **Co$_3$-1a**. Other, minor signals may result from different endo/exo placements of the nitrosyl ligands or from slight decomposition of the cage.

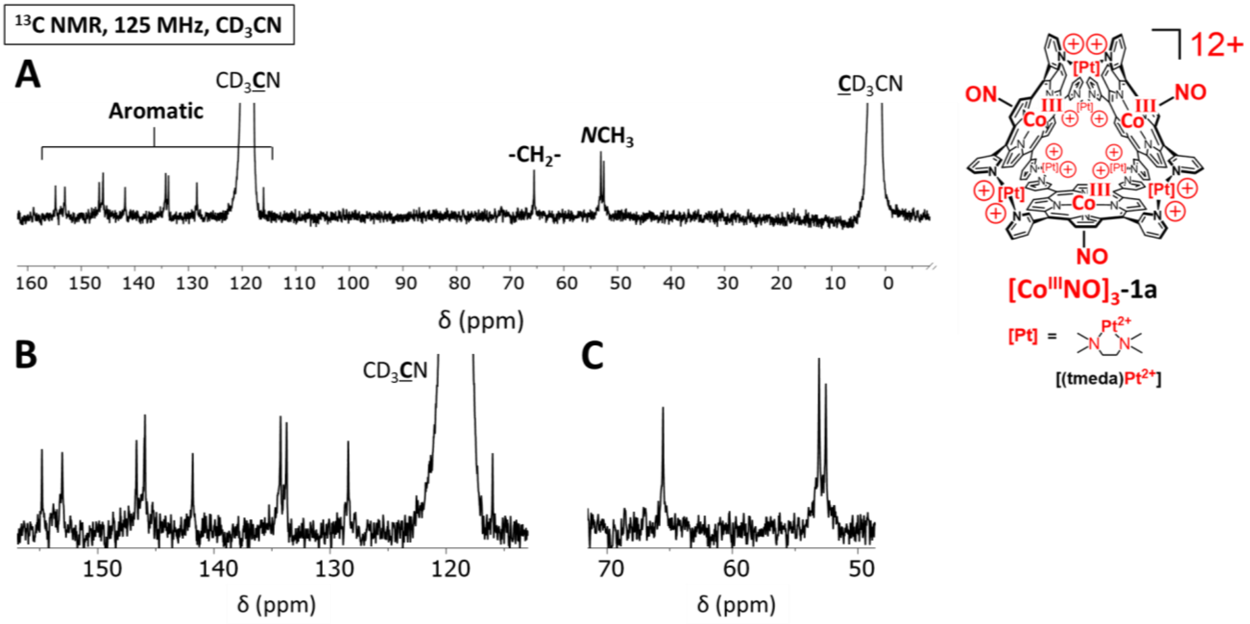

Figure S23. ^{13}C{^{1}H} NMR spectrum of **[Co^{III}NO]$_3$-1a** prepared in situ by reaction of **Co$_3$-1a**•12PF$_6$ with NO in CD$_3$CN. (A) Full spectrum. (B) Aromatic region. Nine of ten expected aromatic signals are observed. (C) Aliphatic region.

5.l. Cage **[Co^{III}NO]$_3$-1b**

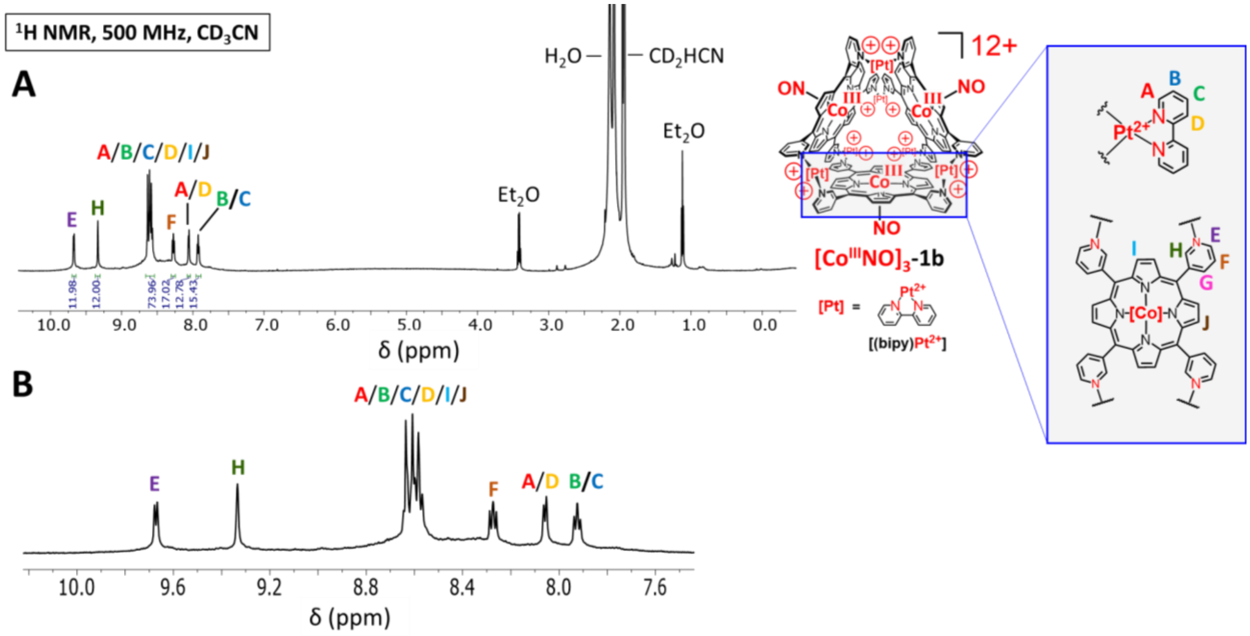

Figure S24. ^{1}H NMR spectrum of **[Co^{III}NO]$_3$-1b** prepared in situ by reaction of **Co$_3$-1b**•12PF$_6$ with NO in CD$_3$CN. (A) Full spectrum. (B) Aromatic region. Major signals confirm formation of the expected tris-Co^{III}NO derivative of **Co$_3$-1b**. The raised baseline from ca. 7.4 – 9.0 ppm suggests slight decomposition of the cage.

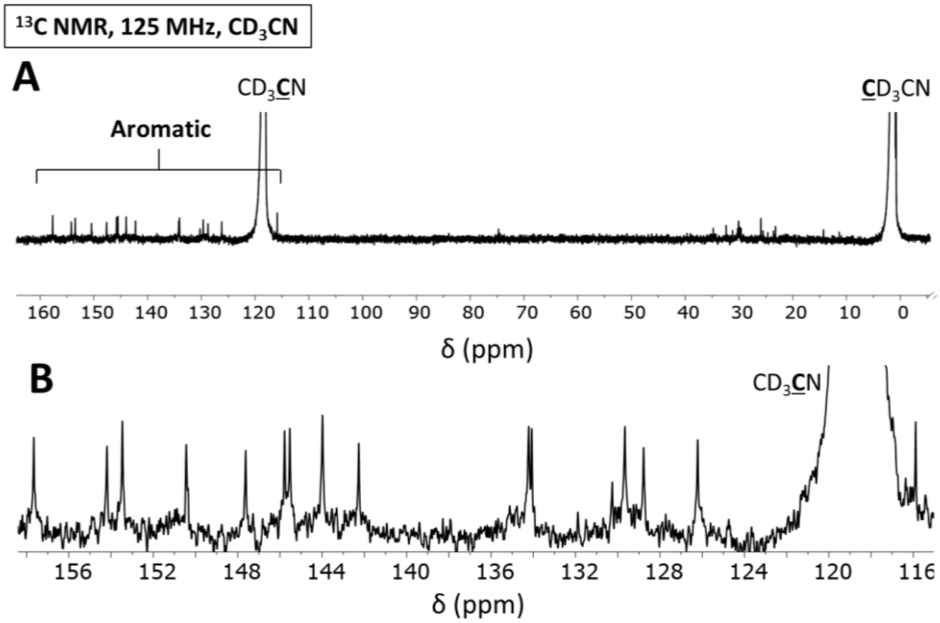

Figure S25. ^{13}C{^{1}H} NMR spectrum of **[Co^{III}NO]$_3$-1b** prepared in situ by reaction of **[Co$_3$-1b]**•12PF$_6$ with NO in CD$_3$CN. (A) Full spectrum. (B) Aromatic region.

5.m. Cage **Zn$_3$-1a**

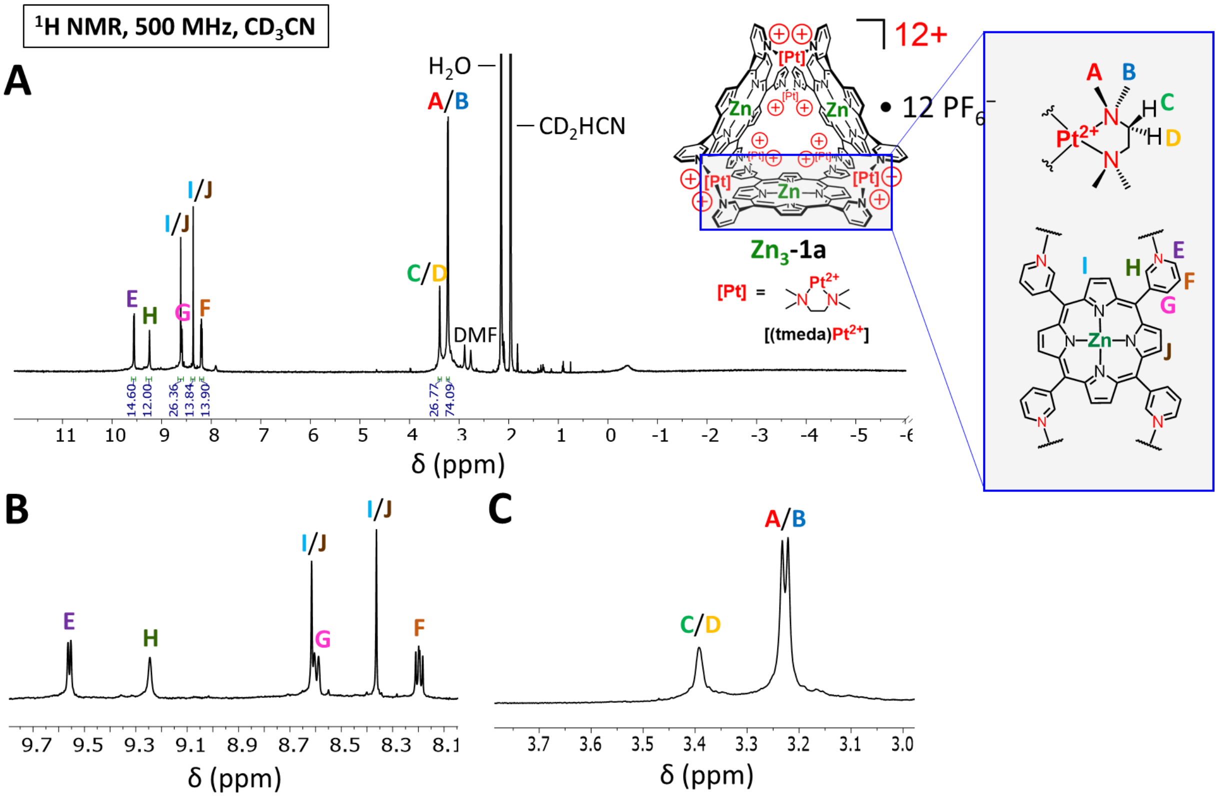

Figure S26. ^{1}H NMR spectrum of **Zn$_3$-1a**•12PF$_6$ in CD$_3$CN. (A) Full spectrum. (B) Aromatic region. (C) Aliphatic region.

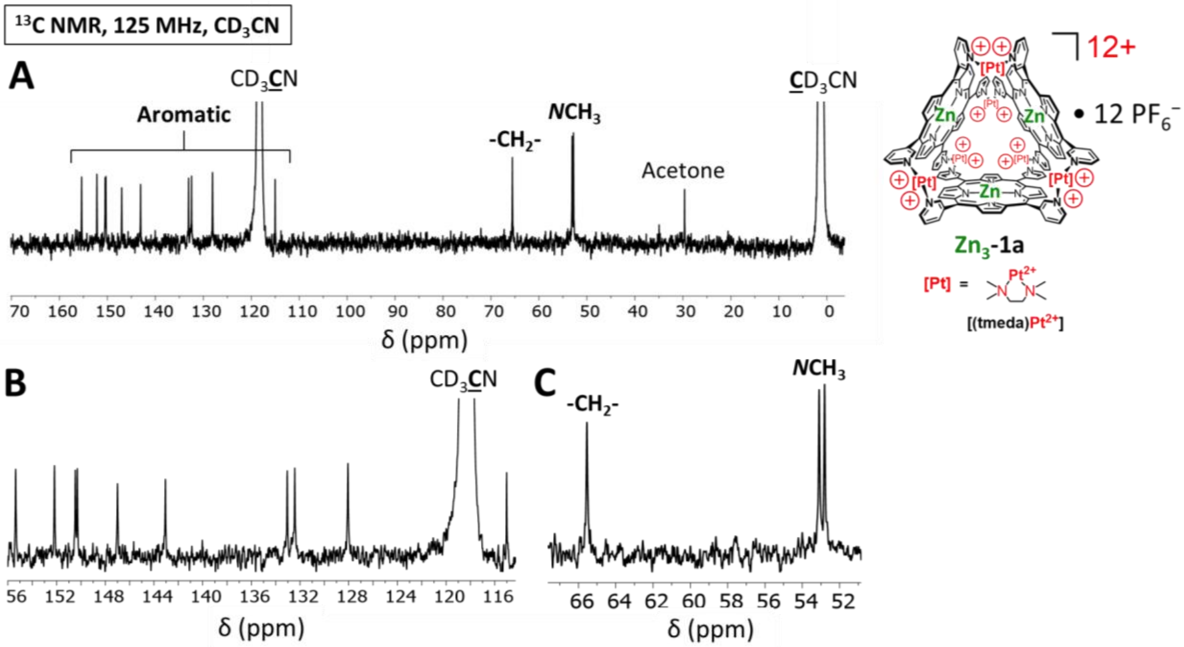

Figure S27. ^{13}C{^{1}H} NMR spectrum of **Zn$_3$-1a**•12PF$_6$ in CD$_3$CN. (A) Full spectrum. (B) Aromatic region. (C) Aliphatic region.

5.n. Cage **Zn$_3$-1b**

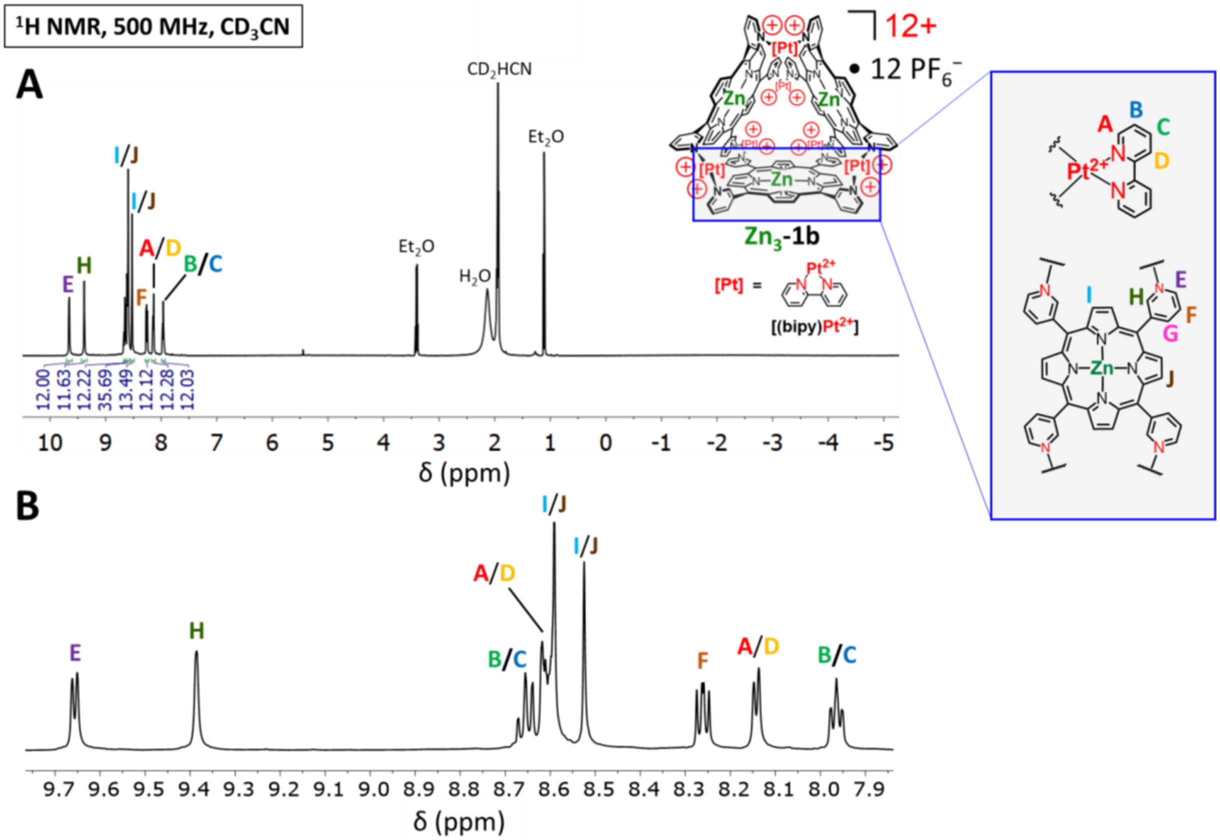

Figure S28. ^{1}H NMR spectrum of **Zn$_3$-1b**•12PF$_6$ in CD$_3$CN. (A) Full spectrum. (B) Aromatic region.

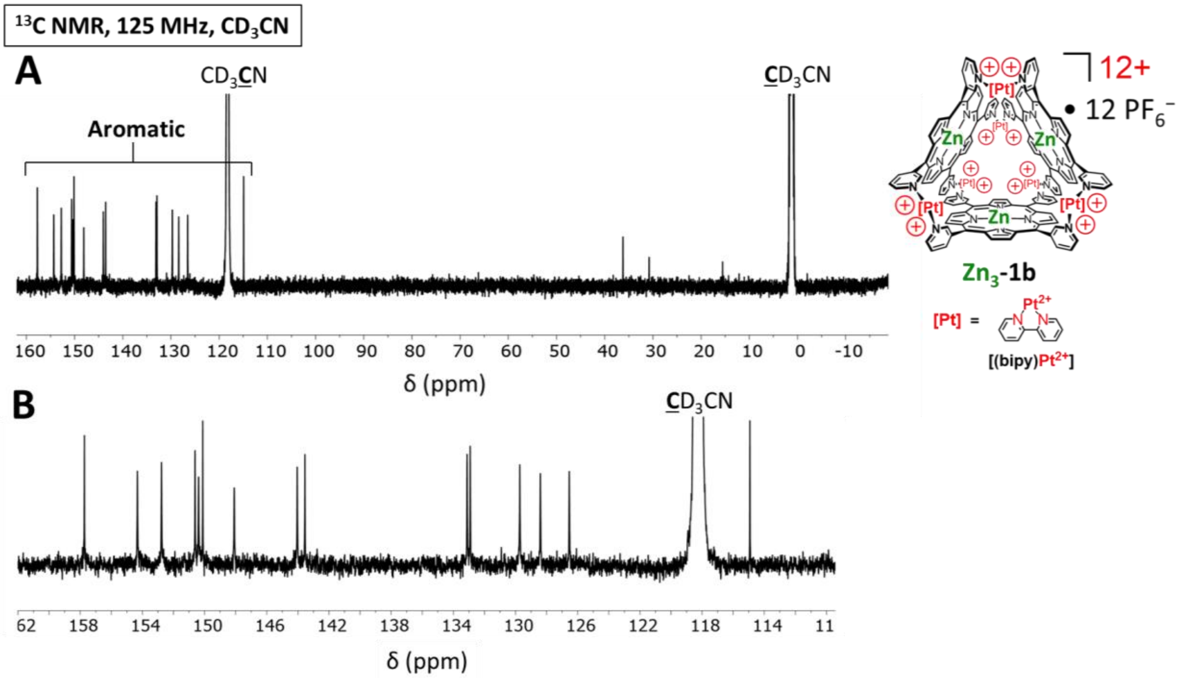

Figure S29. ^{13}C{^{1}H} NMR spectrum of **Zn$_3$-1b**•12PF$_6$ in CD$_3$CN. (A) Full spectrum. (B) Aromatic region.

5.o. Reaction of **Co$^{I}_{3}$-1a** with [Me$_3$O]BF$_4$

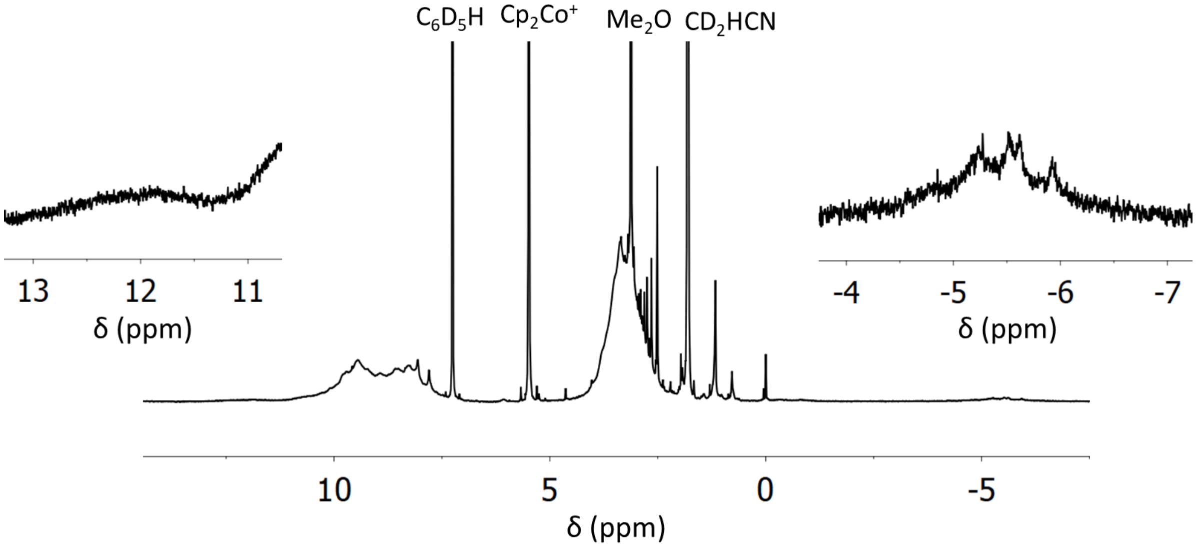

Figure S30. ^{1}H NMR spectrum acquired after adding [Me$_3$O]BF$_4$ (3 equiv.) to a solution of **Co$^{I}_{3}$-1a** prepared in CD$_3$CN as described in Section 3.d. The aromatic and aliphatic regions show broad, poorly defined resonances resulting from the cage and/or its decomposition products. The left inset displays a broad resonance downfield of 11 ppm that suggests formation of some Co^{II} products. The right inset displays broad, poorly defined Co^{III}-CH$_3$ signals.

5.p. Reaction of **Co$^{I}_{3}$-1b** with [Me$_3$O]BF$_4$

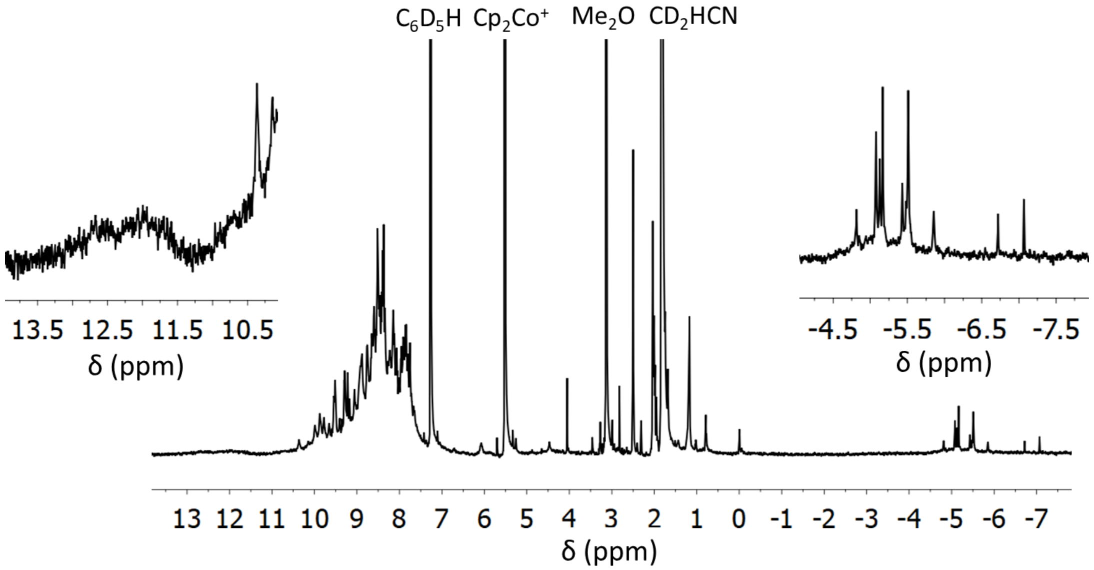

Figure S31.^{1}H NMR spectrum acquired after adding [Me$_3$O]BF$_4$ (3 equiv.) to a solution of **Co$^{I}_{3}$-1b** prepared in CD$_3$CN as described in Section 3.d. The aromatic region shows many overlapping resonances resulting from the cage and/or its decomposition products. The left inset displays a broad resonance downfield of 11 ppm that suggests formation of some Co^{II} products. The right inset displays several Co^{III}-CH$_3$ signals.

5.q. **Co_3-1a** + $AgPF_6$ + pyridine

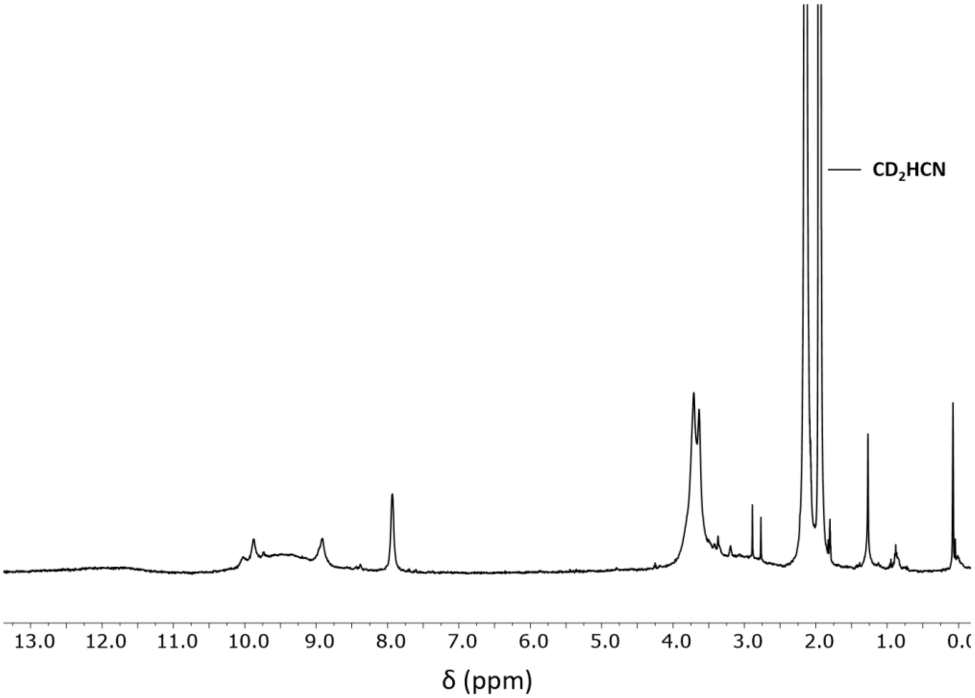

Figure S32. ^{1}H NMR spectrum acquired 30 min after adding $AgPF_6$ (9 equiv.) and pyridine (6 equiv.) to a solution of **Co_3-1a**•12PF_6 in CD_3CN. No substantial change was observed after monitoring for 24 h.

5.r. **Co_3-1b** + $AgPF_6$ + pyridine

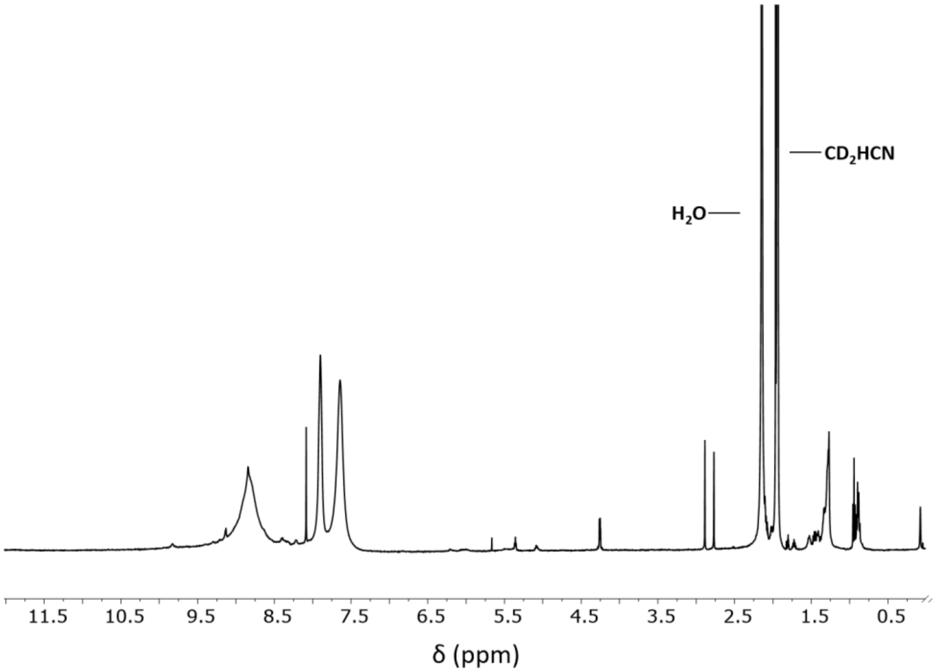

Figure S33. ^{1}H NMR spectrum acquired 30 min after adding $AgPF_6$ (9 equiv.) and pyridine (6 equiv.) to a solution of **Co_3-1b**•12PF_6 in CD_3CN. No substantial change was observed after monitoring for 24 h.

5.s. Oxidation of **Co_3-1a** with thianthrenium

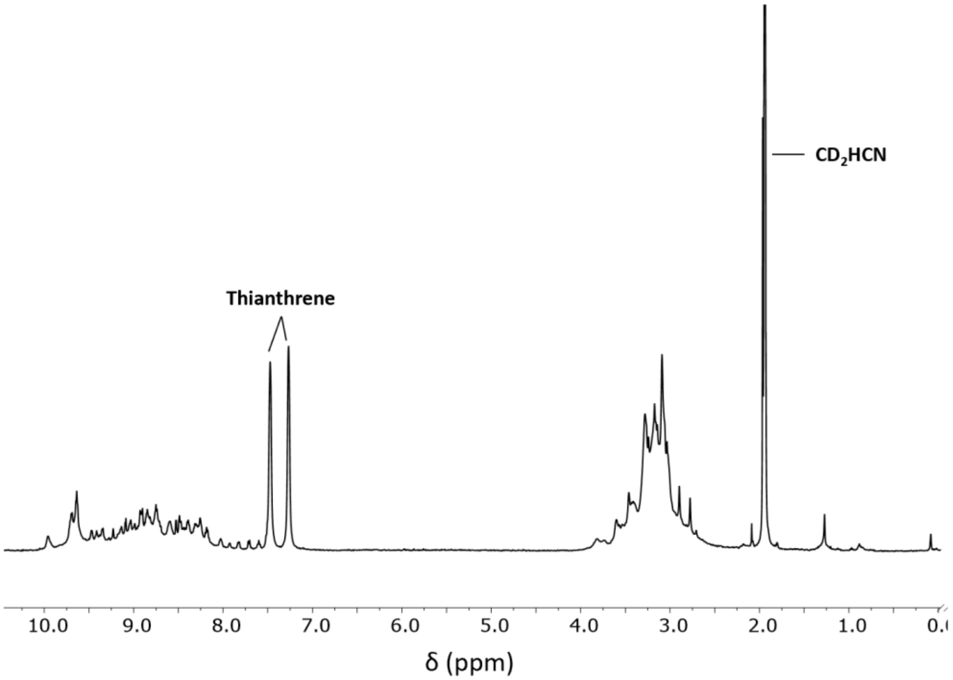

Figure S34. ^{1}H NMR spectrum acquired after adding a solution of thianthrenium (3 equiv.) to a solution of **Co_3-1a**•$12PF_6$ in CD_3CN.

5.t. Oxidation of **Co_3-1b** with thianthrenium

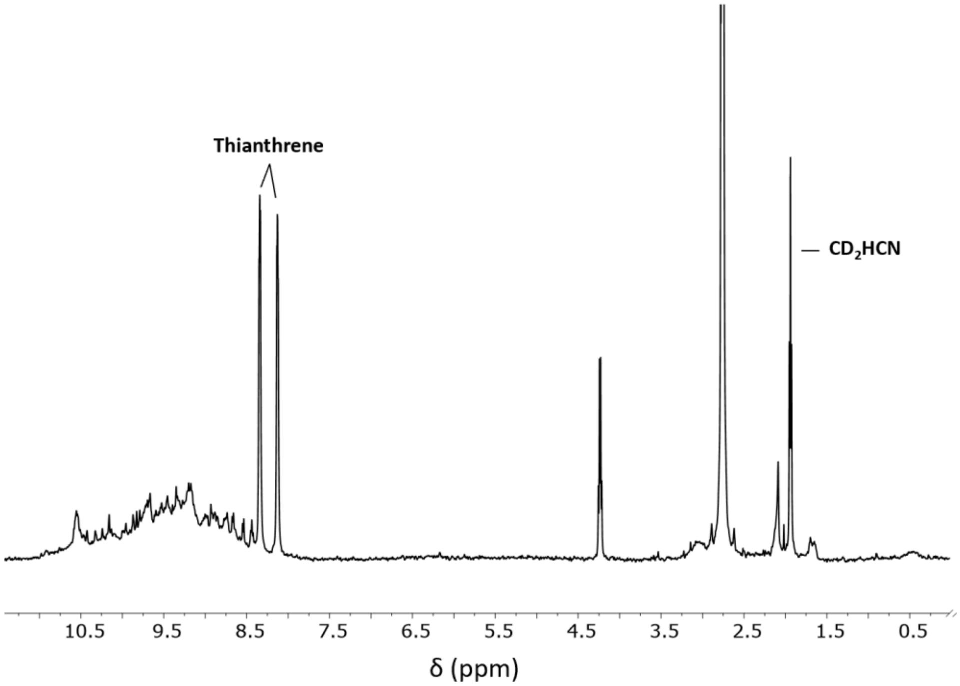

Figure S35. ^{1}H NMR spectrum acquired after adding a solution of thianthrenium (3 equiv.) to a solution of **Co_3-1b**•$12PF_6$ in CD_3CN.

6. DOSY NMR Spectra

Instrumentation: All Diffusion Ordered (DOSY) ^{1}H NMR spectra were measured using a Bruker AVANCE Neo spectrometer with a 500 MHz working frequency. All DOSY spectra were recorded at 298 K.

Data Analysis: DOSY NMR data were processes using Bruker's Dynamic Center software. Reported diffusion constants (D) are the average of the individual diffusion constants determined for each signal of the compound of interest.

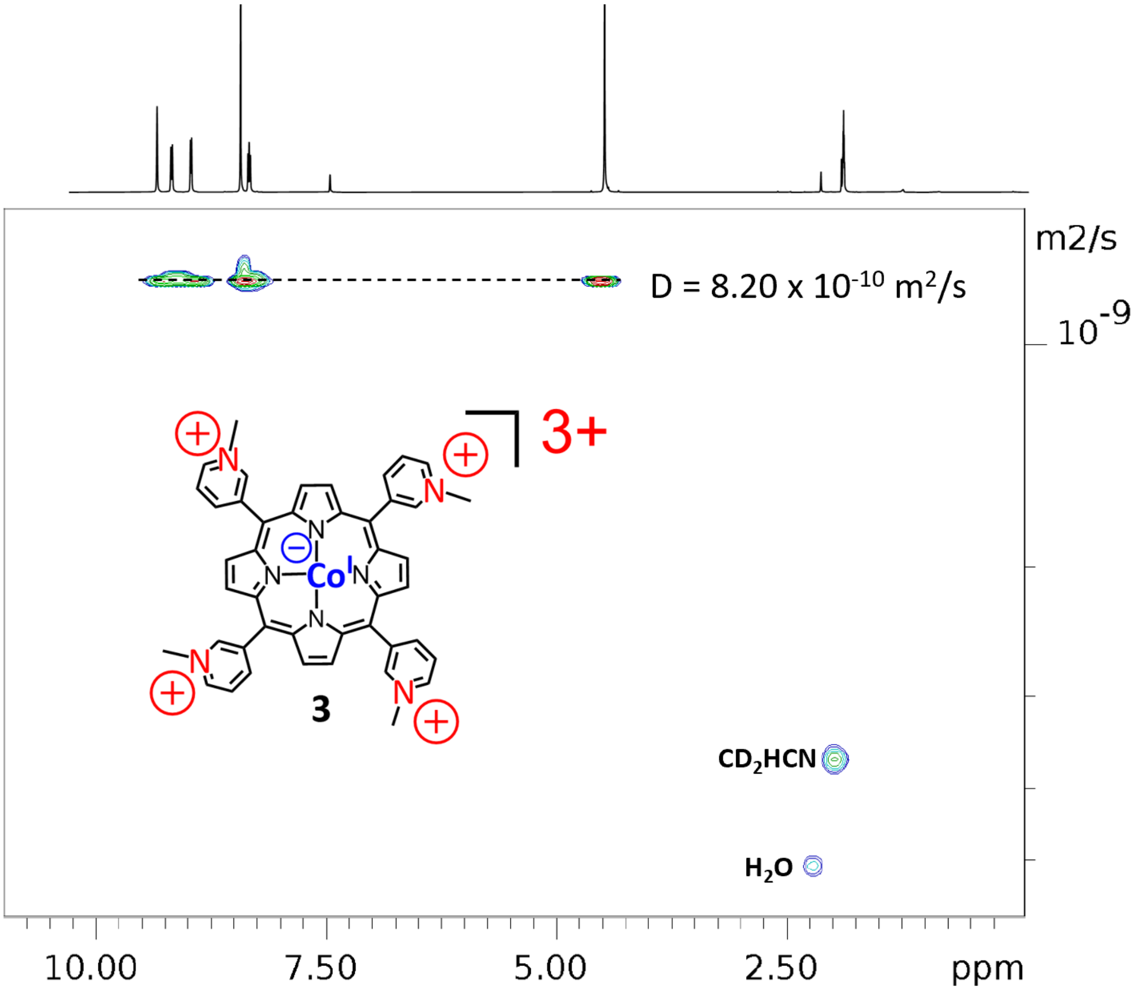

Figure S36. Diffusion ordered (DOSY) ^{1}H NMR spectrum of **3** prepared in situ in CD_3CN by reducing **2**•4PF_6 with a slight excess of Cp_2Co. The experimental diffusion constant (8.20 x 10^{-10} m^2/s) corresponds to a spherical hydrodynamic radius[6] of 7.84 Å.

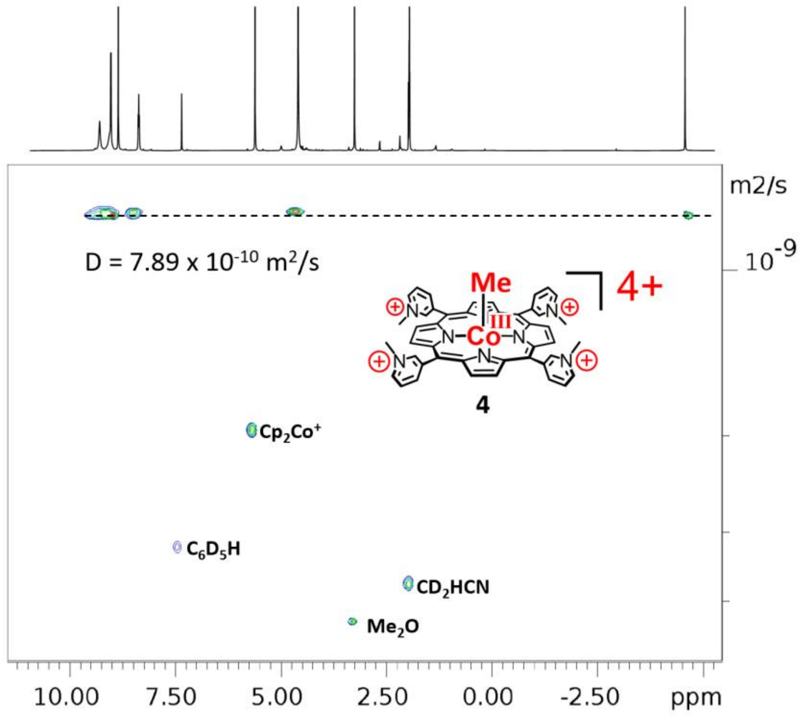

Figure S37. Diffusion ordered (DOSY) ^{1}H NMR spectrum of **4** prepared in situ in CD_3CN by treatment of **2**•$4PF_6$ with Cp_2Co and $[Me_3O]BF_4$. The experimental diffusion constant (7.79 x 10^{-10} m^2/s) corresponds to a spherical hydrodynamic radius[6] of 8.26 Å.

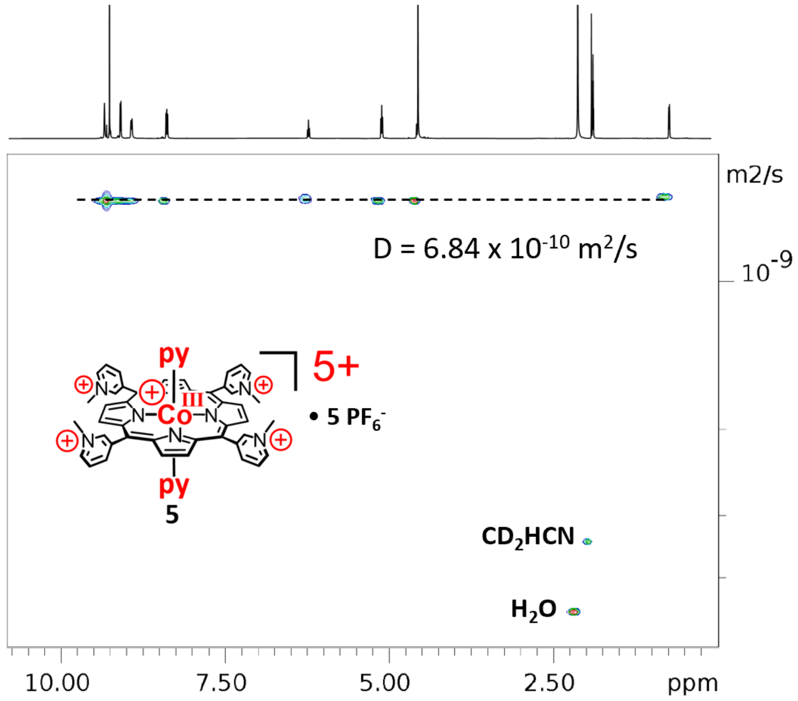

Figure S38. Diffusion ordered (DOSY) ^{1}H NMR spectrum of **5**•$5PF_6$ in CD_3CN. The experimental diffusion constant (6.84 x 10^{-10} m^2/s) corresponds to a spherical hydrodynamic radius[6] of 9.40 Å.

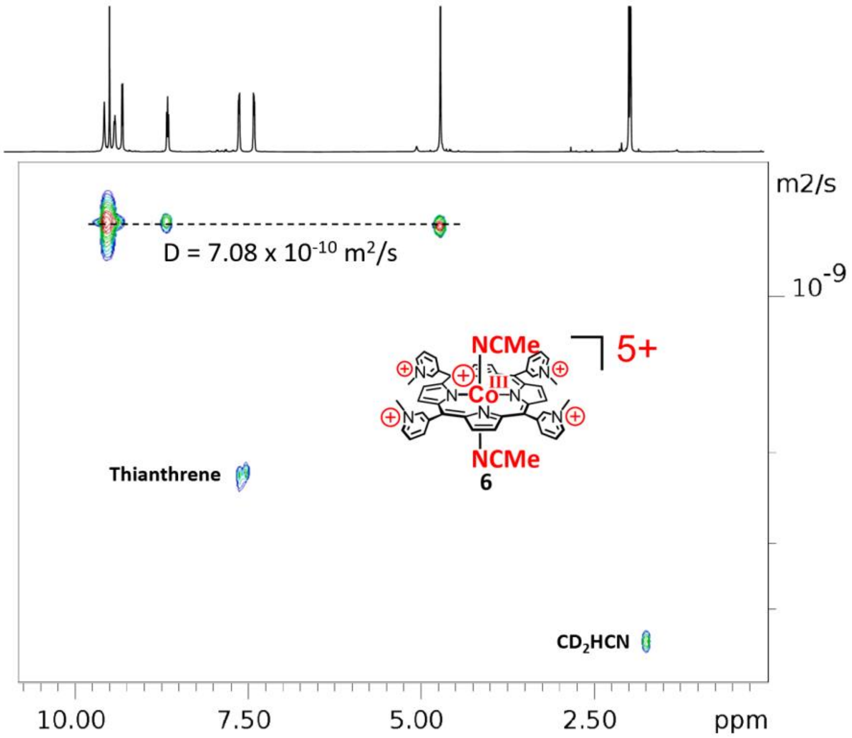

Figure S39. Diffusion ordered (DOSY) ^{1}H NMR spectrum of **6** prepared in situ in CD_3CN by oxidizing **2**•4PF_6 with thianthrenium hexafluorophosphate. The experimental diffusion constant (7.08 x 10^{-10} m^2/s) corresponds to a spherical hydrodynamic radius[6] of 9.08 Å.

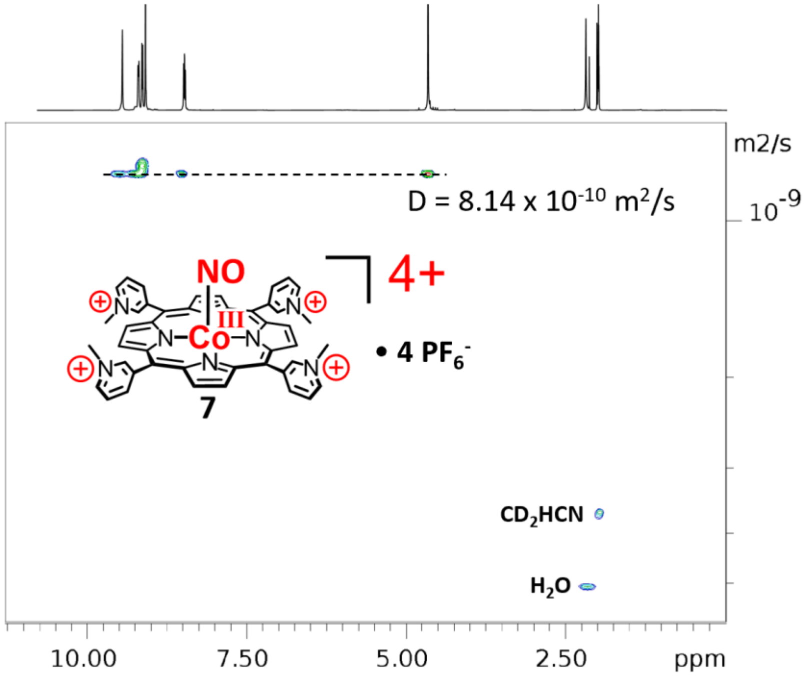

Figure S40. Diffusion ordered (DOSY) ^{1}H NMR spectrum of **7**•4PF_6 in CD_3CN. The experimental diffusion constant (8.14 x 10^{-10} m^2/s) corresponds to a spherical hydrodynamic radius[6] of 7.90 Å.

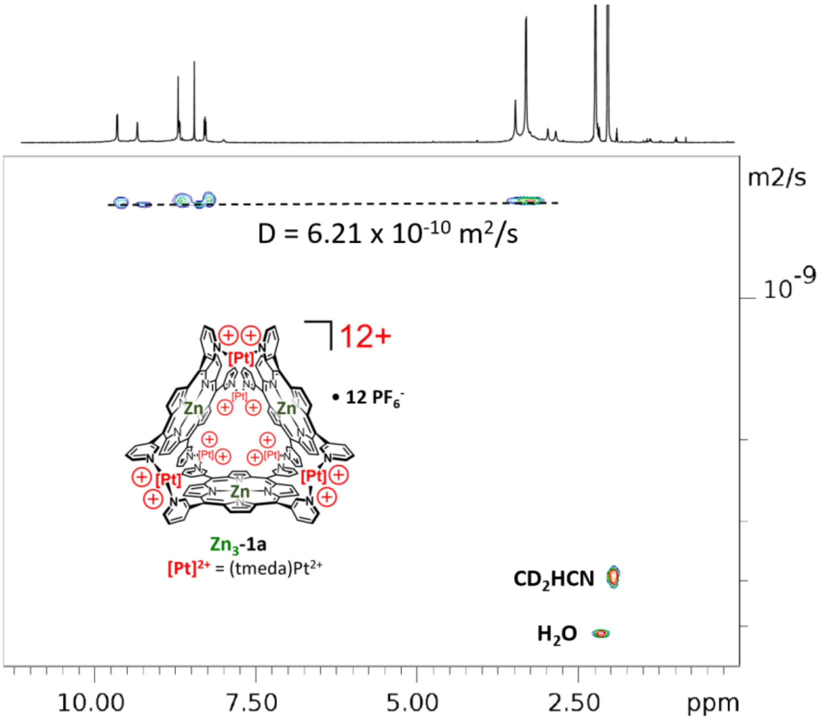

Figure S41. Diffusion ordered (DOSY) ^{1}H NMR spectrum of **Zn$_3$-1a**•12PF$_6$ in CD$_3$CN. The experimental diffusion constant (6.21 x 10^{-10} m^2/s) corresponds to a spherical hydrodynamic radius[6] of 10.36 Å.

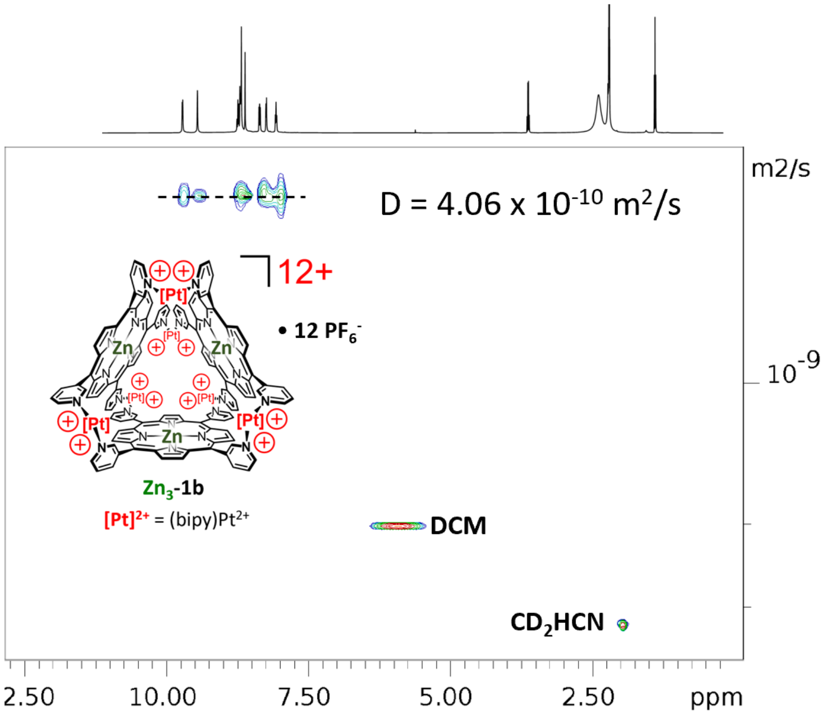

Figure S42. Diffusion ordered (DOSY) ^{1}H NMR spectrum of **Zn$_3$-1b**•12PF$_6$ in CD$_3$CN. The experimental diffusion constant (4.06 x 10^{-10} m^2/s) corresponds to a spherical hydrodynamic radius[6] of 15.84 Å.

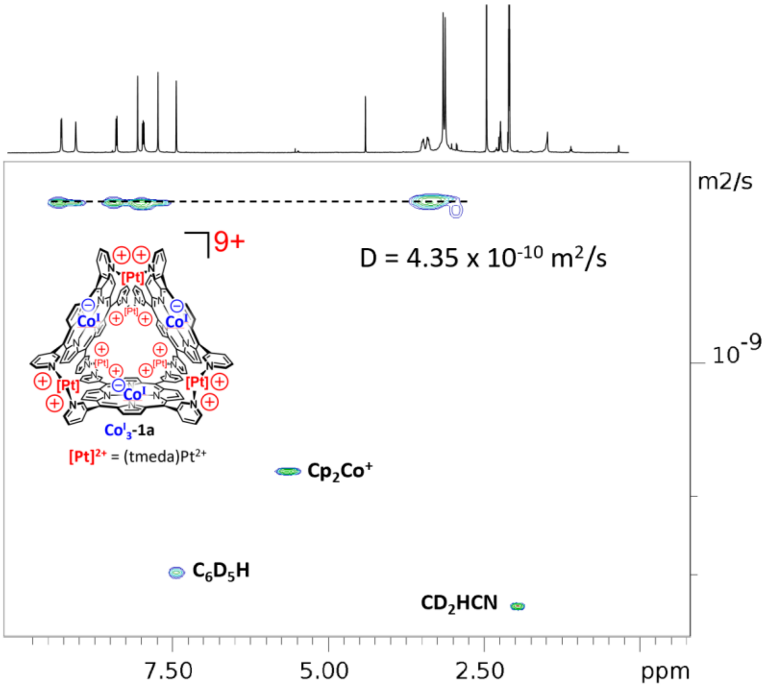

Figure S43. Diffusion ordered (DOSY) ^{1}H NMR spectrum of **Co^I_3-1a** generated in situ by reducing **Co_3-1a**•12PF_6 with a slight excess of Cp_2Co in CD_3CN. The experimental diffusion constant (4.35 x 10^{-10} m^2/s) corresponds to a spherical hydrodynamic radius[6] of 14.79 Å.

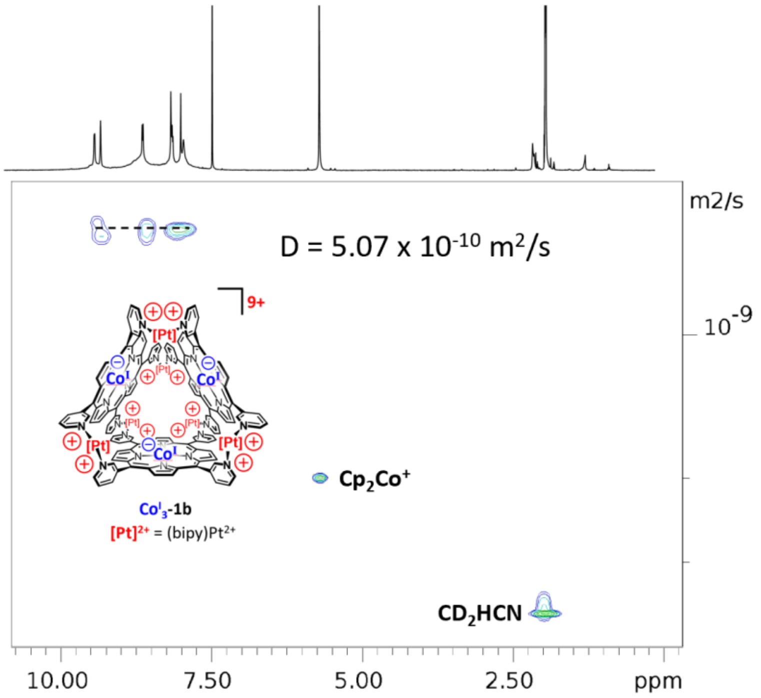

Figure S44. Diffusion ordered (DOSY) ^{1}H NMR spectrum of **Co^I_3-1b** generated in situ by reducing **Co_3-1b**•12PF_6 with a slight excess of Cp_2Co in CD_3CN. The experimental diffusion constant (5.07 x 10^{-10} m^2/s) corresponds to a spherical hydrodynamic radius[6] of 12.69 Å.

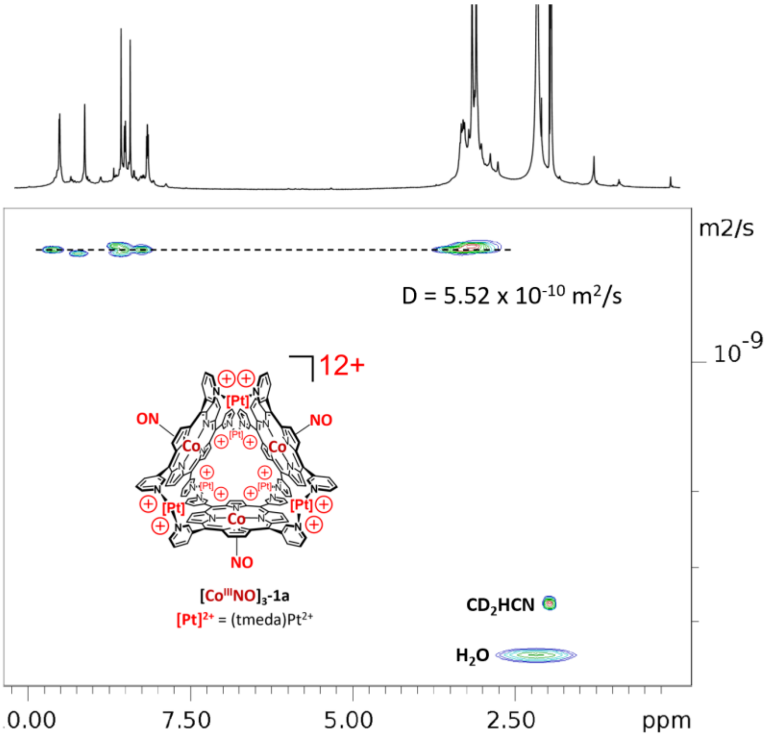

Figure S45. Diffusion ordered (DOSY) ^{1}H NMR spectrum of **[Co^{III}NO]$_3$-1a** generated in situ from **Co$_3$-1a**•12PF$_6$ in CD$_3$CN. The experimental diffusion constant (5.52 x 10^{-10} m^2/s) corresponds to a spherical hydrodynamic radius[6] of 11.65 Å.

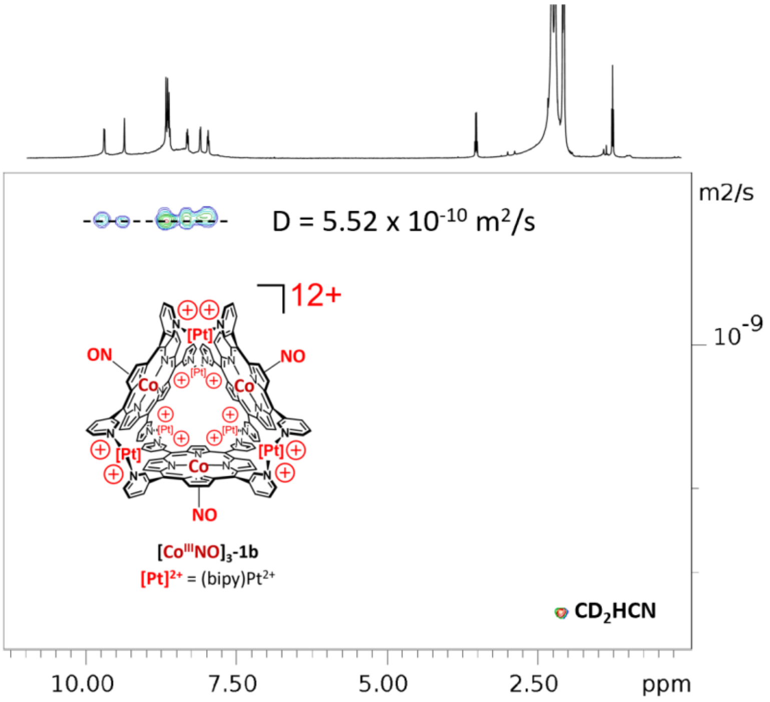

Figure S46. Diffusion ordered (DOSY) ^{1}H NMR spectrum of **[Co^{III}NO]$_3$-1b** generated in situ from **Co$_3$-1b**•12PF$_6$ in CD$_3$CN. The experimental diffusion constant (5.52 x 10^{-10} m^2/s) corresponds to a spherical hydrodynamic radius[6] of 11.65 Å.

7. ESI-MS characterization

High resolution mass spectra were obtained using a Waters Xevo G2-XS QTOF mass spectrometer using an ESI source and positive ion detection. Samples of the complexes (0.01 mmol) in MeCN were introduced by direct infusion (5 µL/min). A standard of Leu-Enkephalin (Waters, Milford, MA) was injected in tandem with the sample for in-process calibration.

7.a. Complex **2**

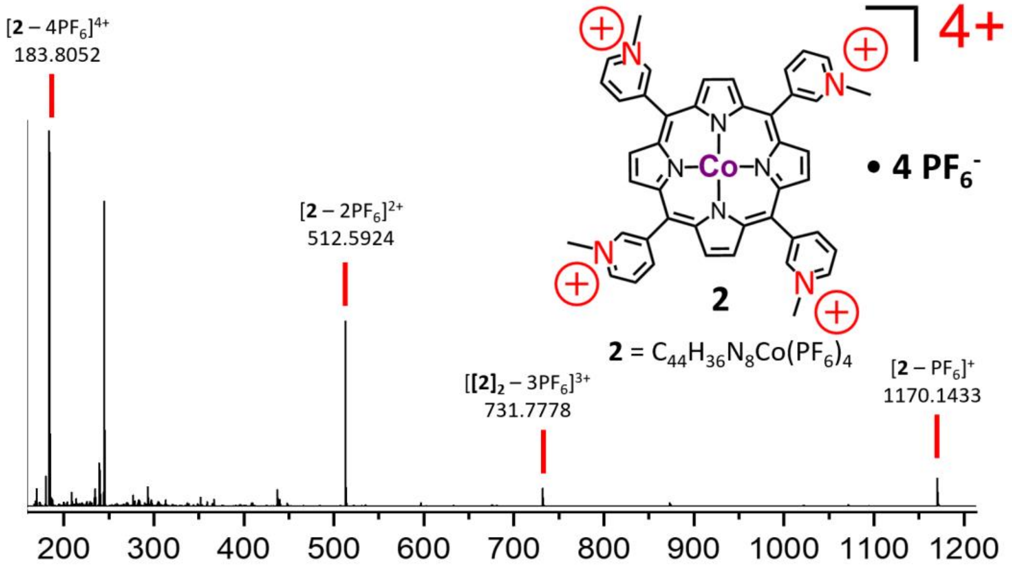

Figure S47. ESI(+)-MS spectrum of **2**•4PF$_6$, showing successive loss of PF$_6^-$ anions, as well as a dimer of two units of **2** held together by five PF$_6^-$ anions ([[**2**]$_2$ – 3PF$_6$]$^{3+}$).

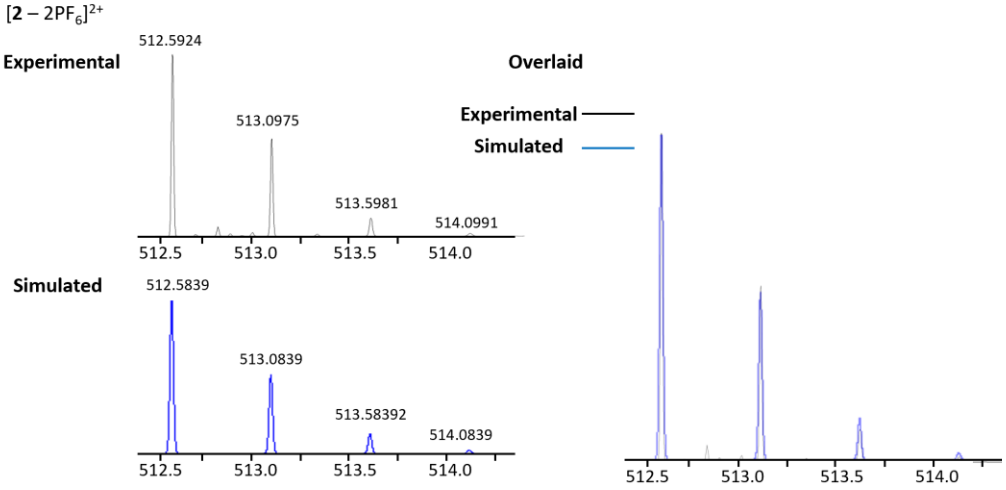

Figure S48. Comparison of the experimental (black) and simulated (blue) isotope patterns of the [**2** – 2PF$_6$]$^{2+}$ mass peak. Overlaying the experimental and simulated isotope pattern shows good agreement

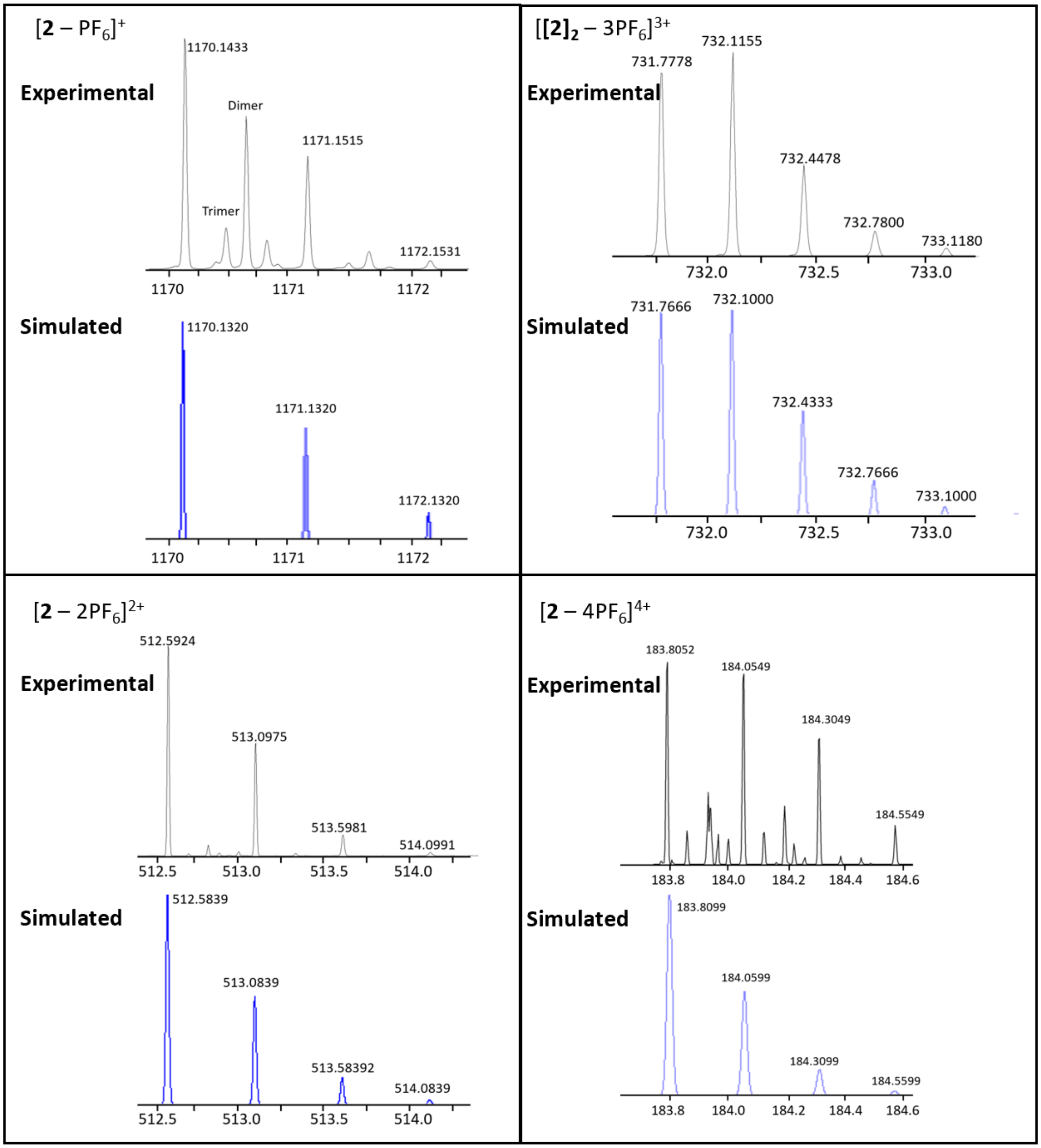

Figure S49. Comparison of the experimental (black) and simulated (blue) isotope patterns for the loss of 1, 2, and 4 $\mathrm{PF_6^-}$ anions from **2**, as well as the loss of 3 $\mathrm{PF_6^-}$ from the dimer **[2]₂**.

7.b. Cage **Co₃-1a**

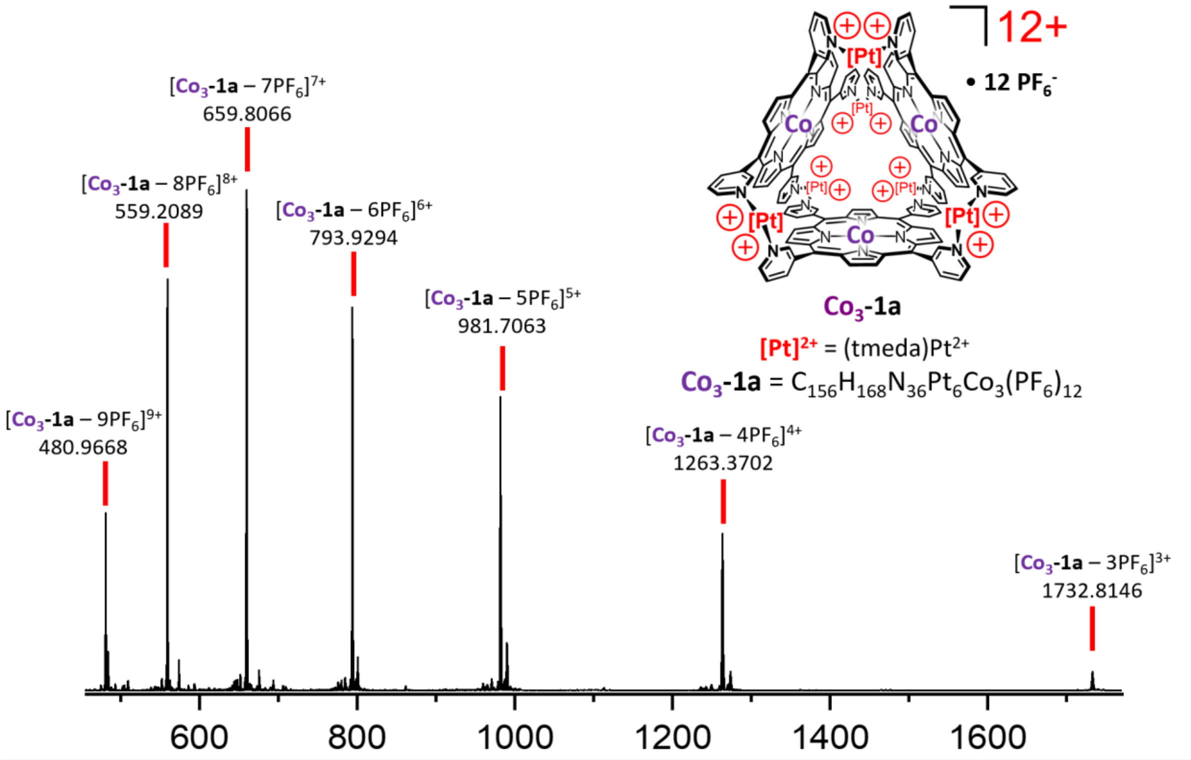

Figure S50. ESI(+)-MS spectrum of **Co₃-1a**•12PF₆, showing successive loss of PF₆⁻ anions.

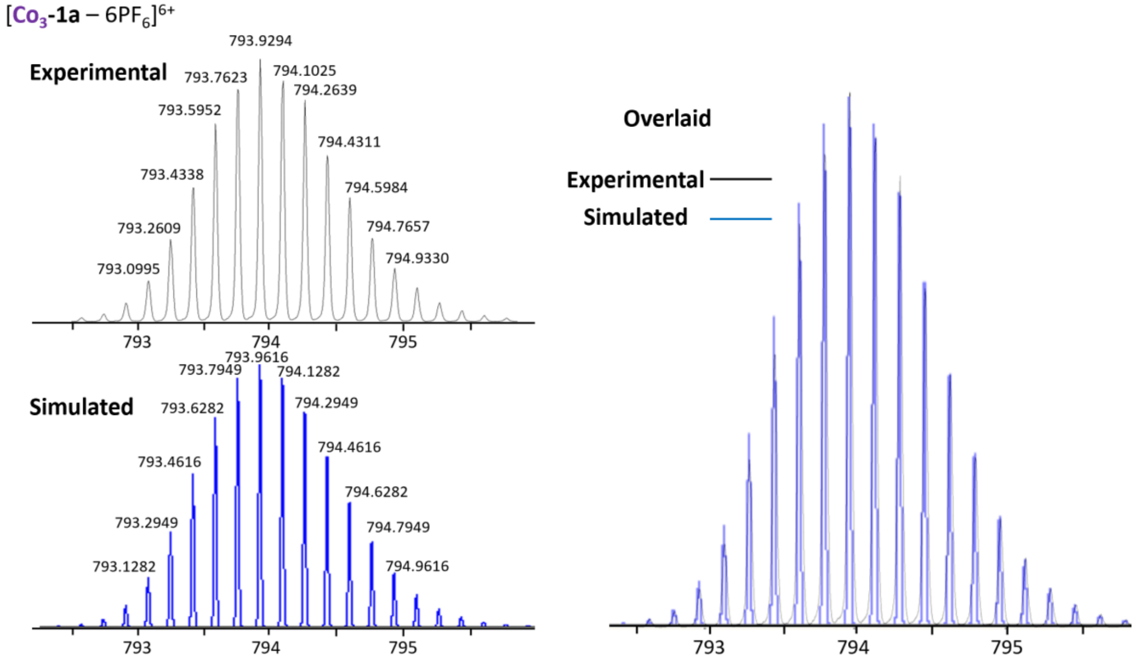

Figure S51. Comparison of the experimental (black) and simulated (blue) isotope patterns of the [**Co₃-1a** – 6PF₆]$^{6+}$ mass peak. Overlaying the experimental and simulated isotope pattern shows good agreement.

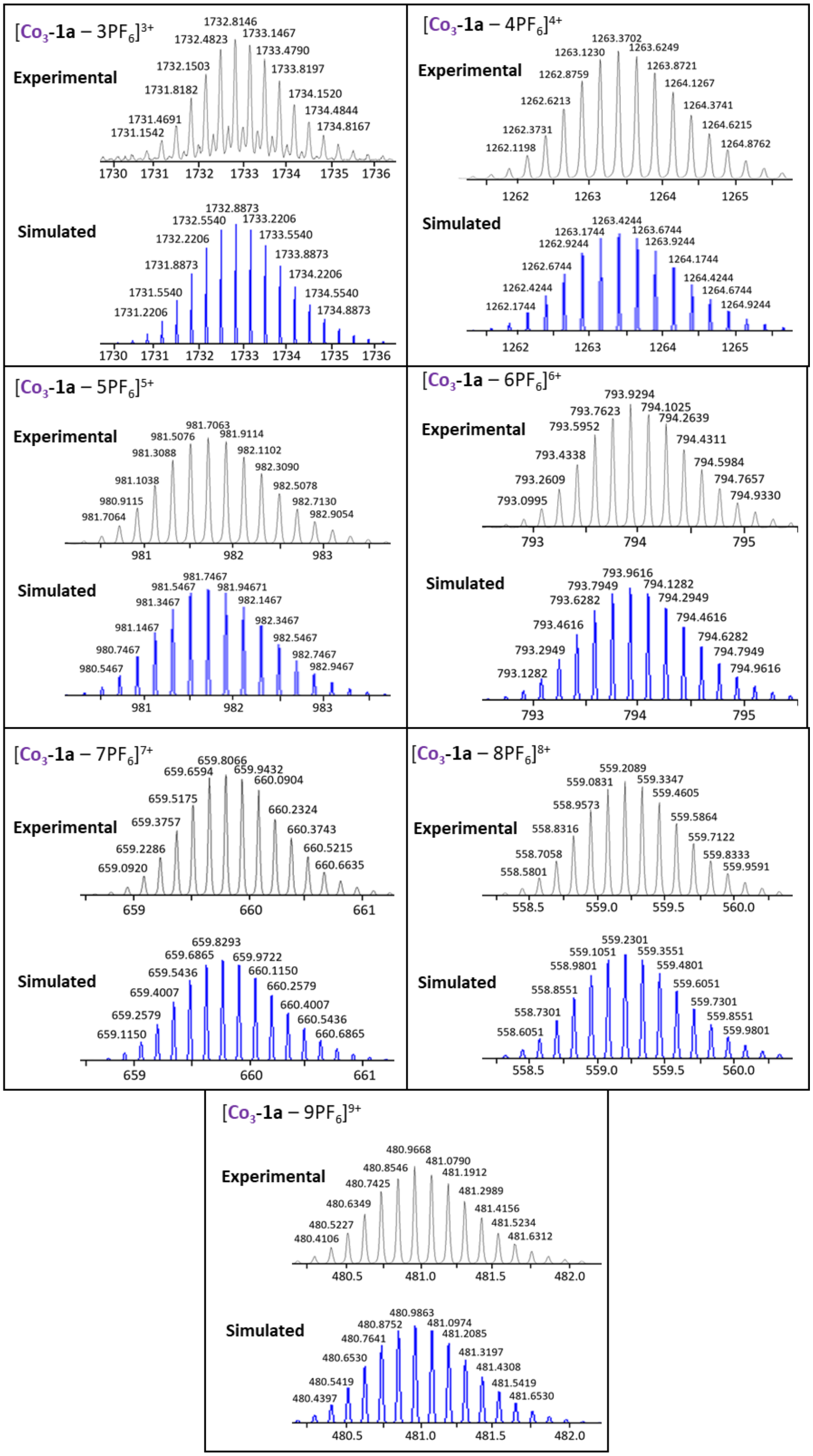

Figure S52. Comparison of the experimental (black) and simulated (blue) isotope patterns for the loss of 3 to 9 PF_6^- anions from **Co$_3$-1a**.

7.c. Cage **Co_3-1b**

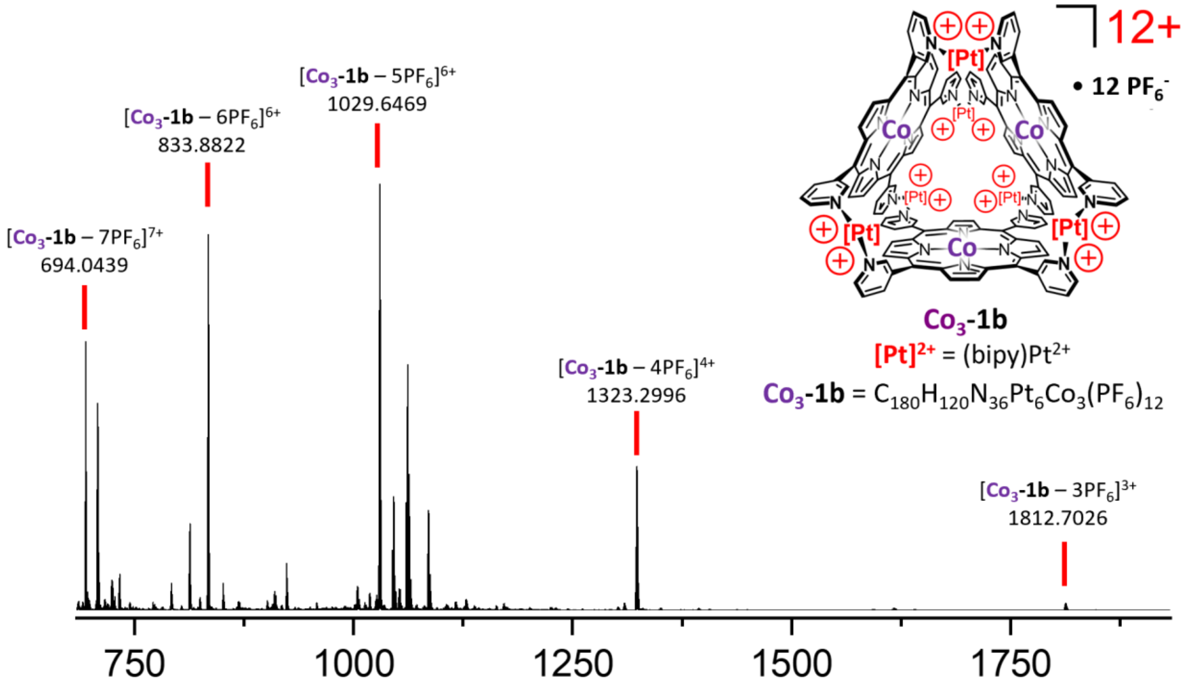

Figure S53. ESI(+)-MS spectrum of **Co_3-1b**•12PF_6, showing successive loss of PF_6^- anions.

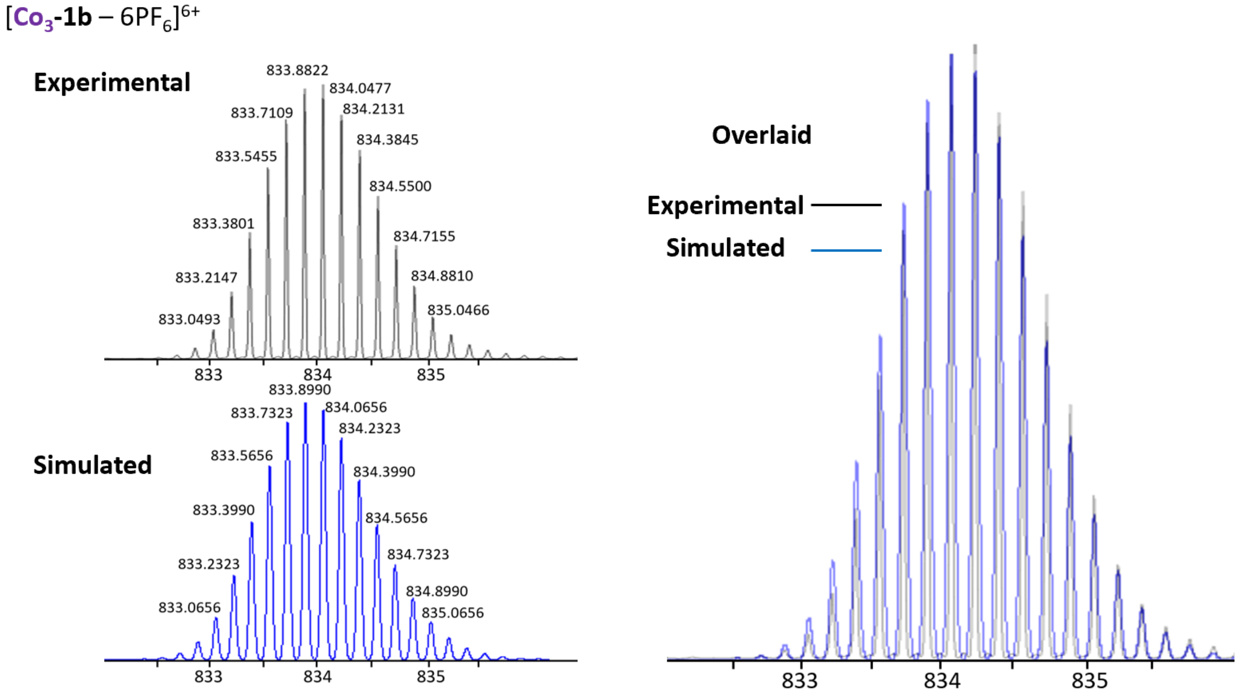

Figure S54. Comparison of the experimental (black) and simulated (blue) isotope patterns of the [**Co_3-1b** – 6PF_6]$^{6+}$ mass peak. Overlaying the experimental and simulated isotope pattern shows good agreement.

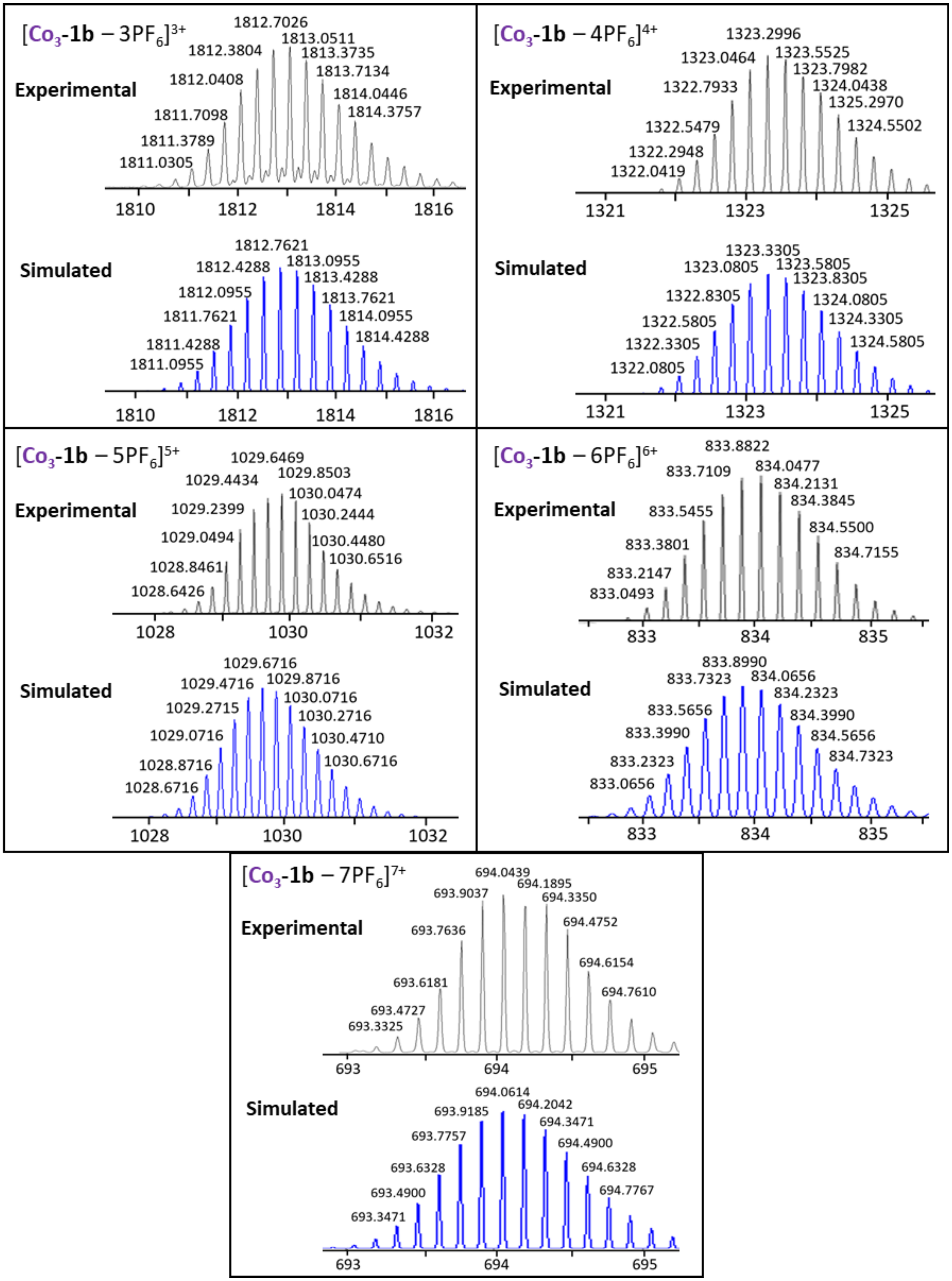

Figure S55. Comparison of the experimental (black) and simulated (blue) isotope patterns for the loss of 3 to 7 PF_6^- anions from **Co$_3$-1b**.

7.d. Cage **Zn$_3$-1a**

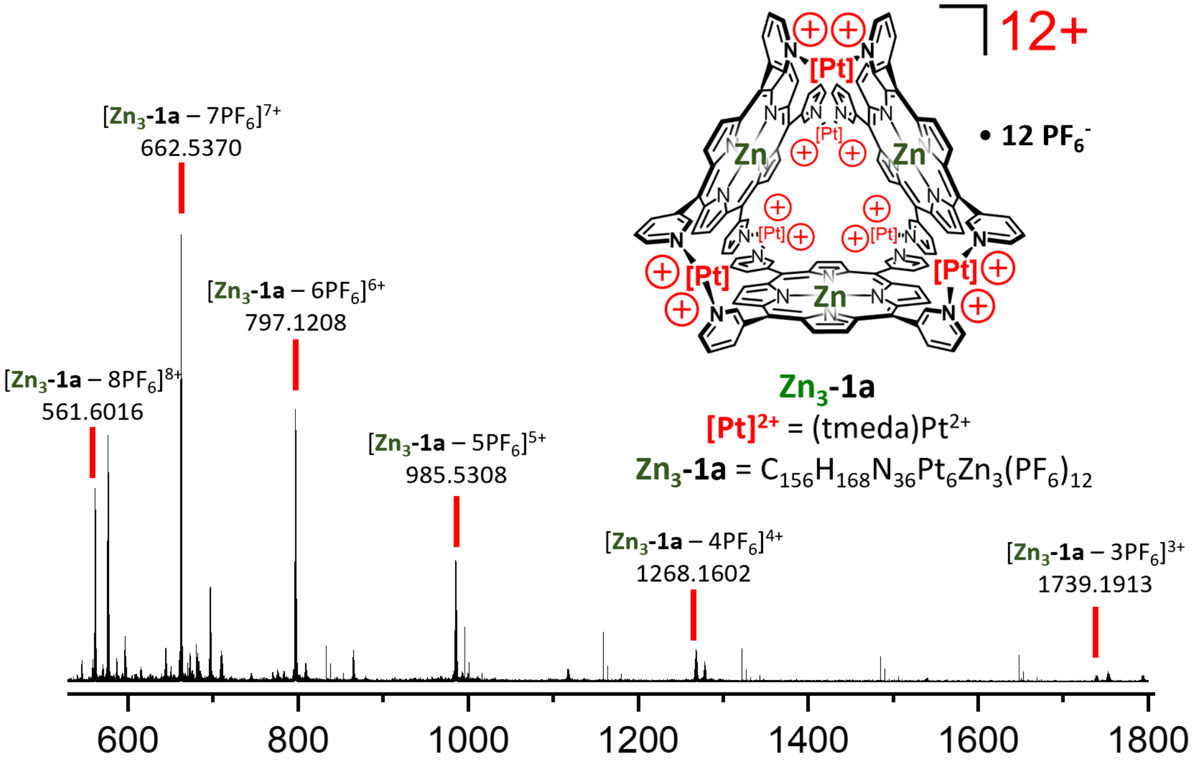

Figure S56. ESI(+)-MS spectrum of **Zn$_3$-1a**•12PF$_6$, showing successive loss of PF$_6^-$ anions.

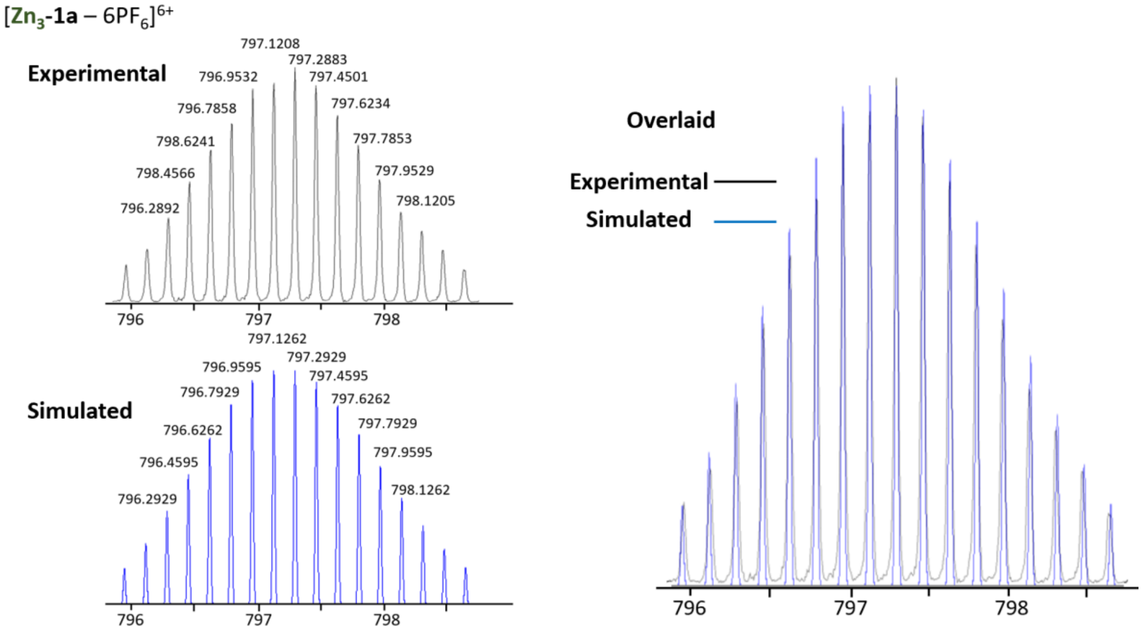

Figure S57. Comparison of the experimental (black) and simulated (blue) isotope patterns of the [**Zn$_3$-1a** – 6PF$_6$]$^{6+}$ mass peak. Overlaying the experimental and simulated isotope pattern shows good agreement.

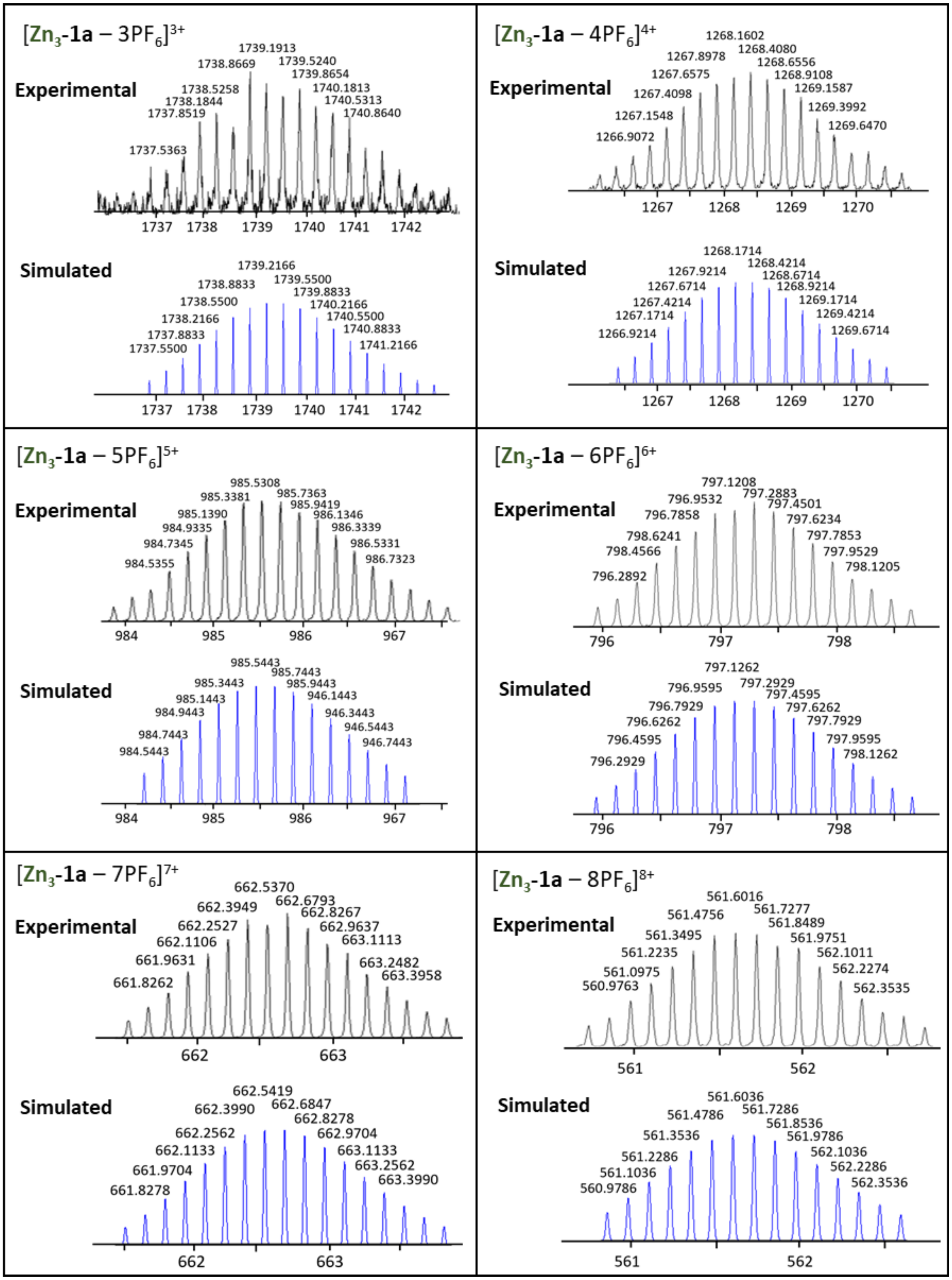

Figure S58. Comparison of the experimental (black) and simulated (blue) isotope patterns for the loss of 3 to 8 PF_6^- anions from **Zn_3-1a**.

7.e. Cage **Zn₃-1b**

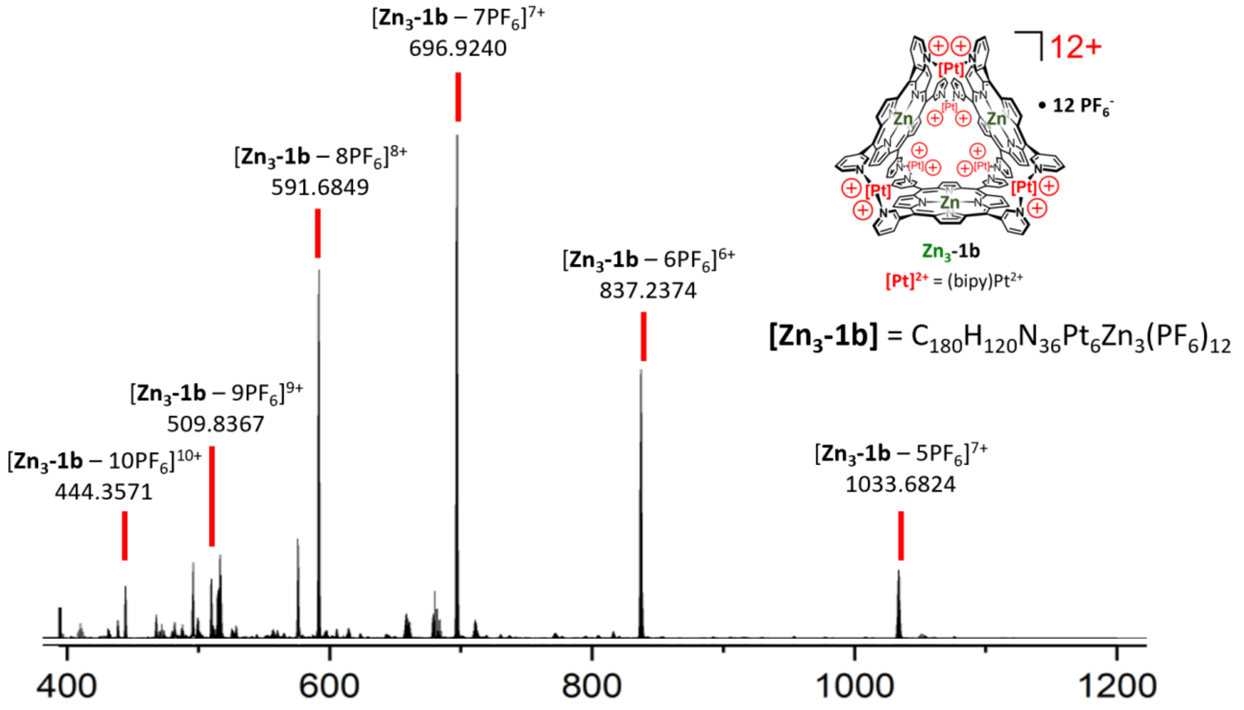

Figure S59. ESI(+)-MS spectrum of **Zn_3-1b**•12PF_6, showing successive loss of PF_6^- from **Zn_3-1b.**

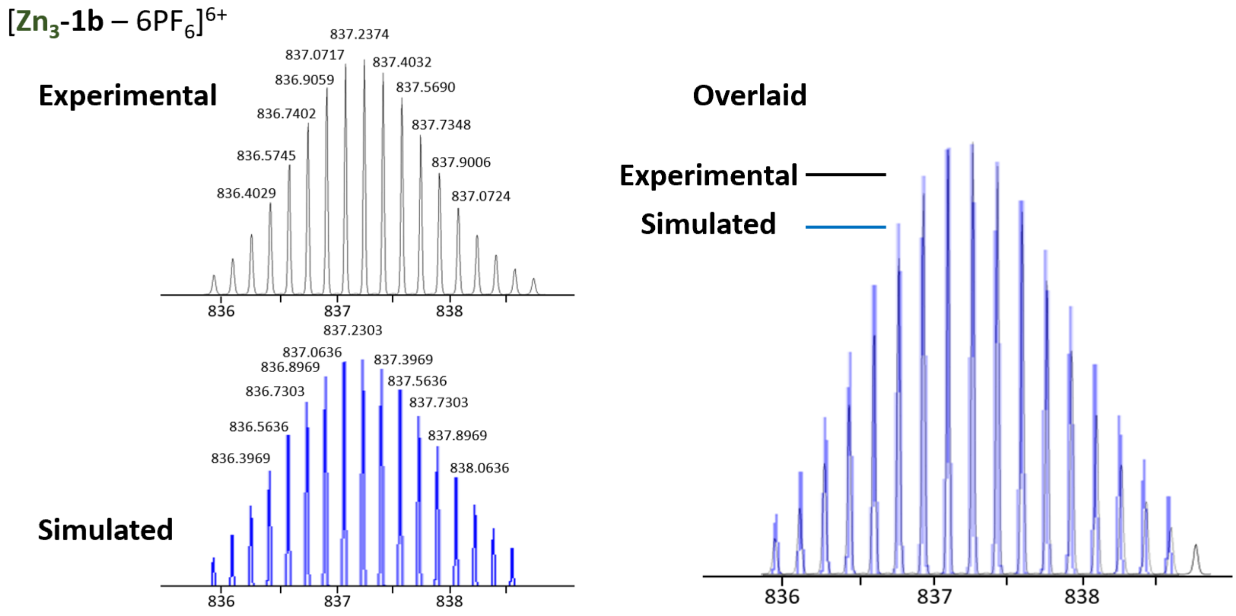

Figure S60. Comparison of the experimental (black) and simulated (blue) isotope patterns of the [**Zn_3-1b** – 6PF_6]$^{6+}$ mass peak. Overlaying the experimental and simulated isotope pattern shows good agreement.

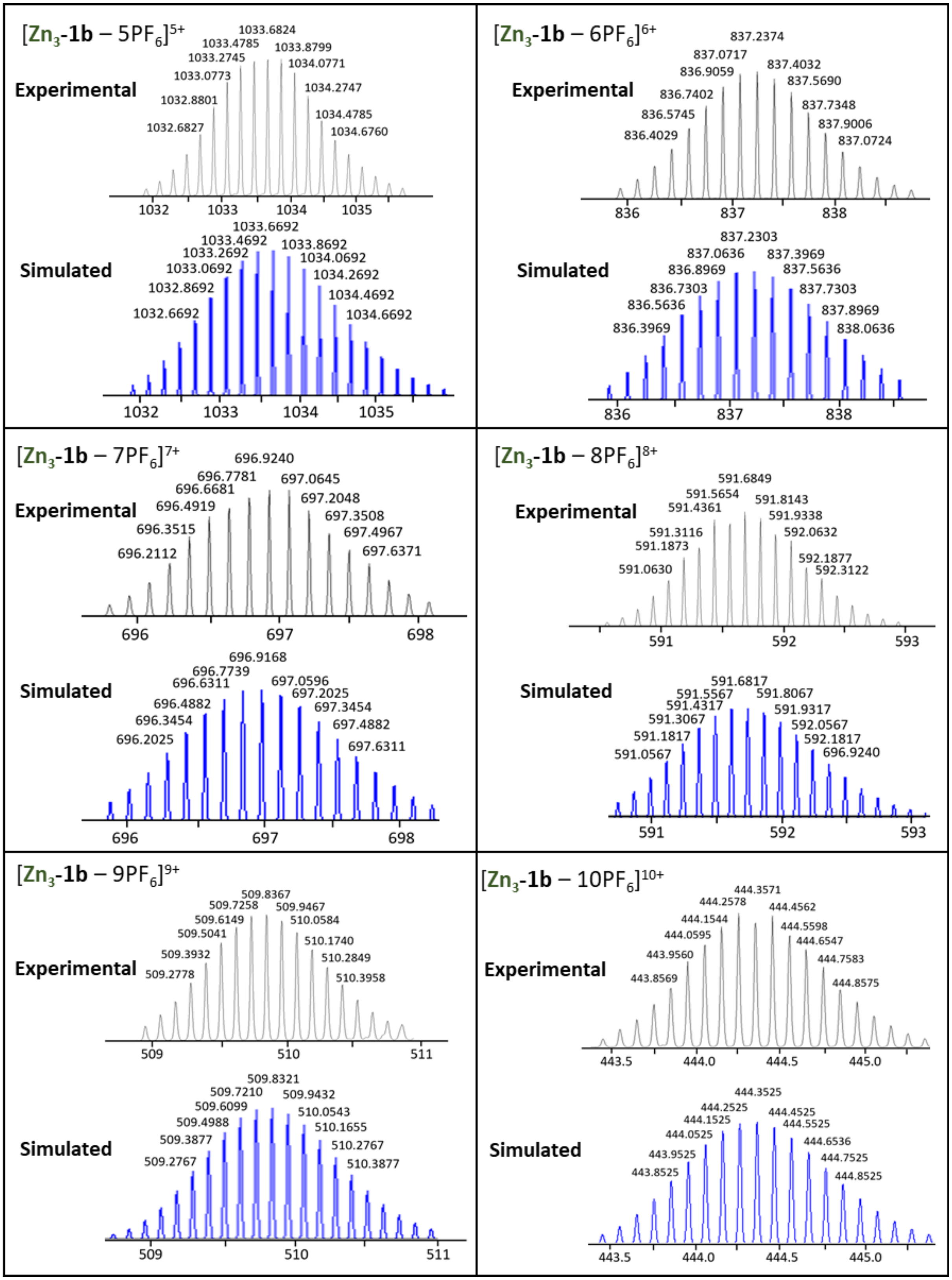

Figure S61: Comparison of the experimental (black) and simulated (blue) isotope patterns for the loss of 5 to 10 PF_6^- anions from **Zn$_3$-1b**.

8. EPR Spectroscopy

EPR experiments were performed using a Bruker Elexsys580e EPR spectrometer operating at X-band microwave frequency. Samples of Co^{II} derivatives were prepared in an air-free mixture of MeCN/toluene (50/50). All experiments were carried out at a temperature of 77 K (with samples kept cold inside a liquid nitrogen finger dewar), a microwave frequency of 9.534 GHz, a microwave power of 2 mW, and a modulation amplitude of 1 mT. Concentrations of the Co^{II} complexes were determined by comparing the integrated EPR signal intensities with an EPR standard of a known number of spins (a $CuSO_4{\cdot}5H_2O$ crystal of known weight in a mineral oil). All EPR simulations were performed using the EasySpin toolbox for MATLAB.[7]

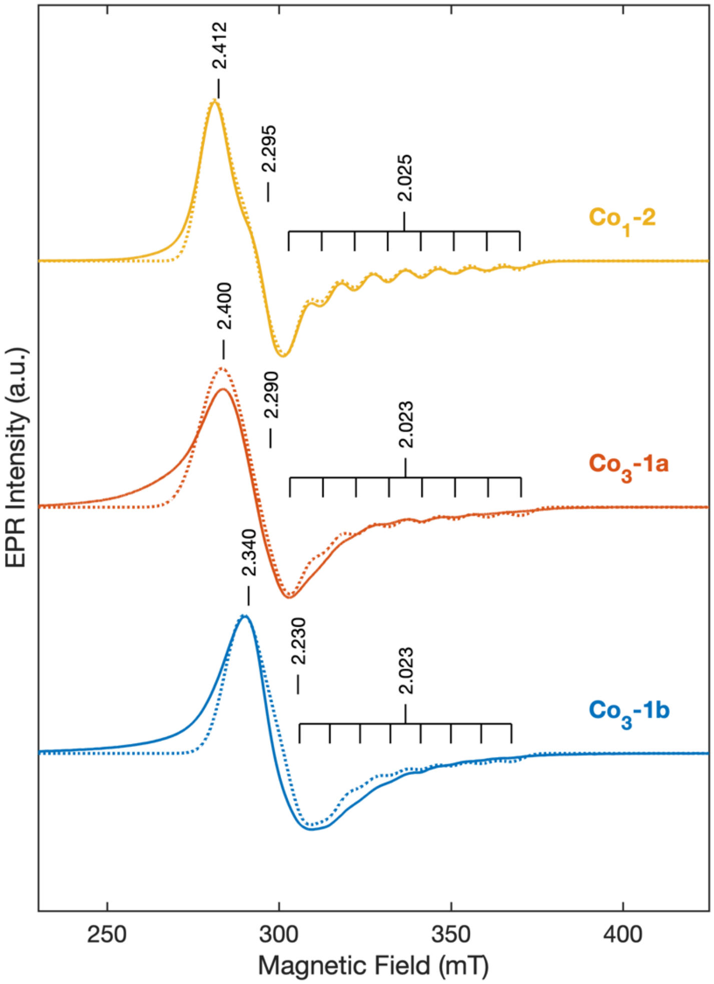

Figure S62. EPR spectra of the monomeric Co^{II} porphyrin complex **2** (3 mM) and the tris-Co^{II} nanoprisms **Co$_3$-1a** (1 mM) and **Co$_3$-1b** (1 mM) in frozen MeCN/toluene (50/50) at 77 K. The experimental spectra are presented with solid lines, and dashed lines depict EPR simulations. Three principal g-factor values are identified in each spectrum along with octets of split lines around g_3 due to hyperfine interactions with ^{59}Co (I = 7/2). Remaining EPR parameters, including full ^{59}Co hyperfine tensors and anisotropic peak broadening, are discussed below. The nanoprisms **Co$_3$-1a** and **Co$_3$-1b** both show noticeably broader EPR peak linewidths as compared to monomeric Co^{II} porphyrin complex **2**; this broadening is a signature of strong dipole-dipole couplings between three Co^{II} spins at a proximal distance of ~8 Å locked in each cage.

EPR characteristics of monomeric Co^{II} porphyrin complex 2

Complex **2** showed an anisotropic EPR signal (yellow solid line in Figure S62) with slightly rhombic g-factor tensors (g_x, g_y, g_z) = (2.412, 2.295, 2.025) and nearly axial ^{59}Co hyperfine tensors (A_x, A_y, A_z) = (17 ± 5, 19 ± 5, 269 ± 2) MHz. This signal is characteristic of a low spin d^7 electron configuration, with an unpaired electron residing on the d_{z2} orbital in Co^{II}. Similar EPR signals, both in terms of g-factors and ^{59}Co hyperfine coupling tensors, have been reported for several Co^{II} porphyrin complexes that include a fifth N-donor ligand coordinated at the axial position.[8.9] While the exact nature of this fifth axial ligand in **2** remains unknown, it is most probably a nitrile nitrogen of solvent MeCN. Strong unresolved ^{14}N hyperfine coupling to this axial MeCN ligand is the main reason for the broad linewidth (ΔB = 5.5 mT) observed in the EPR spectrum of **2**.

EPR characteristics of tris-Co^{II} nanoprisms Co$_3$-1a and Co$_3$-1b

The EPR spectra of **Co$_3$-1a** and **Co$_3$-1b** (red and blue traces in Figure S62, respectively) display the same symmetry in their g-factors and ^{59}Co hyperfine coupling tensors as observed for the monomeric complex **2** (yellow trace in Figure S62). The $g_{x,y}$ values and the ^{59}Co hyperfine A_z coupling in **Co$_3$-1a** and **Co$_3$-1b** show a small change from those in **2**, but remain in the range characteristic of Co^{II} porphyrin complexes with one additional ligand coordinated in an axial position.[8,9] The biggest difference between the EPR spectra of **Co$_3$-1a,b** and that of **2** is a substantially broader EPR linewidth for the nanoprisms. The broader linewidth for **Co$_3$-1a**,**b** is most clearly evident when inspecting the resolution of the ^{59}Co hyperfine splitting around g_z. In EPR simulations for **Co$_3$-1a**,**b** (red and blue dashed traces in Figure S62), an additional (anisotropic) linewidth broadening, ΔB_{dd}, was introduced to account for this broadening.

The EPR linewidth broadening in **Co$_3$-1a**,**b** most likely originates from dipole-dipole and spin-exchange couplings between the three Co^{II} spins held in close proximity. Assuming a perfect equilateral triangular geometry, a distance of ~8 Å is expected between the Co^{II} centres in **Co$_3$-1a**,**b**. At such a short distance, dipole-dipole interactions of a magnitude $D \sim 120$ MHz would be expected between the Co^{II} spins. This estimated D coupling is consistent with the additional (anisotropic) linewidth broadening, $\Delta B_{dd} \sim 120$-300 MHz, that was introduced when fitting the EPR spectra of **Co$_3$-1a**,**b**.

EPR simulation parameters

1. **Monomeric porphyrin Co$_1$-2**:

   Electron g-factor: (g_x, g_y, g_z) = (2.412, 2.295, 2.025)

   Electron g-factor strain: (δg_x, δg_y, δg_z) = (0.04, 0.06, 0.00)

   ^{59}Co hyperfine coupling tensor: (A_x, A_y, A_z) = (17 ± 5, 19 ± 5, 269 ± 2) MHz

   ^{59}Co hyperfine tensor strain: (δA_x, δA_y, δA_z) = (6, 10, 0) MHz

   Inhomogeneous EPR broadening: ΔB = 5.5 mT (resulting from unresolved hyperfine interactions to four pyrrole ^{14}N nitrogens, one additional ^{14}N nitrogen from the axially coordinated MeCN, and also several ^{1}H protons from porphyrin and solvent molecules)

2. **Tri-cage Co_3-1a** (tmeda):

   Electron g-factor: (g_x, g_y, g_z) = (2.40, 2.29, 2.023)

   Electron g-factor strain: (δg_x, δg_y, δg_z) = (0.08, 0.06, 0.00)

   ^{59}Co hyperfine coupling tensor: (A_x, A_y, A_z) = (17 ± 5, 19 ± 5, **269** ± 2) MHz

   ^{59}Co hyperfine tensor strain: (δA_x, δA_y, δA_z) = (6, 10, 0) MHz

   Inhomogeneous EPR broadening: ΔB = 5.5 mT

   Additional (anisotropic) EPR broadening: ΔB_{dd} = (200, 300, **120**) MHz (resulting from dipole-dipole couplings between three Co^{2+} electron spins locked in tri-cages)

3. **Tri-cage Co_3-1b** (bipy):

   Electron g-factor: (g_x, g_y, g_z) = (2.34, 2.23, 2.023)

   Electron g-factor strain: (δg_x, δg_y, δg_z) = (0.06, 0.08, 0.00)

   ^{59}Co hyperfine coupling tensor (A_x, A_y, A_z) = (17 ± 5, 19 ± 5, **249** ± 2) MHz

   ^{59}Co hyperfine tensor strain (δA_x, δA_y, δA_z) = (6, 10, 0) MHz

   Isotropic EPR broadening: ΔB = 5.5 mT

   Additional (anisotropic) EPR broadening: ΔB_{dd} = (200, 250, **140**) MHz

9. UV-vis-NIR characterization

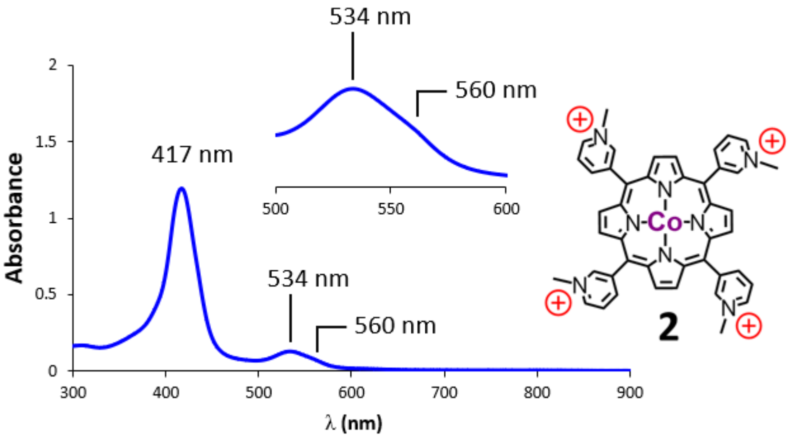

Figure S63. UV-vis spectrum (1 mm path) of a 0.1 mM solution of **2**•4PF$_6$ in MeCN. The inset shows an expanded view of the q-peak, revealing a shoulder at 560 nm.

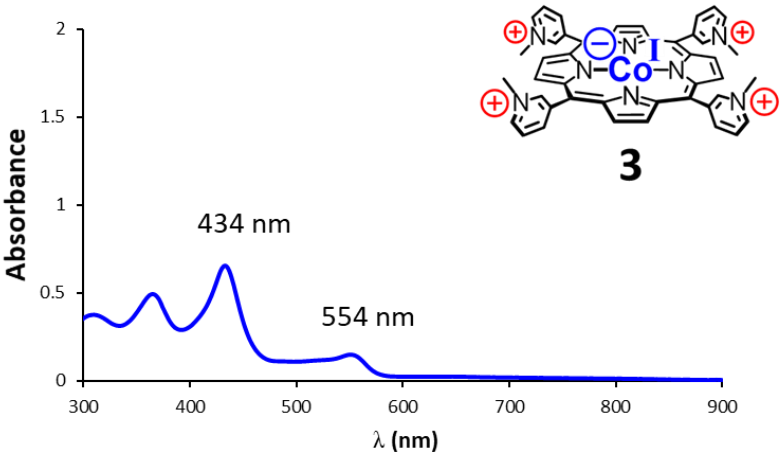

Figure S64. UV-vis spectrum (1 mm path) of a 0.1 mM solution of **3** in MeCN.

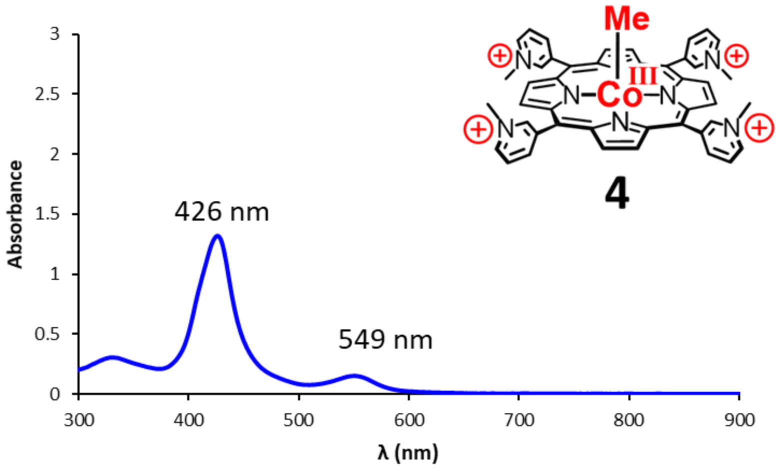

Figure S65. UV-vis spectrum (1 mm path) of a 0.1 mM solution of **4** in MeCN.

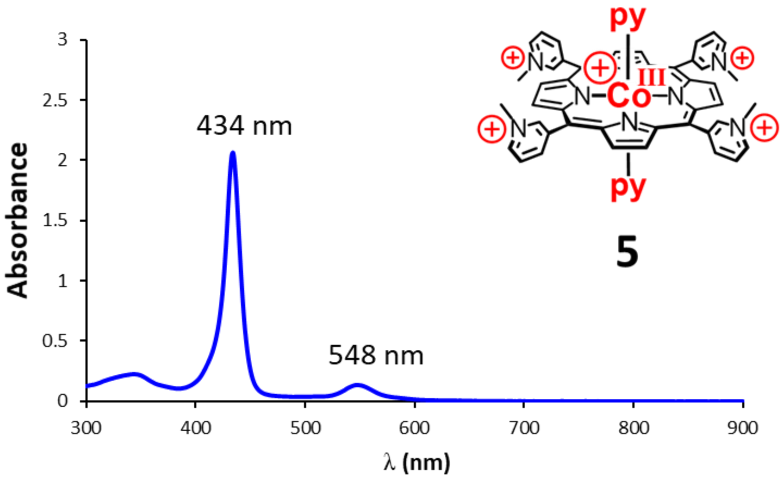

Figure S66. UV-vis spectrum (1 mm path) of a 0.1 mM solution of **5**•5PF$_6$ in MeCN.

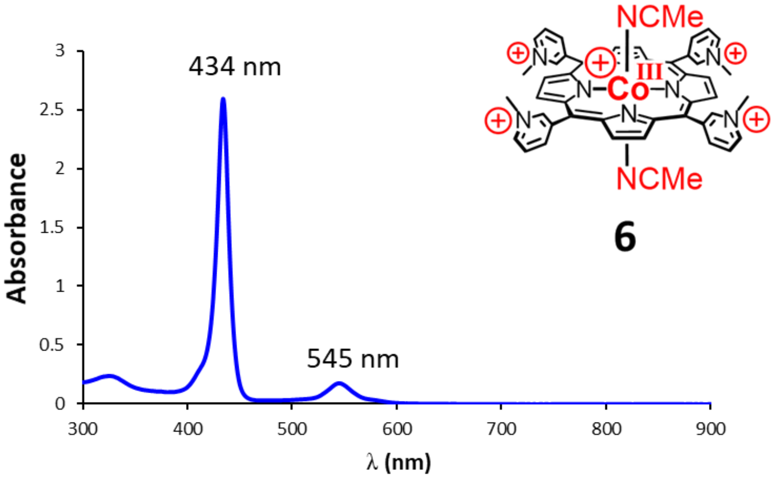

Figure S67. UV-vis spectrum (1 mm path) of a 0.1 mM solution of **6** in MeCN.

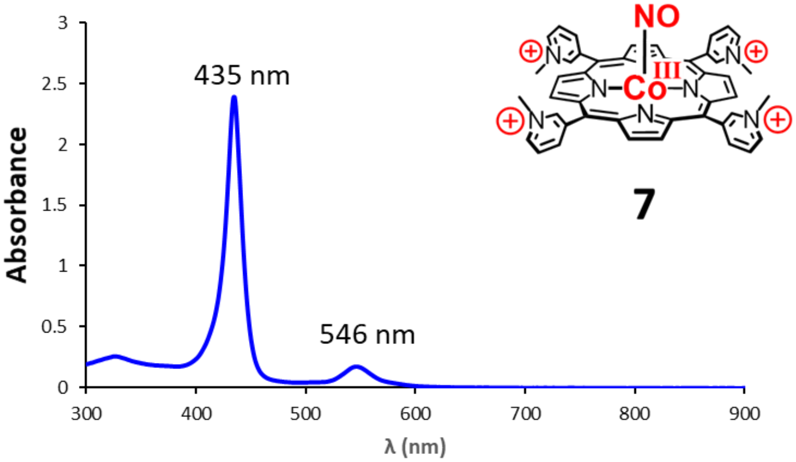

Figure S68. UV-vis spectrum (1 mm path) of a 0.1 mM solution of **7**•4PF$_6$ in MeCN.

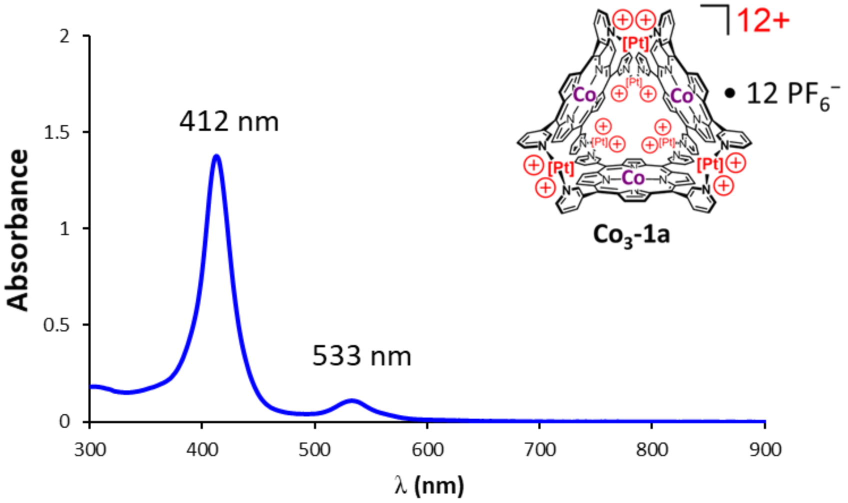

Figure S69. UV-vis spectrum (1 mm path) of a 0.033mM solution of **Co_3-1a**•12PF_6 in MeCN.

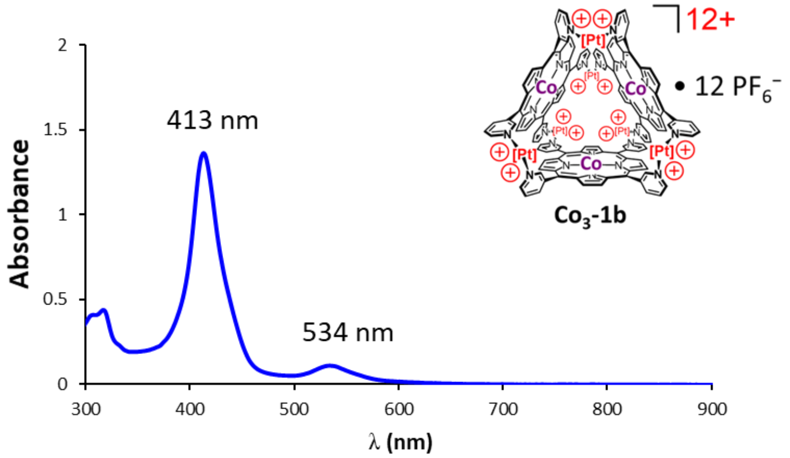

Figure S70. UV-vis spectrum (1 mm path) of a 0.033mM solution of **Co_3-1b**•12PF_6 in MeCN.

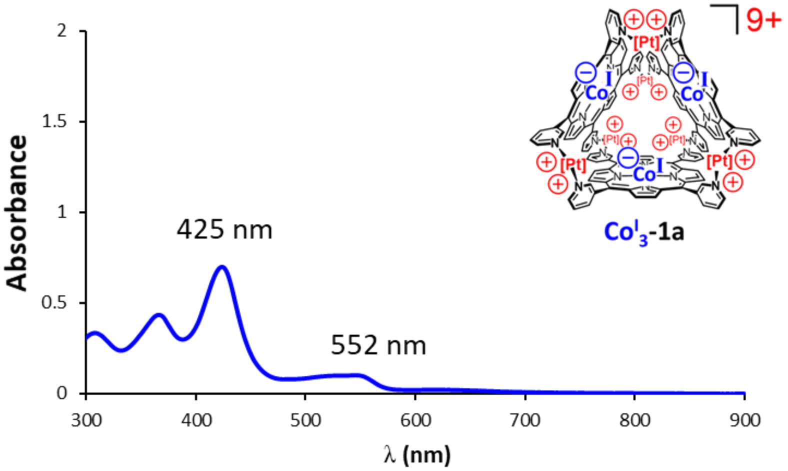

Figure S71. UV-vis spectrum (1 mm path) of a 0.033mM solution of **Co^I_3-1a** in MeCN.

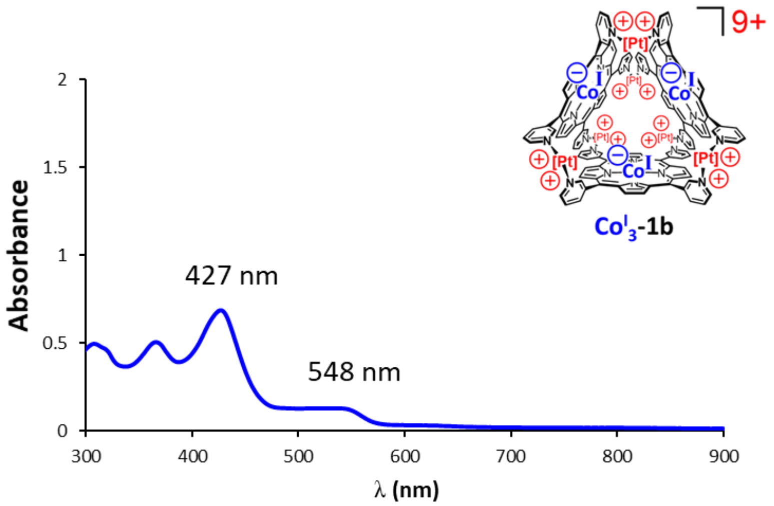

Figure S72. UV-vis spectrum (1 mm path) of a 0.033mM solution of **Co$^{I}_{3}$-1b** in MeCN.

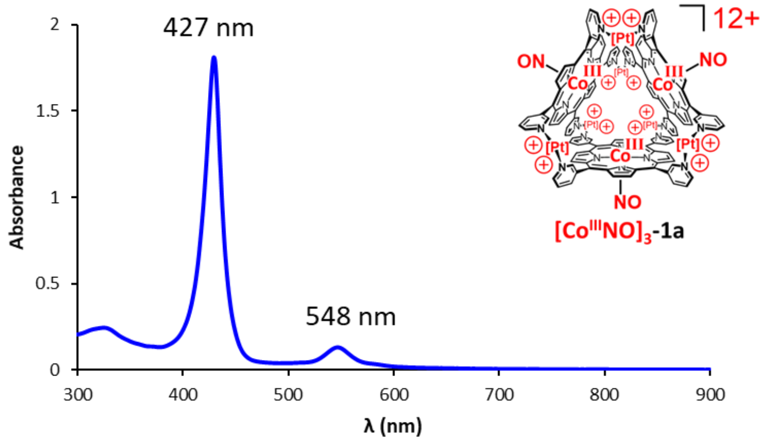

Figure S73. UV-vis spectrum (1 mm path) of a 0.033 mM solution of **[Co^{III}NO]$_3$-1a** in MeCN.

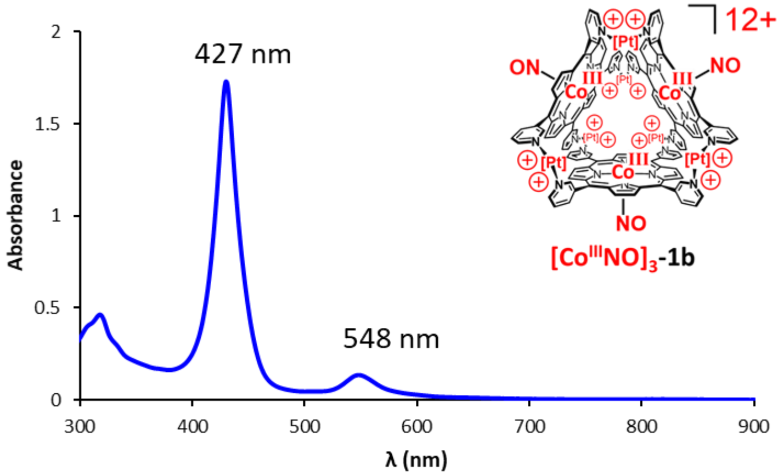

Figure S74. UV-vis spectrum (1 mm path) of a 0.033mM solution of **[Co^{III}NO]$_3$-1b** in MeCN.

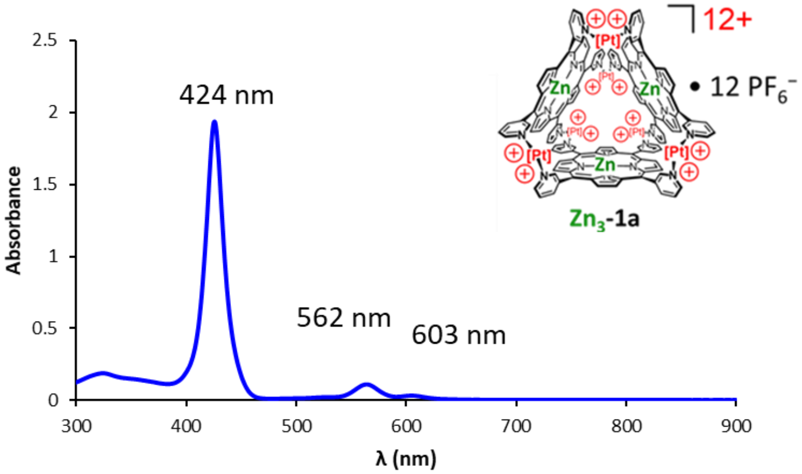

Figure S75. UV-vis spectrum (1 mm path) of a 0.033mM solution of **Zn_3-1a**•12PF_6 in MeCN.

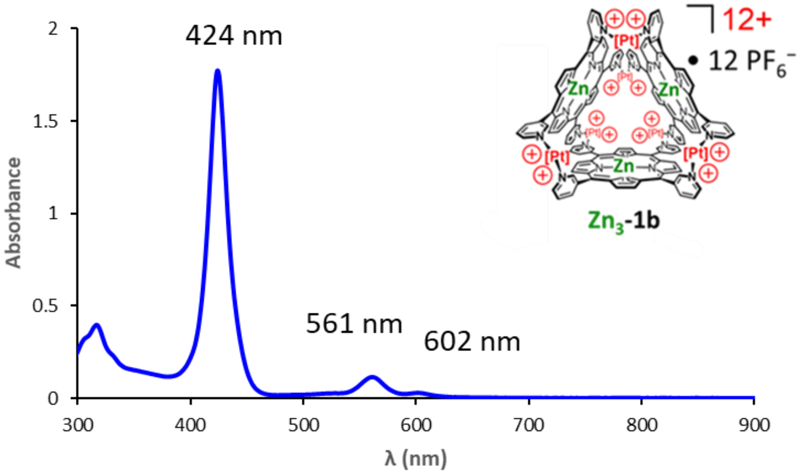

Figure S76. UV-vis spectrum (1 mm path) of a 0.033mM solution of **Zn_3-1b**•12PF_6 in MeCN.

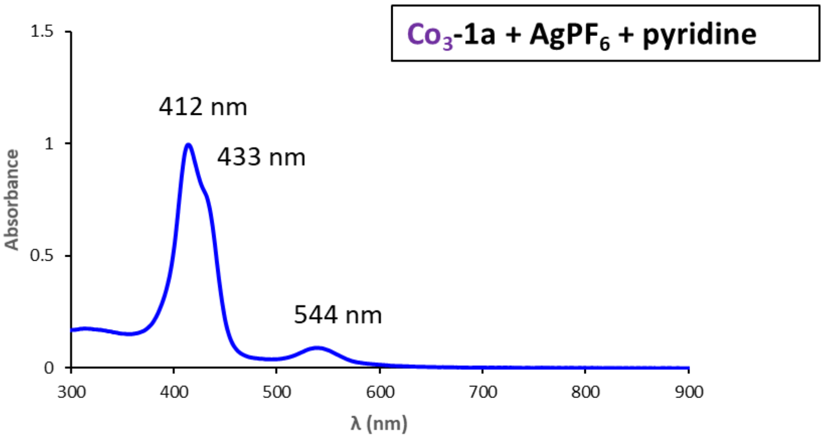

Figure S77. UV-vis spectrum (1 mm path) of a 0.033mM solution of **Co_3-1a**•12PF_6 after addition of 9 equiv. of $AgPF_6$ and 6 equiv. pyridine in MeCN.

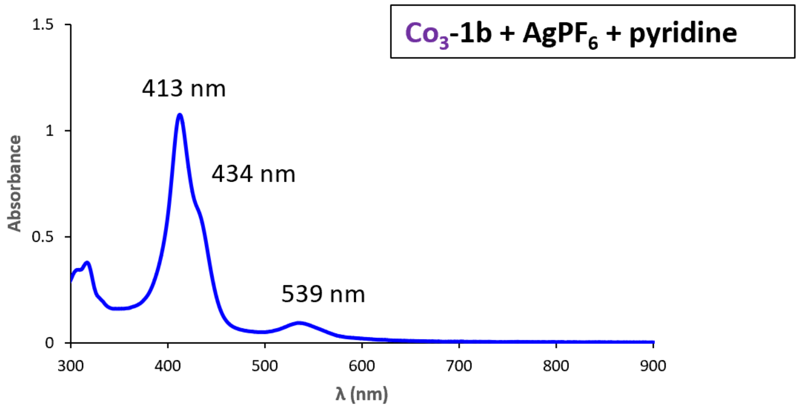

Figure S78. UV-vis spectrum (1 mm path) of a 0.033mM concentration solution of **Co_3-1b**•12PF_6 after addition of 9 equiv. of $AgPF_6$ and 6 equiv. pyridine in MeCN.

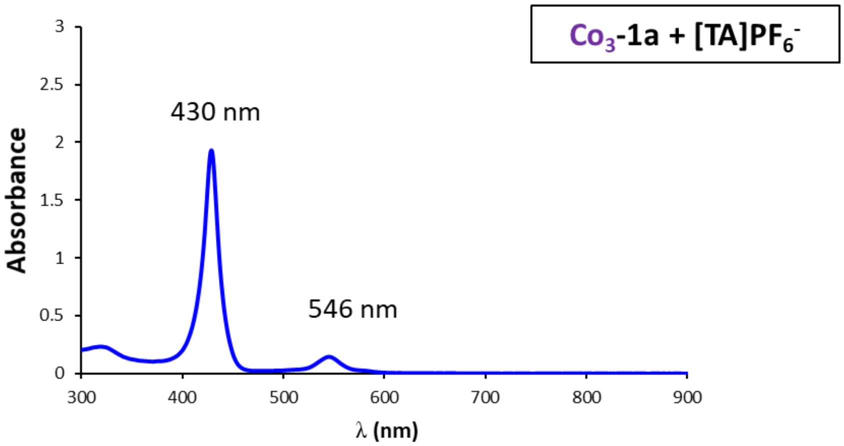

Figure S79. UV-vis spectrum (1 mm path) of a 0.033mM concentration solution of **Co_3-1a**•12PF_6 after addition of 3 equiv. of thianthrenium hexafluorophosphate ([TA]PF_6) in MeCN.

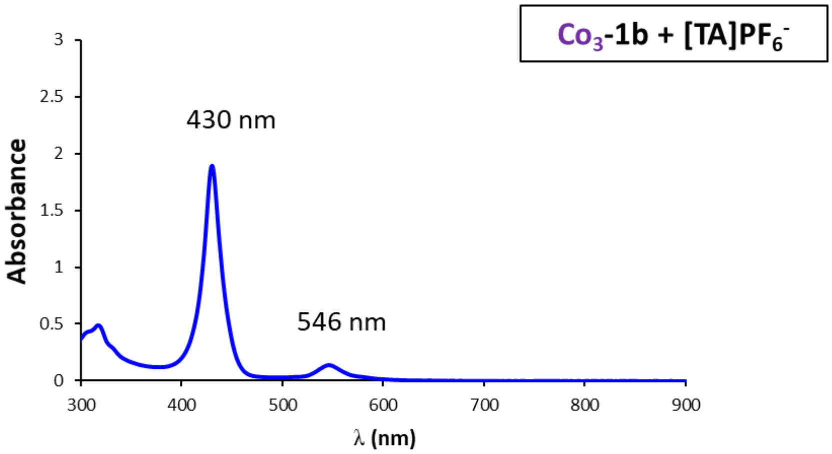

Figure S80. UV-vis spectrum (1 mm path) of a 0.033mM concentration solution of **[Co_3-1b]**•12PF_6 after addition of 3 equiv. of thianthrenium hexafluorophosphate ([TA]PF_6) in MeCN.

10. Cyclic Voltammetry

Cyclic voltammograms (CVs) were recorded with a CH Instruments 600E potentiostat. Dry MeCN was used as the solvent with 0.1 M tetrabutylammonium hexafluorophosphate (TBAPF$_6$) as a supporting electrolyte. CVs were recorded using a 3 mm glassy carbon working electrode, a platinum wire counter electrode, and a silver wire pseudoreference electrode which was confined in a polypropylene body that provided contact with the analyte solution via a porous zeolite bead or a glass frit. Potentials were referenced to the Fc$^{+/0}$ couple of an internal ferrocene standard or by calibrating the pseudo-reference electrode vs. the Fc$^{+/0}$ couple of an external solution of ferrocene immediately before use (note: keeping the pseudo-reference electrode isolated from the bulk sample limits drift of the reference potential over numerous CV experiments). For clarity, we present the CVs that do not include the Fc$^{+/0}$ wave, and in all cases the measured potentials of redox processes were consistent with those determined with the internal Fc$^{+/0}$ redox couple included along with the analyte. Positive feedback iR compensation was applied during all CV experiments. The 2nd cycle out of three is presented unless otherwise stated.

10.a. CVs of Complex **2**

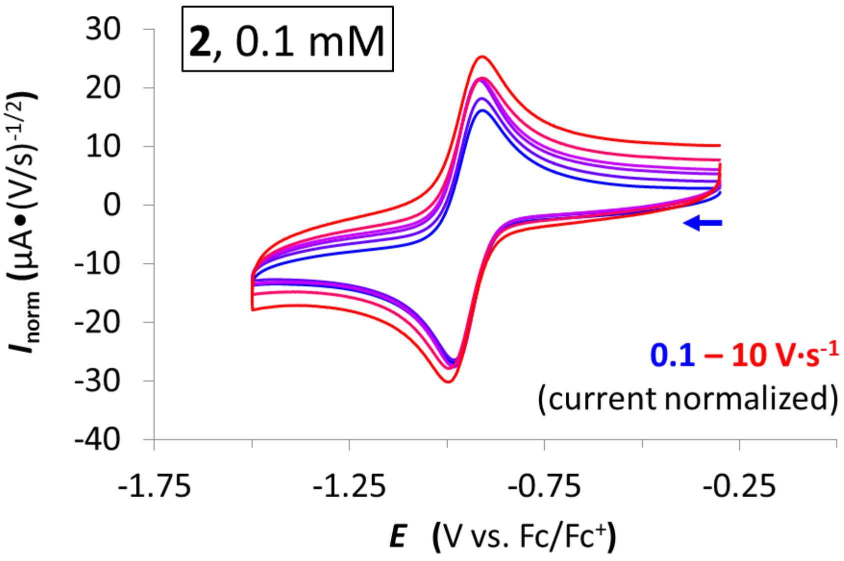

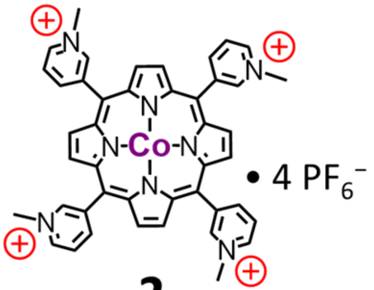

2

Figure S81. Cyclic voltammogram measured from −0.30 V to −1.50 V vs Fc$^{0/+}$ on a 0.1 mM solution of **2**•4PF$_6$ in MeCN containing 0.1 M TBAPF$_6$ as a supporting electrolyte. CVs were recorded at a scan rate of 100 mV·s^{-1}, 200 mV·s^{-1}, 500 mV·s^{-1}, 1 V·s^{-1}, 5 V·s^{-1}, and 10 V·s^{-1} with the current scaled by the square root of the scan rate. These CVs show the reversible Co^{II}/Co^{I} redox couple of **2** at $E_{1/2}$= −0.95 V vs. Fc$^{0/+}$.

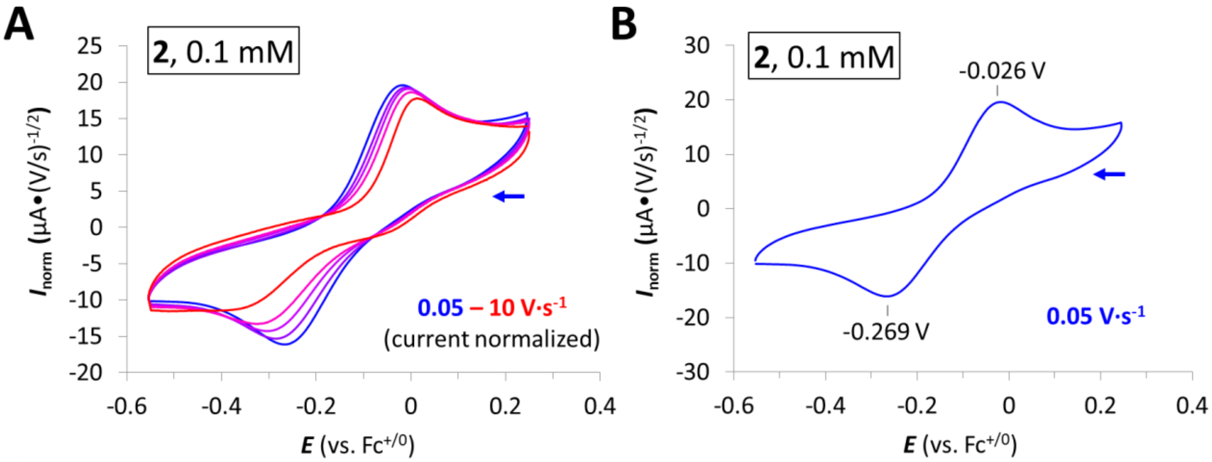

Figure S82. Cyclic voltammograms measured from +0.25 V to −0.55 V vs Fc$^{0/+}$ on a 0.1 mM solution of **2**•4PF$_6$ in MeCN containing 0.1 M TBAPF$_6$ as a supporting electrolyte. (A) CVs recorded at a scan rate of 50 mV·s^{-1}, 100 mV·s^{-1}, 200 mV·s^{-1}, 500 mV·s^{-1}, 1 V·s^{-1}, 5 V·s^{-1}, and 10 V·s^{-1} with the current scaled by the square root of the scan rate. (B) CV recorded at a scan rate of 50 mV·s^{-1}, from which the $E_{1/2}$ value of −0.15 V was determined for the quasireversible Co^{III}/Co^{II} of **2**.

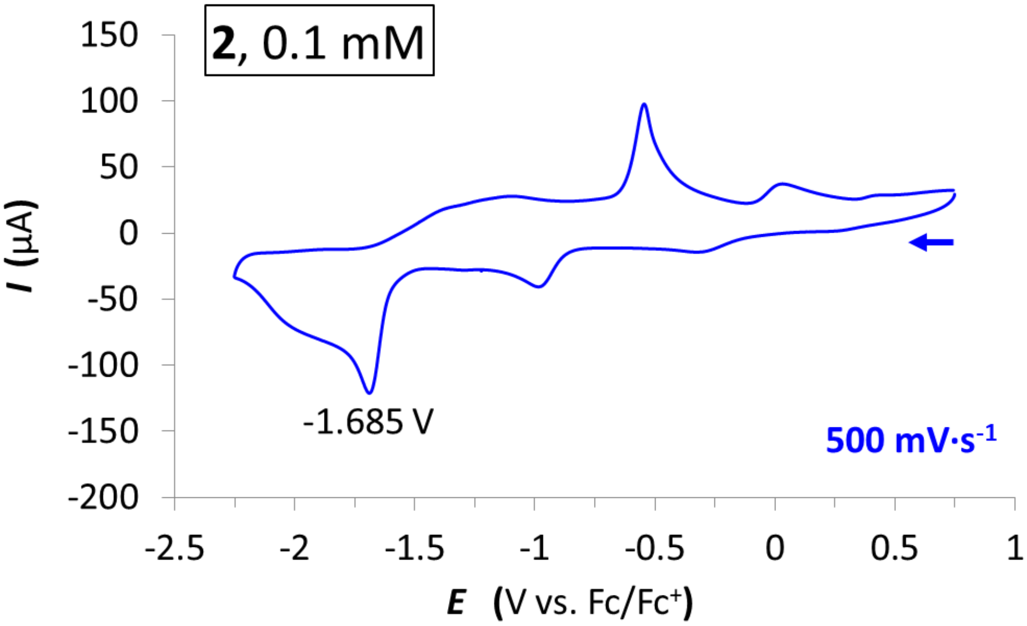

Figure S83. Cyclic voltammogram measured from +0.75 V to −2.25 V vs Fc$^{0/+}$ on a 0.1 mM solution of **2**•4PF$_6$ in MeCN containing 0.1 M TBAPF$_6$ as a supporting electrolyte, recorded at a scan rate of 500 mV·s^{-1}. The cathodic wave at E_{pc} = −1.685 V is attributed to the reduction of the pyridinium groups of **2** based on comparison with a similar feature in the CVs of unmetallated tetrakis(*N*-Me-3-pyridinium)porphyrin.[1]

10.b. CVs of Cage **Co₃-1a**

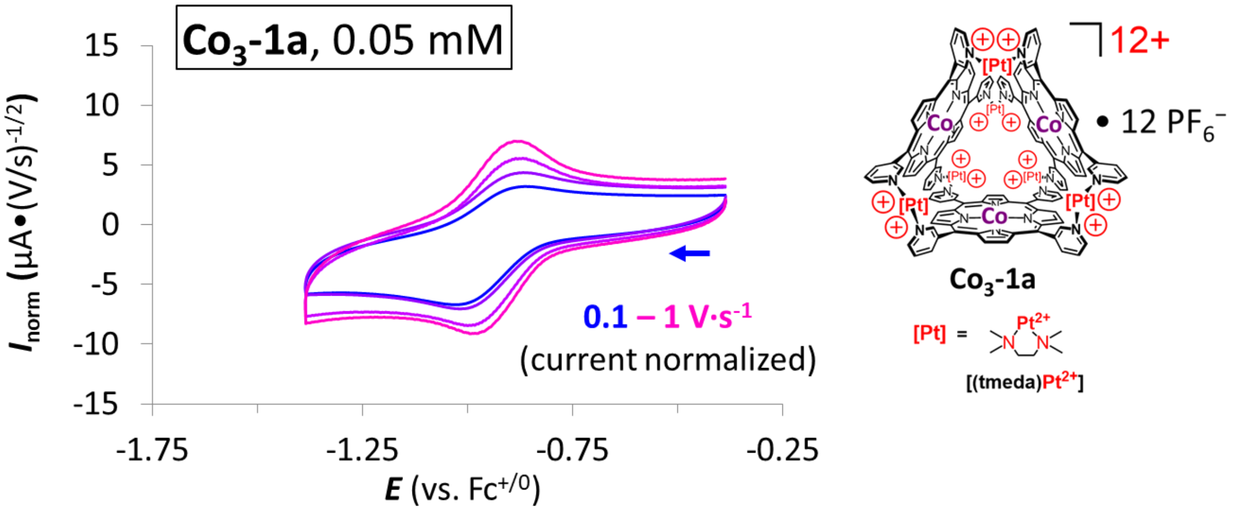

Figure S84. Cyclic voltammograms measured from −0.43 V to −1.43 V vs $\mathrm{Fc}^{0/+}$ on a 0.05 mM solution of **$\mathrm{Co_3}$-1a**•$12\mathrm{PF_6}$ in MeCN containing 0.1 M $\mathrm{TBAPF_6}$ as a supporting electrolyte. CVs were recorded at a scan rate of 100 $\mathrm{mV{\cdot}s^{-1}}$, 200 $\mathrm{mV{\cdot}s^{-1}}$, 500 $\mathrm{mV{\cdot}s^{-1}}$, and 1 $\mathrm{V{\cdot}s^{-1}}$ with the current scaled by the square root of the scan rate. These CVs show the reversible $\mathrm{Co^{II}/Co^{I}}$ redox couple of **$\mathrm{Co_3}$-1a** at $E_{1/2}$= −0.98 V vs. $\mathrm{Fc}^{0/+}$.

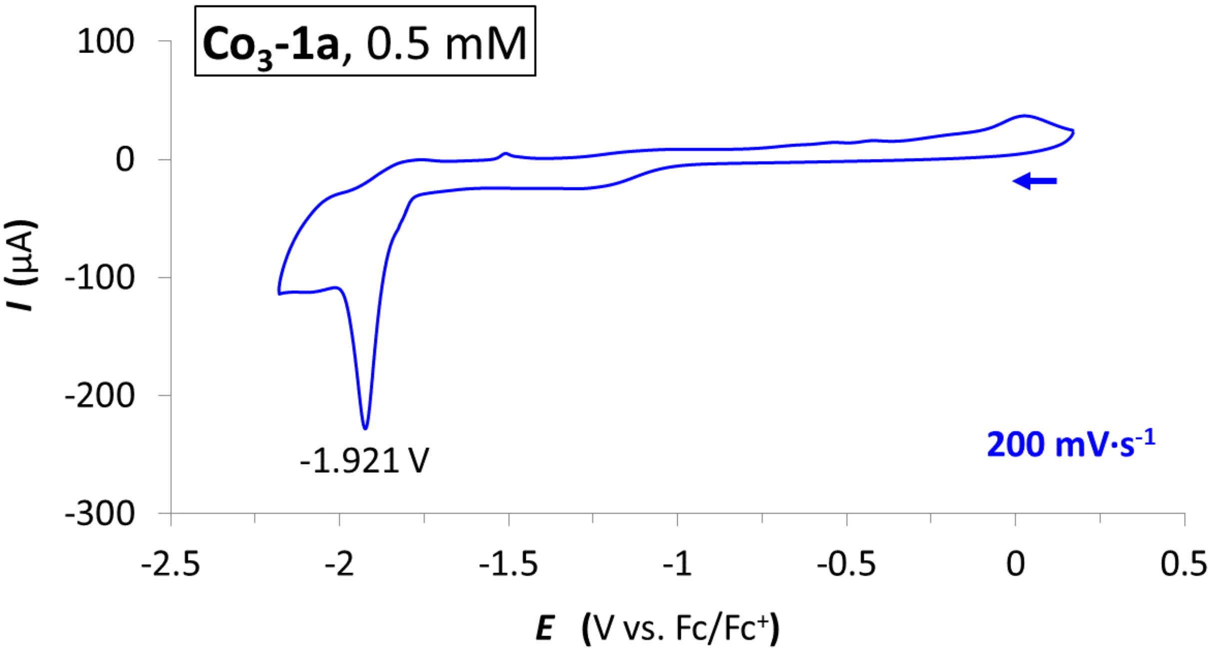

Figure S85. Cyclic voltammogram measured from +0.17 V to −2.18 V vs $\mathrm{Fc}^{0/+}$ on a 0.5 mM solution of **$\mathrm{Co_3}$-1a**•$12\mathrm{PF_6}$ in MeCN containing 0.1 M $\mathrm{TBAPF_6}$ as a supporting electrolyte, recorded at a scan rate of 200 $\mathrm{mV{\cdot}s^{-1}}$. The cathodic wave at E_{pc} = −1.921 V is attributed to the irreversible reduction of the Pt^{2+} centers of the $[\mathrm{(tmeda)Pt}]^{2+}$ linkers based on comparison with a similar feature in the CVs of **1a**.[1]

10.c. CVs of Cage **Co$_3$-1b**

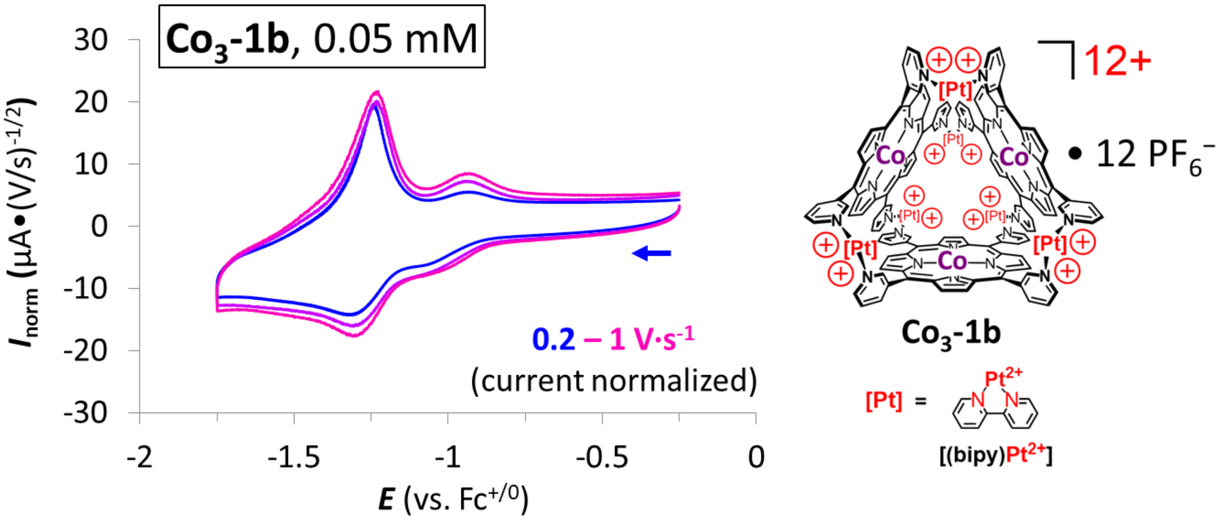

Figure S86. Cyclic voltammograms measured from +0.25 V to −1.75 V vs Fc$^{0/+}$ on a 0.05 mM solution of **Co$_3$-1b**•12PF$_6$ in MeCN containing 0.1 M TBAPF$_6$ as a supporting electrolyte. CVs were recorded at scan rates of 200 mV·s^{-1}, 500 mV·s^{-1}, and 1 V·s^{-1} with the current scaled by the square root of the scan rate. These CVs shows the reversible Co^{II}/Co^{I} redox couple of **Co$_3$-1b** at $E_{1/2}$= −0.98 V vs. Fc$^{0/+}$, followed by the first reversible reduction of the bipyridine ligands of the [(bipy)Pt]$^{2+}$ linkers at E$_{1/2}$= −1.26 V vs. Fc$^{0/+}$.

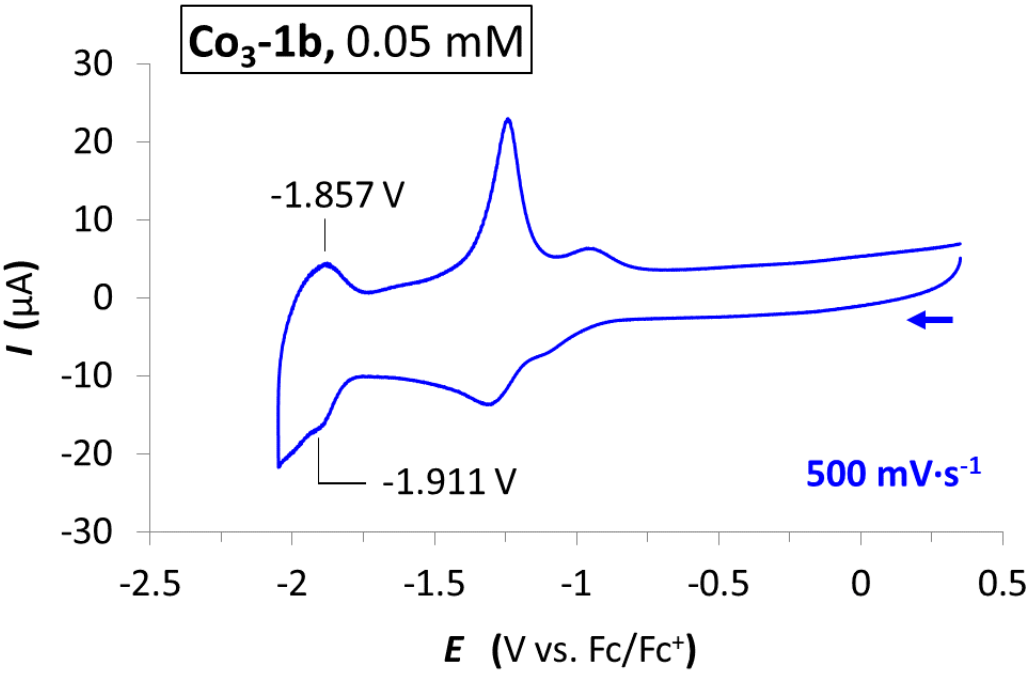

Figure S87. Cyclic voltammogram (CVs) measured from +0.35 V to −2.05 V vs Fc$^{0/+}$ on a 0.5 mM solution of **Co$_3$-1b**•12PF$_6$ in MeCN containing 0.1 M TBAPF$_6$ as a supporting electrolyte, recorded at a scan rate of 500 mV·s^{-1}. The redox couple at $E_{1/2}$ = −1.88 V is assigned to the second reversible reduction of the bipyridine ligands of the [(bipy)Pt]$^{2+}$ linkers based on comparison with CVs of **1b**.[1]

11. FTIR Measurements

FTIR experiments were conducted using a Thermo Scientific Smart OMNI-Transmittance FTIR. Samples were prepared in an N_2 atmosphere glovebox by grinding together 3 mg of a sample with 50 mg KBr before pressing into pellets. To minimized exposure to air, the pellets were transported form the glovebox in sealed plastic bags and removed just before acquiring spectra.

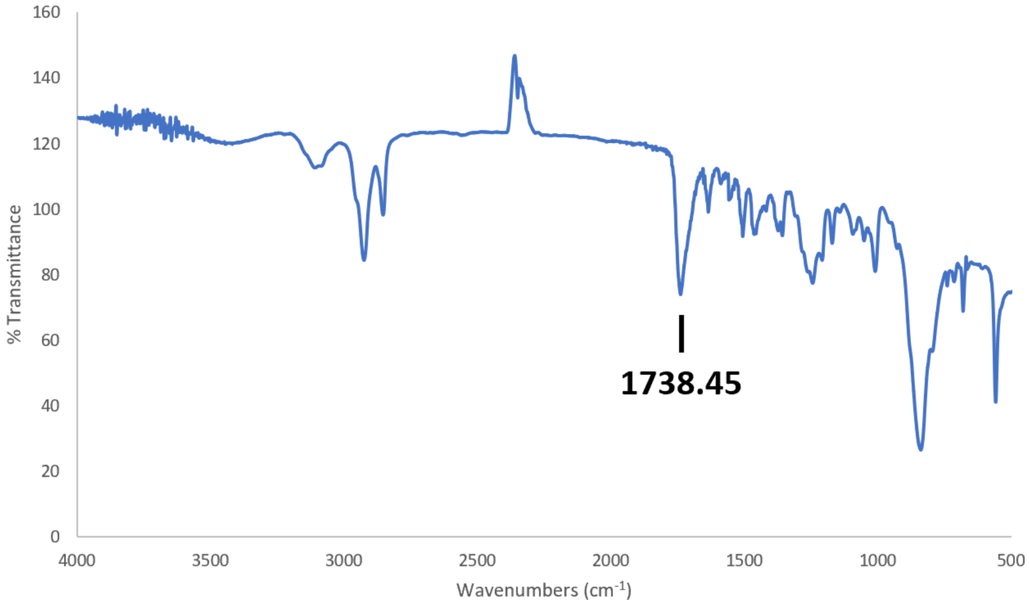

Figure S88. FTIR spectra of **7** showing a stretch at 1738.5 cm^{-1} that is consistent with the NO stretch of a nitrosyl ligand bound to a cobalt porphyrin.[10]

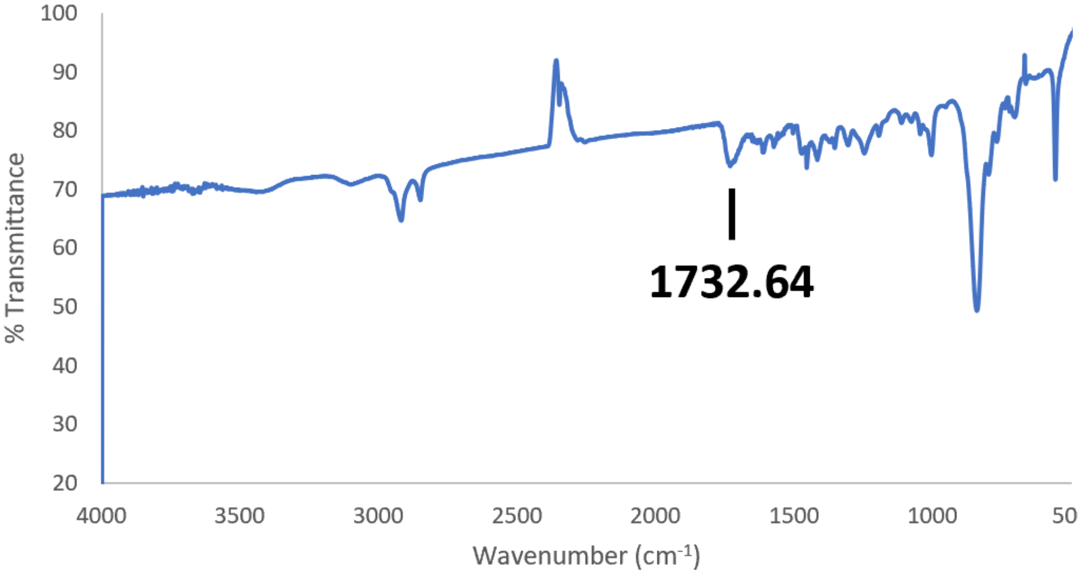

Figure S89. FTIR spectra of **$[Co^{III}NO]_3$-1a** showing a stretch at 1732.6 cm^{-1} that is consistent with the NO stretch of a nitrosyl ligand bound to a cobalt porphyrin.[10]

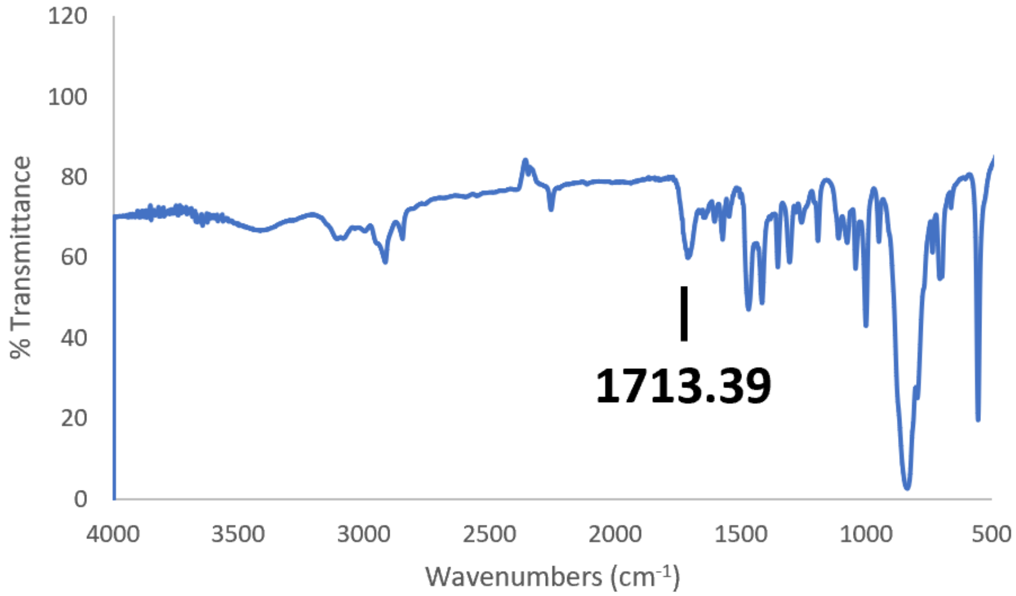

Figure S90. FTIR spectra of **[Co^{III}NO]$_3$-1b** showing a stretch at 1713.4 cm^{-1} that is consistent with the NO stretch of a nitrosyl ligand bound to a cobalt porphyrin.[10]

12. References:

[1] K. G. Dutton, D. A. Rothschild, D. B. Pastore, T. J. Emge and M. C. Lipke, *Inorganic Chemistry* **2020**, *59*, 12616-12624.
[2] M. B. Berezin, N. M. Berezina, M. I. Bazanov, A. I. V'yugin, A. S. Semeikin and A. V. Glazunov, *Russian Journal of Physical Chemistry A* **2010**, *84*, 1449-1451.
[3] B. K. Bandlish and H. J. Shine, *The Journal of Organic Chemistry* **1977**, *42*, 561-563.
[4] S. A. Baldwin and G. Van Weert, *Hydrometallurgy* **1996**, *42*, 209-219.
[5] G. R. Fulmer, A. J. M. Miller, N. H. Sherden, H. E. Gottlieb, A. Nudelman, B. M. Stoltz, J. E. Bercaw and K. I. Goldberg, *Organometallics* **2010**, *29*, 2176-2179.
[6] L. Allouche, A. Marquis and J.-M. Lehn, *Chemistry – A European Journal* **2006**, *12*, 7520-7525.
[7] S. Stoll in *Chapter Six - CW-EPR Spectral Simulations: Solid State*, *Vol. 563* Eds.: P. Z. Qin and K. Warncke), Academic Press, **2015**, pp. 121-142.
[8] G. C. Wagner, I. C. Gunsalus, M. Y. Wang and B. M. Hoffman, *Journal of Biological Chemistry* **1981**, *256*, 6266-6273.
[9] F. A. Walker, *Journal of the American Chemical Society* **1970**, *92*, 4235-4244.
[10] G. B. Richter-Addo, S. J. Hodge, G.-B. Yi, M. A. Khan, T. Ma, E. Van Caemelbecke, N. Guo and K. M. Kadish, *Inorganic Chemistry* **1996**, *35*, 6530-6538.